The Great Strides of Iron Photosensitizers for Contemporary Organic Photoredox Catalysis: On Our Way to the Holy Grail?

Felix Glaser,[1] Akin Aydogan,[2] Benjamin Elias[2,*] and Ludovic Troian-Gautier[2,*]

[1]Johannes Gutenberg University Mainz, Department of Chemistry, Duesbergweg 10–14, Mainz 55128, Germany

[2]Université catholique de Louvain (UCLouvain), Institut de la Matière Condensée et des Nanosciences (IMCN), Molecular Chemistry, Materials and Catalysis (MOST), Place Louis Pasteur 1, bte L4.01.02, 1348 Louvain-la-Neuve, Belgium

*Correspondence to: Ludovic.Troian@uclouvain.be, Benjamin.Elias@uclouvain.be

Abstract. The scarcity of 2nd and 3rd row transition metals such as ruthenium, iridium, rhodium and osmium, coupled with a global desire for sustainable chemistry has led to the resurgence of research centered on earth-abundant metal-based photosensitizers. Amongst these, iron photosensitizers have often been considered a 'holy grail' because of iron's high abundance in the earth's crust, low toxicity, and low environmental impact. In the last years especially, two different concepts to use these photosensitizers for photoredox catalysis were developed and an overview of both approaches will be presented herein. The first one is related to the inner sphere reactivity of *in situ* generated photosensitizers that allows the activation of several ligand classes for radical-based transformations using simple iron salts. The second one covers the diffusional excited-state reactivity for recently developed structurally well-defined photosensitizers. For both approaches the applications are structured according to the (proposed) photoactivation step in the light-driven applications and discussed based on the versatile examples recently reported in this highly emerging research field.

Keywords: Photoredox, Catalysis, Iron, Electron Transfer, Radicals.

1) INTRODUCTION: CHALLENGES AND OPPORTUNITIES FOR IRON PHOTOCATALYSTS 3

1.1) LIGHT-DRIVEN REACTIONS: A LONG HISTORY 3
1.2) THE EVOLUTION TOWARDS LIGHT-DRIVEN CATALYSIS 5
1.3) CHALLENGING CANDIDATES: IRON-BASED ANALOGUES OF $[Ru(bpy)_3]^{2+}$ 6
1.4) TOWARDS EXTENDING THE EXCITED-STATE LIFETIME FOR PHOTOREDOX CATALYSIS APPLICATIONS 8
1.5) A DIFFERENT APPROACH: *IN SITU* COMPLEX FORMATION AND LIGAND DISSOCIATION 9
1.6) A GUIDED TOUR OF THE REVIEW 10

2) PHOTOREDOX CATALYSIS USING *IN SITU* GENERATED PHOTOCATALYSTS 12

2.1) LIGAND-TO-METAL CHARGE TRANSFER WITH COORDINATED CARBOXYLATES 13
2.2) LIGAND-TO-METAL CHARGE TRANSFER WITH COORDINATED ALKOXIDES 16
2.3) LIGAND-TO-METAL CHARGE TRANSFER WITH COORDINATED LIGANDS AND SUBSEQUENT HAT CATALYSIS 18
2.4) MISCELLANEOUS 28

3) PHOTOREDOX CATALYSIS USING WELL DEFINED PHOTOSENSITIZERS 36

3.1) THE CASE OF $[Fe(bpy)_3]^{2+}$ AND ITS DERIVATIVES 38
3.2) PHOTOREDOX CATALYSIS USING LMCT EXCITED STATES 43
3.3) PHOTOREDOX CATALYSIS USING MLCT EXCITED STATES 53
3.4) PHOTOREDOX CATALYSIS USING A MULTI-PHOTON EXCITATION PATHWAY 54
3.5) PHOTOREDOX CATALYSIS USING DISSOCIATIVE EXCITED STATES 58

4) CONCLUSIONS AND PERSPECTIVES 65

DECLARATION OF COMPETING INTEREST 67

ACKNOWLEDGMENTS 67

REFERENCES 68

1) Introduction: Challenges and Opportunities for Iron Photocatalysts

1.1) Light-driven reactions: a long history

In the realm of synthesis, the use of light to trigger chemical transformations has been a powerful and widely used approach towards the formation of diverse and intricate molecules with high degree of complexity.[1-12] In the past century, distinctive molecular transformations were developed using reactivities of excited states to enable pathways not available through ground-state chemistry. A seminal example is the [2+2] photocycloaddition of carvone to carvone camphor, as reported by Ciamician and Silber in 1908 (**Figure 1a**).[1, 13] However, this reaction proceeded upon exposure to intermittent sunlight irradiation for several months. Similar approaches using better focused lamps were later developed. For example, almost hundred years later, Skrikrishna and Ramasastry reported the synthesis of (+)-solanascone proceeding *via* a key light-activated [2+2] cyclization within 2 hours of (high-power) ultraviolet (UV) light irradiation starting from an enantiomerically pure *(R)*-carvone (**Figure 1b**).[14, 15] Similar light-induced photocyclizations following a direct excitation of the substrate with (UV) light were exploited for the synthesis of natural products and derivatives thereof.[16] [4, 17]

As shown through these examples, light is an energy vector that can trigger chemical reactions, constituting an interesting approach towards the synthesis of complex organic architectures from simpler building blocks.[18] However, these organic molecules usually possess a very low molar absorption coefficient in the visible range and are thus often limited to near or even far UV irradiation range, thus restricting the accessibility, scalability and the versatility of the organic photochemistry due to the low natural availability of this range of the light spectrum. In addition, UV light being so energetic might also trigger unwanted photoreactions, such as photodegradation of the reagents or products, or lead to undesired photoproducts. Consequently, different approaches have been developed over the years to perform these challenging reactions with visible light using organic and inorganic chromophores - mostly referred to as photosensitizers or photocatalysts. For example, in 2012 the group of Yoon reported sensitized [2+2] cycloadditions using an Ir^{III} photosensitizer and visible light, hence avoiding the need for potentially harmful UV light excitation (**Figure 1c**).[19] This protocol was then exploited to perform the key step in the synthesis of (±)-cannabiorcicyclolic acid. In this context, complexes of precious transition metals (TM) have been under numerous investigations as potential photosensitizers for [2+2] cycloadditions.[20] In a more general way, they play a central role in a variety of light-triggered chemical processes ranging from photoredox catalysis[21, 22] and artificial solar energy conversion[23, 24] to the

development of photoprobes or photoreagents for biomolecules as diagnostic and/or therapeutic agents for various diseases.[25, 26]

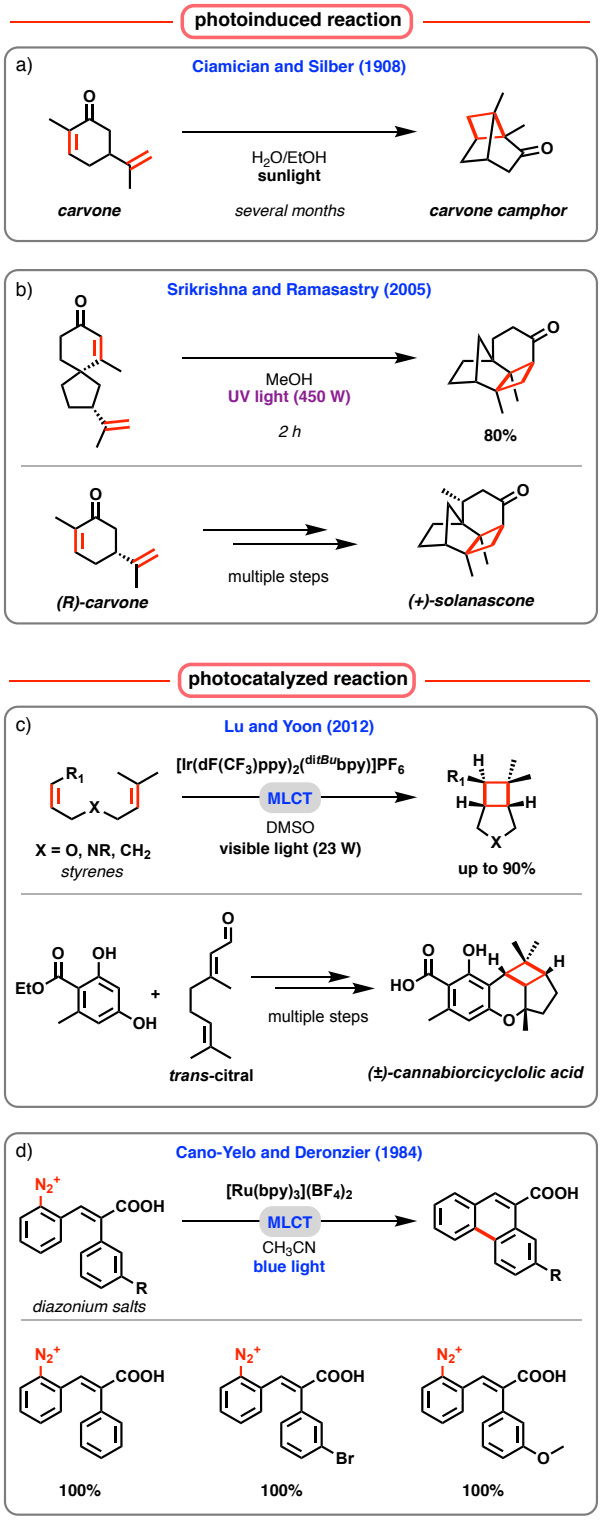


Figure 1. From photoinduced reaction with UV light to photo(redox) catalysis with visible light. A) Ciamician and Silber's [2+2] photocycloaddition of carvone yielding carvone camphor.[13] b) Srikrishna and Ramasastry's [2+2] photocycloaddition to yield solanascone derivatives.[14, 15] c) Lu and Yoon's [2+2] photocycloaddition using an Ir^{III} photosensitizer and visible light irradiation.[19] d) Phenanthrene formation from stilbene diazonium salts reported by Cano-Yelo and Deronzier.[27, 28] MLCT = metal-to-ligand charge transfer.

1.2) The evolution towards light-driven catalysis

From a broader perspective, the use of photocatalysts for light-driven transformations as an alternative to direct substrate irradiation or to thermal reaction has started to attract interest in the second half of the last century.[29] One of the very first example of photosensitized catalysis – generally referred to as *photoredox catalysis* – was developed in the late eighties using a ruthenium-based metal complex.[27, 28] In this light-mediated reaction, a $[Ru(bpy)_3]^{2+}$ photosensitizer (bpy = 2,2'-bipyridine) absorbs visible light and populates a $^{3*}[Ru(bpy)_3]^{2+}$ excited-state, which consists of a metal-to-ligand charge transfer (MLCT) with a formally reduced ligand and oxidized metal center. The facilitated electron transfer in comparison to the ground state enables excited state quenching with suitable substrates or sacrificial reagents. Using the above-mentioned ruthenium-based photosensitizer, Cano-Yelo and Deronzier successfully converted stilbene diazonium salts into phenanthrenes with excellent yield in degassed acetonitrile using visible light (**Figure 1d**).

These 4d and 5d metal-based photosensitizers possess several key properties that contribute to their usefulness in the field of photochemistry. Most of them absorb light in the visible region of the electromagnetic spectrum which leads to the population of an excited state that usually persists for several hundreds of nanoseconds or even microseconds. For example, the excited-state lifetime of $^{3*}[Ru(bpy)_3]^{2+}$ in acetonitrile is around 1100 ns in the absence of oxygen, which is sufficiently long to engage in bimolecular interactions in solution phase.[30, 31] In addition, the excited state also exhibits enhanced electrochemical properties, where the catalyst in its excited state is both a stronger reductant and oxidant than the corresponding ground state.[32, 33] An important condition for an efficient bimolecular reactivity from an excited photocatalyst is that the excited-state lifetime must be sufficiently long to allow the excited photosensitizer and a quencher to diffuse towards each other and form an encounter complex.[34] This condition is often successfully met for the prototypical Ru^{II}, Ir^{III} and Os^{II} photosensitizers due to their reasonably long lifetimes within the nanosecond to microsecond timescale.[35, 36] Although these compounds are amongst the most widely employed systems in various light-induced applications, they are amongst the least abundant elements in the Earth's crust. With the urgency of sustainability, the scarcity and the high cost of these metals constitute major drawbacks. Organic photosensitizers such as acridinium and triphenylpyrylium ions or donor-acceptor fluorophores are often considered as an alternative as they exhibit excited-state lifetime between 3 and 20 ns, which is usually long enough to promote bimolecular reactivity with sufficiently large concentrations of quencher present in

solution.[37-44] Another alternative is to use first row transition metals photosensitizers as these are very abundant elements.[45-47] Over the past decade, a regained interest in earth-abundant metal-based photosensitizer led to spurt of development in the field. Indeed, major advances have been made with photosensitizers based on elements such as copper, tungsten, molybdenum, nickel, zirconium, chromium, cobalt and iron as alternatives to complexes based on precious and rare metals.[45-64]

1.3) Challenging candidates: iron-based analogues of $[Ru(bpy)_3]^{2+}$

Iron represents an interesting case as, after oxygen, silicon and aluminum, it is the most abundant element in the Earth's crust. In addition, the isoelectronicity of the d^6 valence electronic configuration of Fe^{II} compared to Ru^{II}, Os^{II} and Ir^{III} in principle renders it an obvious potentially suitable candidate for their replacement.[65] $[Fe(bpy)_3]^{2+}$ was first synthesized in the 1960's,[66] and exhibits intense visible absorption features with comparable molar absorption coefficients as its heavier $[Ru(bpy)_3]^{2+}$ and $[Os(bpy)_3]^{2+}$ analogues.[67] In contrast to the spectral similarity in the ground state, the excited-state behavior is very different between the 3d and the 4d/5d metal complexes. Transient absorption spectroscopy of $[Ru(bpy)_3]^{2+}$ leads to a bleach of the metal-to-ligand charge transfer (MLCT) transition and novel absorption bands in the UV and past 550 nm. The bleach is assigned to the formal oxidation of Ru^{II} to Ru^{III} whereas the novel absorption bands are attributed to ligand-centered reduction due to the formally reduced ligand. Hence, the excited state of $[Ru(bpy)_3]^{2+}$ is often described as $^{3*}[Ru^{III}(bpy)_2(bpy^{\bullet-})]^{2+}$. Similar features are observed initially for $[Fe(bpy)_3]^{2+}$ using femtosecond transient absorption spectroscopy, *i.e.* positive excited-state absorption in the blue and red spectral range and a ground-state bleach of the MLCT band in the green spectral range. The initial excited-state of $[Fe(bpy)_3]^{2+}$ with a MLCT character is hence also depicted as $^{*}[Fe^{III}(bpy)_2(bpy^{\bullet-})]^{2+}$. However, despite initially very similar transient absorption signals compared to $[Ru(bpy)_3]^{2+}$, the lifetime of these excited states is very different and the transient absorption spectra of $^{*}[Fe(bpy)_3]^{2+}$ rapidly evolves within 100 fs and is converted into an overall bleached signal. These observations indicate that the visible light excitation ultimately results in the formation of an excited state whose nature is different compared to the typical MLCT state in $[Ru(bpy)_3]^{2+}$ (**Figure 2a**). The lack of positive transient absorption of $[Fe(bpy)_3]^{2+}$ in the blue region (near 400 nm) was proposed to constitute a strong evidence that the excited state was not a charge-transfer species but rather a ligand-field state, without clarifying the exact spin-state ($^3T_1$ or $^5T_{2g}$).[68-71] This assumption was confirmed by McCusker and coworkers assuming that the nature of the lowest excited-state of $[Fe(bpy)_3]^{2+}$ is a ligand-field high-spin

$^5T_{2g}$ state, formed upon ultrafast intersystem crossing from ^{1}MLCT to $^5T_{2g}$ (**Figure 2a**).[70, 72] The relaxation of the metal-centered dark excited state was modeled by a single exponential decay with a lifetime of 18±2 ns.[73, 74] Bergkamp *et al.* determined that the formation quantum yield of the $^5T_{2g}$ state of $^*[Fe(phen)_3]^{2+}$ (phen = 1,10-phenanthroline) was nearly 100 %.[75, 76]

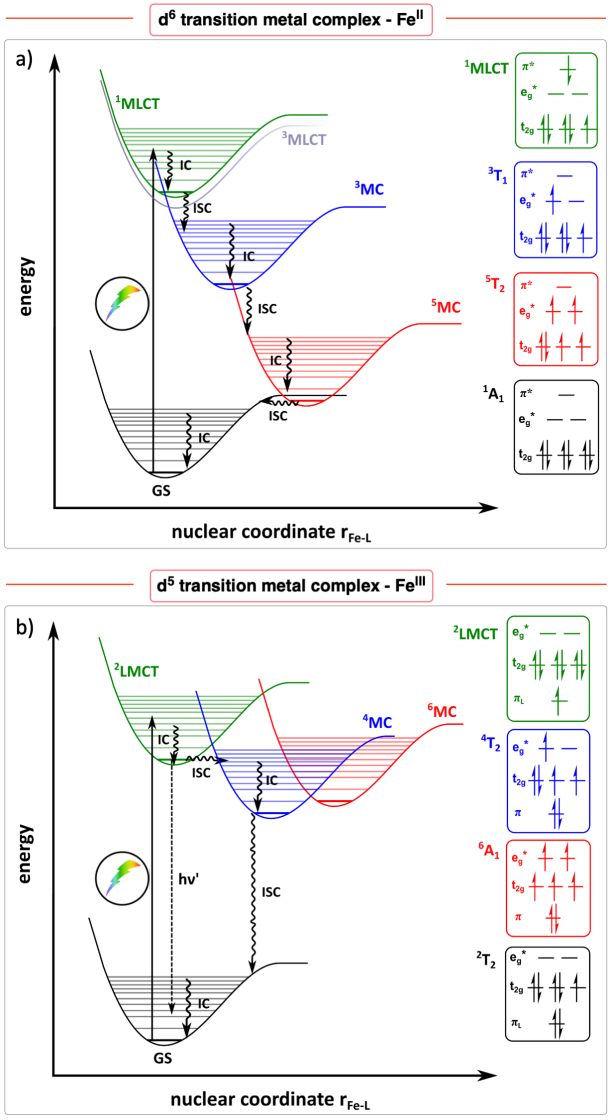


Figure 2. Schematic potential energy surfaces and relevant electronic states for the excited-state decay of a) Fe^{II} and b) Fe^{III} transition metal complexes. Electron configurations are given for O_h symmetry for simplicity. Radiative decay pathways are denoted as dotted straight lines while non-radiative decay pathways are presented as wavy lines. GS = ground state, IC = internal conversion, ISC = intersystem crossing, MLCT = metal-to-ligand charge transfer, LMCT = ligand-to-metal charge transfer, MC = metal-centered.

In summary, almost immediately after its photo-generation, the ^{1}MLCT state in $[Fe(bpy)_3]^{2+}$ decays and is converted on a ~100 fs time scale to low-lying metal-centered ligand-field states of the iron core, populating a high-spin quintet excited state ($^5T_{2g}$). For any classical polypyridyl-type ligand, the resulting Fe^{II} complexes generally follow this photophysical pathway (**Figure 2a**).[68, 72, 73, 77, 78] In contrast to the ^{3}MLCT excited state of Ru^{II}

complexes, there is thus no long-lived net charge separation upon formation of the excited state in Fe^{II} complexes. Hence, the overall remarkable difference between $[Ru(bpy)_3]^{2+}$ and $[Fe(bpy)_3]^{2+}$ in the excited state is caused by a change of the lowest excited state from a MLCT state to a metal-centered state (**Figure 2a**). Because of its ligand-field nature and its lower energy relative to its ^{1}MLCT state,[79] its reactivity is fundamentally different and less appealing in iron catalysis compared to the ^{3}MLCT state of Ru^{II} complexes.[80]

1.4) Towards extending the excited-state lifetime for photoredox catalysis applications

The extremely short excited-state lifetime of Fe^{II} polypyridyl photosensitizers and related Fe^{III} photosensitizers (*vide infra*) represents a drastic limitation and renders diffusion-based photoredox catalysis challenging with iron catalysts. Within the last years, two different approaches to use iron catalysts for photoredox catalysis have been developed. One strategy that is followed by several research groups are new concepts to change the excited-state energy landscape to (hopefully) extend the lifetime of the charge separated excited states and prevent or diminish the population or deactivation through metal-centered state. This concept represents a possibility to make iron catalysts more appealing for photoredox catalysis. Thus, strategies to extend their excited-state lifetimes have been investigated over the past years. These have been described in excellent reviews towards which the reader is directed,[46, 47, 52, 56, 65, 81-85] and will hence only be very briefly summarized hereafter. The main rational is to extend the lifetime of the MLCT states, either by stabilizing it or by destabilizing the metal-centered (MC) states involved in the ultrafast deactivation.[56, 65, 86] Strategies to achieve this goal include the use of (i) highly σ-donating ligands to strengthen the ligand-field and, thereby, increasing the separation between t_{2g} and e_g molecular orbitals, (ii) ligands having low energy π* orbitals to stabilize MLCT states, (iii) complexes with a geometry approaching the perfect octahedron to increase the field strength of the ligands, and (iv) metal centers presenting a break of the symmetry of the coordination sites. Theoretical calculations indicate that an asymmetry in this first coordination sphere should also induce a larger energy difference between MLCT states and MC states.[87] In recent years, these approaches have allowed to increase the excited-state lifetime of iron-based photosensitizers with MLCT excited states from ~10 ps in 2013[58] to 528 ps in 2018 with several gradual steps in between.[88] The current record for iron-based photosensitizers with MLCT excited states is around 1-1.25 ns.[89, 90] An iron photosensitizer with an excited-state lifetime of ~2.5 ns has been reported in 2019 by the Herbert group.[91] Although it was initially proposed to be an MLCT excite state, recent results tend to suggest that this state could be a charge-transfer state or even a metal-centered state. Very recently, an

Fe^{III} complex, $[Fe(ImP)_2]^+$ (HImP = 1,1'-(1,3-phenylene)bis(3-methyl-1-imidazol-2-ylidene)), with two symmetric tridentate cyclometalated *N*-heterocyclic carbene (NHC) ligands and exhibiting a Janus-type dual emission from ligand-to-metal charge transfer (LMCT) and metal-to-ligand charge transfer states (MLCT) has been reported.[92] The ^{2}LMCT exhibited an excited-state lifetime of 240 ps whereas the ^{2}MLCT state exhibited a new excited-state lifetime record for iron photosensitizers of 4.6 ns. It was however very recently shown that this long-lived species originated from the presence of an impurity with a photoluminescence centered at 450 nm.[93]

With respect to purely LMCT emitters, a Fe^{III} photosensitizer with six carbene ligands exhibits an unconventional low-lying luminescent doublet ligand-to-metal charge transfer (^{2}LMCT) excited-state and an excited-state lifetime of ~2.2 ns.[94] In contrast to the spin-forbidden phosphorescence from the ^{3}MLCT state in Fe^{II} complexes, the observed emission is in this case a spin-allowed fluorescence from the ^{2}LMCT to the ground state ^{2}GS (= $^2T_2$, **Figure 2b**). Taking into consideration the different strategies discussed earlier to prolong the excited state lifetimes of d^6 metal complexes with MLCT excited states, in this polycarbene Fe^{III} complex, deactivation *via* vibrational modes rather than ^{4}MC states was found to be a limiting factor of the excited-state lifetime.[95] Nevertheless, these lifetimes are comparable to the singlet states of (short-lived) organic chromophores and diffusion-controlled encounters in solution are possible and can (potentially) allow applications of these complexes in photoredox catalysis (section 3).

1.5) A different approach: *in situ* complex formation and ligand dissociation

The progress with respect to the excited-state lifetimes has been impressive within the last years (see **section 1.3**). Nevertheless, these lifetimes fall within the picosecond to low nanosecond timescales which implies that diffusion-controlled rate constants for bimolecular quenching and/or high concentrations of quencher are needed for successful catalysis. Rather than tuning the excited-state lifetimes of these iron photosensitizers, an alternative approach consists in utilizing an electronic sequence to populate metal-centered states for unique reactivities.[96] For well-defined photosensitizers with designed ligand structures, a population of MC states - e.g. $^3T_1$ and $^5T_2$ in **Figure 2a** - is often undesired as this is often one of the main deactivation pathways preventing long excited-state lifetime,[56, 65] but for the light-induced reaction of coordinated substrates, this aspect can be beneficial.[97-102] This approach has received particular attention for photoredox catalysis with Fe^{III} catalysts. With suitable ligands, a homolysis of the bond between the Fe^{III} catalyst (or other 3d metal complexes) and an attached

substrate as ligand in a ligand-to-metal charge transfer (LMCT) excited state can therefore result in ligand-centered radical intermediates. Typically, this involves the population of anti-bonding metal-centered orbitals and the depopulation of ligand-dominated bonding σ-bonds.[100, 101, 103] As a consequence of the weaker coordination of the ligands in first-row transition metal complex, this pathway is facilitated with iron catalyst (and other 3d metals)[96] compared to analogue complexes based on 4d or 5d transition metals.[46, 101] In general, different (monodentate) ligands like alkoxides, carboxylates or halides can be coordinated *in situ* to the iron center. This leads to the formation of iron photosensitizers that can undergo light-induced formation of reactive radicals for various applications in photoredox catalysis (**section 2**). In the literature, this process is sometimes also discussed under the more general term of visible light induced homolysis.[100, 101]

1.6) A guided tour of the review

Achieving excited-state lifetimes reaching the (short) nanosecond timescale has boosted the use of these photosensitizers in photoredox catalysis with a special emphasis on mechanistic determinations. In the synthetically oriented community, the *in situ* activation of substrates with iron-based photocatalysts has received considerable attention in the last years. These two different, yet complementary, research fields of well-defined photocatalysts and of *in situ* generated ones, are herein considered and discussed. The reader is also directed to an excellent perspective that was published during the evaluation of the present review.[85] Our overview here essentially focuses on organic transformations using iron photocatalysis in homogeneous solution whereas research on heterogenous systems and dye-sensitized solar cells is not covered.[104-113]

In the subsequent pages, the reader is guided through two main segments **(Figure 3)**. The first one is dedicated to *in situ* generated photocatalysts that undergo ligand-to-metal charge transfer (LMCT) catalysis with selected substrates. These *in situ* generated photocatalysts have shown great promise in the field of photoredox catalysis where the emphasis has often been placed on functional group tolerance and large substrate scope investigations. Due to the substantial number of reports, only representative examples are presented and collected and discussed according to the functional group chelated to the iron center. The second segment of this review gathers the examples of well-defined $Fe^{II/III}$ molecular photosensitizer that have been developed over the years. A brief history of the evolution of the excited-state lifetime with specific ligand design is given, but the emphasis is placed on the use of these well-defined

photosensitizers for photoredox catalysis applications. In this part the overall number of examples are more limited up to now and more representative substrate scopes are shown.

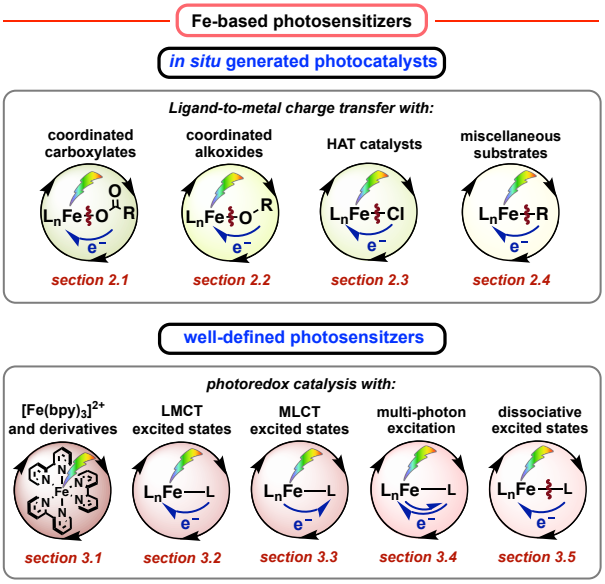


Figure 3. Overview over the different topics covered in this review article.

2) Photoredox catalysis using *in situ* generated photocatalysts

The field of photo(redox) catalysis and its synthetic applications has expanded enormously in recent years with several new approaches that have been developed.[114] Amongst these, an interesting concept with several reported methodologies is related to the *in situ* activation of the substrate, for example with modifications of the substrate to facilitate light-driven chemical transformations,[115-117] or with precatalyst activations – in combination with electrochemistry,[118-120] hydrogen atom transfer (HAT) catalysis,[121-123] metallaphotoredox catalysis,[124] or multi-photonic approaches.[10] Not all of these approaches are easily adaptable to photoredox catalysis with iron-based photosensitizers, but systems that exhibit rapid bond cleavage of *in situ* coordinated substrates can be used as earth-abundant complexes to achieve selected transformations.[96, 97, 125-127] This is especially interesting for first-row transition metals due to the smaller orbital overlap between ligands and metals with subsequently lower anti-bonding or non-bonding MC states and the facilitated light-induced ligand exchange.[80]

In contrast to systems with well-defined complexes that typically rely on diffusional encounters between an excited state and the substrates or sacrificial quenchers (**section 3**), metal complexes where the coordinated substrate is part of the photoactive catalyst can undergo excited-state reactivity *via* inner-sphere mechanisms that do not rely on diffusional processes. Therefore, this strategy circumvents some of the challenges of well-defined photosensitizers and especially their need for reasonably long excited-state lifetimes.[96] In general, two different methods of activation can be distinguished for *in situ* generated photocatalysts with iron: either the substrate is part of the photoactive species and a direct activation *via* a ligand-to-metal charge transfer excitation and fast bond cleavage leads to a direct substrate activation (**Figure 4a**) or an oxidized ligand (e.g. chlorine radical) induces a subsequent reaction for example by HAT catalysis as a pathway for indirect substrate activation (**Figure 4b**). In both cases a cleavage of the coordinated ligand is crucial for a successful light-driven catalysis. In fact, ligand-to-metal charge-transfer to coordinated labile ligands has not been developed solely for iron catalysis, but the general reactivities are also known from other (first-row) transition metal complexes like copper and cerium-based systems.[128-132] Different review articles with a focus on LMCT excitations in 3d metal complexes for synthetic applications were recently published.[96, 102, 133] Here, we especially focus on the different reactivities with iron photocatalysts and their applications in photoredox catalysis. The synthetic transformations are discussed according to their *in situ* coordinated ligand in their proposed photoactive form,

for example carboxylates (**section 2.1**), alkoxides (**section 2.2**), halides and HAT catalysts (**section 2.3**), and other cases that do not perfectly fit in one of the mentioned categories (**section 2.4**).

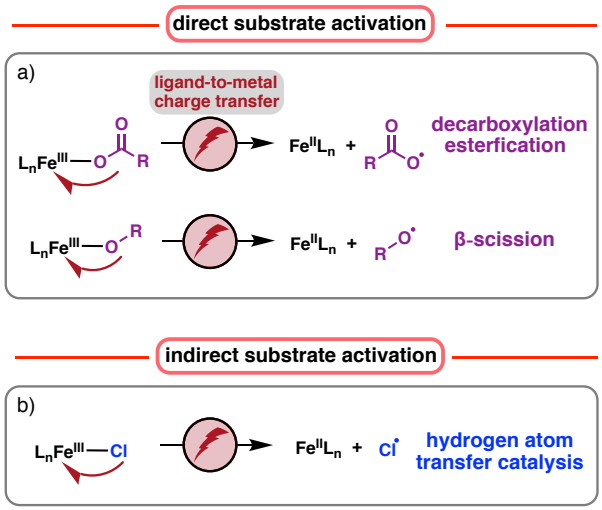


Figure 4. Different general activation modes for ligand-to-metal charge transfer relevant for *in situ* generated photocatalysts used for direct and indirect substrate activation.

2.1) Ligand-to-Metal Charge Transfer with coordinated carboxylates

Carboxylic acids have long been known as ligands for cationic metals.[134-136] In light-driven catalysis, two different approaches were investigated in recent years: i) outer-sphere electron transfer *via* diffusional excited-state quenching,[137-140] and ii) coordination as ligands to metal complexes for a light-induced substrate activation in an inner sphere electron transfer *via* ligand-to-metal charge transfer.[96, 133, 141] The latter reactivity has also been adapted for iron catalysts and the different examples are discussed hereafter.

An early example for LMCT activation from a substrate to an iron catalyst was presented in 2019, where a coordinated carboxylate was proposed to form the photoactive iron photocatalyst (**Figure 5a**).[142] Different amine- and pyridine-based bi- and tridentate ligands were tested as ligands for iron-based photocatalysis. Blue light irradiation led to the subsequent formation of aliphatic and benzylic carbon-centered radicals after decarboxylation. Trapping the corresponding radicals with doubly cyanated alkenes or azodicarboxylates was developed for a series of substrates with different substitution patterns (**Figure 5a**).

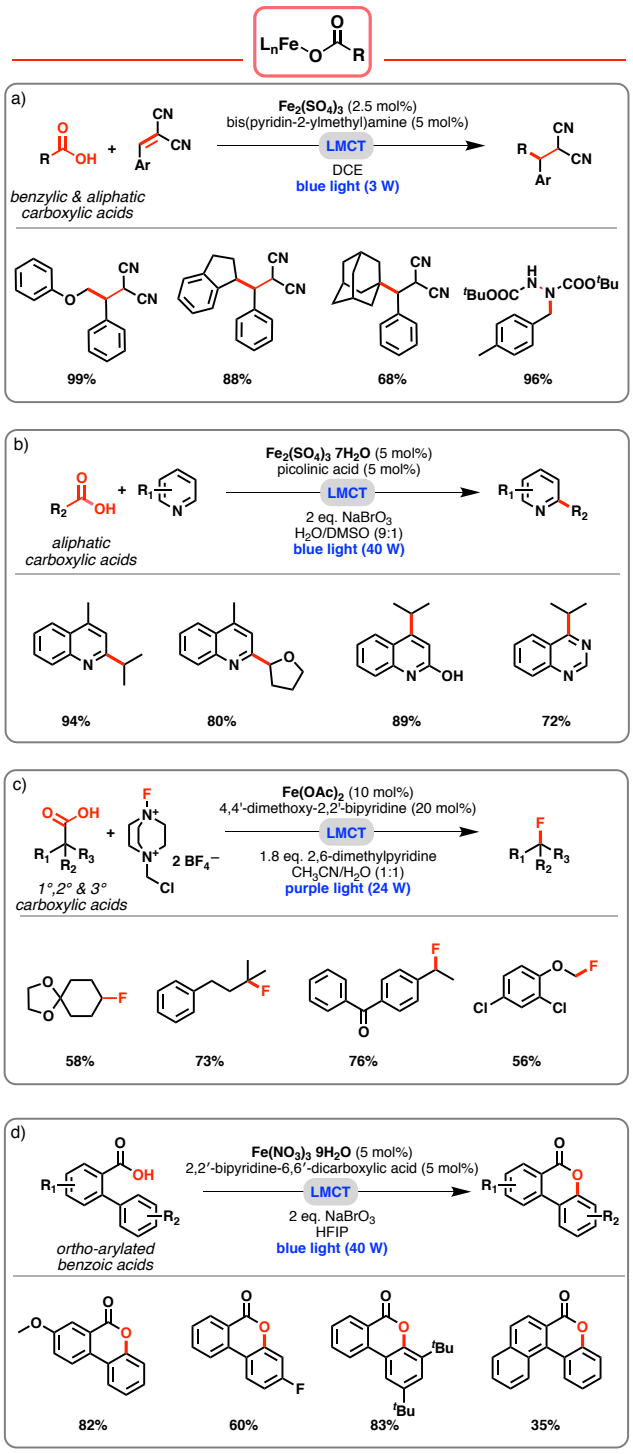


Figure 5. Ligand-to-metal charge-transfer activation of coordinated carboxylic acids with iron precursors.[142-145] HFIP = hexafluoroisopropanol.

The formation of carbon-carbon or carbon-nitrogen bonds in overall-redox neutral reactions without the need for sacrificial reagents was made possible by the use of electrophiles with electron-poor double bonds to trap the radical intermediate. The alkylation of heteroaromatic structures like pyridines, quinolines, quinoxalines or other nitrogen-containing heteroaromatic substrates with aliphatic carboxylic acids was achieved for Minisci-type reactions under blue

light irradiation using a similar concept in the presence of $NaBrO_3$ as sacrificial electron acceptor (**Figure 5b**).[143] Again, a pyridine-based ligand (picolinic acid) enabled a reaction using visible light. Such reactivity was already known for a long time using stoichiometric amounts of $Fe_2(SO_4)_3$ under light irradiation,[146, 147] but the present report describes the use of catalytic concentrations of iron and drastically increased the substrate scope.

The strategy using aliphatic carboxylic acids as precursors for the formation of radical intermediates upon elimination of CO_2 *via* single electron oxidation has also been successfully adapted to the radical fluorination of aliphatic substrates with an Fe^{II} precatalyst in the presence of (poly)pyridine ligands (**Figure 5c**).[145] LMCT of the active Fe^{III} catalyst led to the formation of the corresponding Fe^{II} with a dissociated carboxylate radical that underwent CO_2 release and formed the corresponding aliphatic radical. Selectfluor was used as fluorine source to fluorinate the aliphatic radical while the intermediate amine based radical was proposed to regenerate the Fe^{III} state. For this transformation, comparably high catalyst loadings of 10 mol% were used and electron-rich substituted pyridine-based ligands were found to be optimal to achieve moderate to good yields for product formation.

In 2020, the group of Jin successfully investigated an intramolecular cyclisation with *ortho*-arylated benzoic acid substrates (**Figure 5d**).[144] When biphenyl benzoic acids were used, the corresponding carboxyl radical intermediate was trapped by the neighboring aromatic ring which stands in contrast to the decarboxylative pathway for aliphatic carboxylic acids discussed previously (**Figure 5a-b**). Overall, the formation of a new carbon-oxygen bond was achieved, presumably *via* an intramolecular radical homolytic substitution, in the presence of an amine-based ligand for the iron precatalyst and a sacrificial electron acceptor (**Figure 5d**). Different substitutions bearing electron-withdrawing or electron-donating groups on one of the aromatic rings were tolerated for this intramolecular reaction. The difference in reactivity between aromatic and aliphatic carboxylic acids is not exclusive for iron catalysis, and an oxygen-based radical reactivity instead of decarboxylation of aromatic compounds is also feasible for other reactions involving (aromatic) carboxyl radical intermediates.[138, 148-150] Decarboxylation of aliphatic substrates is typically very efficient but for aromatic carboxylic acids derivatives, competing deactivation pathways (e. g. HAT reactivity or back-electron transfer) can prevent efficient decarboxylation.[130, 138, 151-153] In fact, very sophisticated systems are needed to achieve (light-driven) decarboxylations of benzoic acids and only quite a few examples have been reported to date.[130, 138, 151] Note that transition-metal free (photo)catalytic decarboxylative borylations of aryl *N*-hydroxyphthalimide esters have also been reported, although the exact mechanism is not entirely clear in all cases.[154-156]

2.2) Ligand-to-Metal Charge Transfer with coordinated alkoxides

Alkoxides are also suitable substrates to coordinate a metal center with subsequent inner-sphere ligand-to-metal charge transfer with Fe^{III} catalysts. The generated alkoxy radicals undergo facile β-scission to cleave a carbon-carbon bond and form the corresponding ketone, aldehyde or carboxylic acid (**Figure 6**).[157] Interestingly, in contrast to reactions involving carboxylic acids (**Figure 5**), no additional pyridine-based ligands are needed to perform the light-driven reactions using an iron photocatalyst.

In 2022, various versions of similar reactions following this conceptual idea of an LMCT involving aliphatic alcohols as substrates have been published. For example, a ring opening of cyclic alcohols has been demonstrated by the group of Zeng using iron acetylacetone as catalyst precursor (**Figure 6a-b**).[158, 159] Under blue light irradiation, a carbon-carbon bond cleavage yielded an aliphatic radical that was trapped with suitable reagents. The formation of a new carbon-nitrogen bond together with a ketone was demonstrated with *di-tert*-butyl azodicarboxylate to trap the carbon-centered radical intermediate (**Figure 6a**). Screening of different Fe^{III}-based precursors indicated that iron alkoxides are especially well suited as catalysts, although a closer analysis of the mechanism was not presented. Aliphatic secondary as well as tertiary carbon centers bearing a benzylic alcohol were found to be suitable substrates as well as heteroaromatic groups that were tolerated with moderate to good yields. In a closely related study, the same concept was adapted for the bromination and iodination of cyclic aliphatic alcohols (**Figure 6b**).[159] Halogenated succinimides were investigated as electrophiles to obtain a halogenated product bearing a ketone moiety after LMCT excitation of the corresponding iron alkoxide complex and β-scission. Sodium bromate ($NaBrO_3$) as additional oxidant was found to enhance the product yield and the linear halogenated ketones were generally obtained in moderate to good yields. Overall, these two examples point towards a more general usability of this ring-opening approach for cyclic alcohols and open various possibilities to intercept the radical intermediate and potentially perform different transformations to access functionalized alkyl ketones.

When this approach was adapted to acyclic alcohols, the corresponding ketone and the dissociated radical can be located in different products. For example, primary, secondary and tertiary alcohols have been shown to yield on the one hand a ketone or aldehyde and on the other hand the coupling product from the reaction between the aliphatic radical intermediate and the electrophile using iron catalyst under blue light irradiation (**Figure 6c**).[160] Several benzylic and aliphatic alcohols and trapping reagents with electron-deficient double bonds were

successfully utilized and - depending on the substrate - moderate to excellent yields with up to 93% were obtained. Unlike the previous examples involving alcoholic substrates (**Figure 6a-b**), the generation of the alkoxy radical intermediate was proposed to occur not *via* direct LMCT of the iron complex, but *via* a light-driven chlorine radial formation and subsequent base-assisted hydrogen atom transfer. While a detailed analysis of the mechanism is not presented, the presence of substoichiometric amounts of chloride salts were needed for a successful product formation.

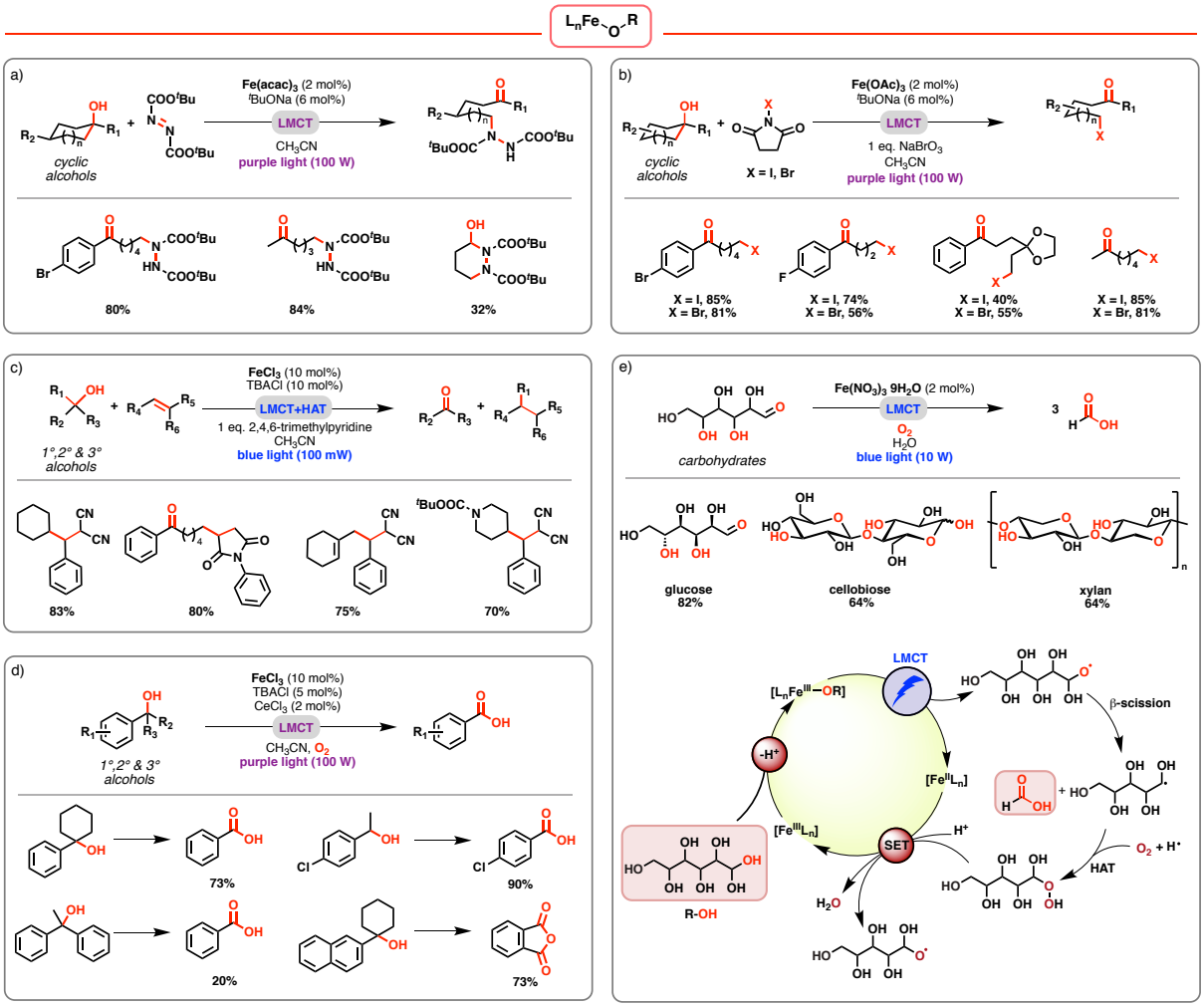


Figure 6. Transformations using ligand-to-metal charge-transfer activation of coordinated alcohols with Fe^{III} precursors.[158, 160, 161] [159, 162] acac = acetylacetone, TBACl = tetra-*n*-butylammonium chloride, tBuONa = sodium *tert*-butoxide

The cleavage of carbon-carbon bonds of alcohol substrates with light-driven iron catalysis to form the corresponding carboxylic acid was recently achieved by the groups of Guo and Zeng that investigated this reactivity using 390 nm UV light irradiation under an oxygen atmosphere (**Figure 6d**).[162] Different primary, secondary and tertiary alcohols were successfully transformed to the corresponding carboxylic acid with moderate to excellent yields. The addition of 10 mol% of tetra-*n*-butylammonium chloride and 2 mol% of Ce^{III}

chloride as ligand and cocatalyst, respectively, were advantageous for the overall reaction yield, although the actual role of the additional lanthanide remained unclear. Light-driven LMCT activation and β-scission of coordinated alcohols has previously been reported with cerium salts.[131, 163-166] However, in the present case, no product formation was observed in the absence of iron catalyst. For naphthalenyl-containing substrates (**Figure 6d**) the reaction conditions allowed an oxidation of the naphthalene ring to form phthalic anhydrides. A superoxide radical anion, which is generated from the Fe^{II} intermediate to recover the Fe^{III} catalyst, is proposed to assist the second light-driven oxidation of the ketone intermediate using the iron catalyst after the first alcohol oxidation step.

Very recently, the synthesis of formic acid from small sugars – for example glucose, arabinose or cellobiose as well as the polysaccharide of xylan – was reported under blue light irradiation with iron nitrate as precatalyst (**Figure 6e**).[161] Small-scale reactions with these carbohydrates were performed in water under an oxygen atmosphere at atmospheric pressure and resulted in moderate to good yields of formic acid. With glucose, a gram-scale reaction was developed that proceeded with yields of 70%. The iron photocatalyzed degradation of cellulose to formic acid in 37% yield was also achieved when the solubility of cellulose was increased in 5wt% sulfuric acid through the addition of lithium chloride. Mechanistically, a LMCT from the coordinated alcohol to the iron catalyst was proposed, followed by a β-scission to shorten the carbon chain by one carbon unit and release formic acid (**Figure 6e**). The carbon-centered radical was proposed to capture oxygen followed by a hydrogen atom transfer to form a peroxide intermediate that was able to regenerate the Fe^{II} catalyst to the initial Fe^{III} state while forming another alcohol-based radical that results in a subsequent cleavage of a second equivalent of formic acid.

2.3) Ligand-to-Metal Charge Transfer with coordinated ligands and subsequent HAT catalysis

A direct coordination of the substrate to the iron precatalyst with deprotonated alcohols or carboxylic acids is attractive due to the operational simplicity, where – in some cases with the addition of suitable ligands – photoactive intermediates are directly formed. A ligand-to-metal charge transfer excitation directly generates the radical intermediate of the substrate upon ligand dissociation (**Figure 4**) and the subsequent reactivity is mainly dominated by the properties of the substrate (**Figure 5 and 6**). A main drawback of this approach is the need for corresponding functional groups to coordinate to the metal center. A conceptually different strategy is the generation of reactive intermediates or active cocatalysts to initiate the desired

light-driven reactivity. In this case, the transient radical determines the scope of possible transformations and the iron catalyst is mainly needed for an (effective) generation of the substrate-activating species (**Figure 4**). In fact, this approach with indirect substrate activation is known for the combination between photoredox and hydrogen-atom transfer (HAT) catalysis using different photoredox catalysts.[121, 122, 165, 167-172] Similar to previously shown examples with copper, cerium or nickel catalysts,[96, 98, 173-178] a LMCT excitation of $FeCl_3$ can lead to a bond dissociation, generating the reduced Fe^{II} catalyst as well as a chlorine radical ($Cl^{\bullet}$). The latter intermediate has previously been explored as useful HAT catalyst,[96, 179, 180] and its formation with iron precursors has been extensively investigated in recent years (**Figure 7**). In comparison to the previous approaches to generate reactive intermediates by excitation of *in situ* generated iron complexes with coordinated substrates, unfunctionalized substrates are also exploitable with this strategy and carbon-centered radicals are accessible simply *via* the abstraction of a hydrogen atom to formally generate hydrogen chloride. Unsurprisingly, this concept of generating catalytic concentrations of $Cl^{\bullet}$ has been adapted to the transformation of several substrates with various photocatalysts in recent years.[179, 181, 182] The interception of the generated carbon-centered radical is either investigated with Michael acceptors (**Figure 7)** or with other functional groups (**Figure 8**).

The first examples of an iron photocatalyst used for the functionalization of sp^3-hybridized carbon centers, including non-activated carbon-hydrogen bonds, were investigated by the group of Rovis (**Figure 7a-b**). The main class of substrates involved C–H bonds distal from electron withdrawing functional groups like ketones, cyanides or acyl chlorides.[183] The corresponding carbon-centered radical intermediate generated upon HAT from the photo-generated chlorine radicals was trapped by various electrophiles with electron-deficient double bonds (**Figure 7a**). With substoichiometric concentrations of $FeCl_3$ (25 mol%), moderate yields of alkylated products were obtained after 36 h of irradiation with a purple LED. The reaction conditions were especially investigated for substrate bearing *tert*-butyl groups next to the electron-withdrawing moiety (**Figure 7b**).[184] With these substrates, light-driven alkylation reactions were also possible under LED irradiation, but product distribution was shown to depend on reaction conditions. At room temperature, a trapping of the carbon-centered radical by an electron-deficient alkene is competing with an intramolecular rearrangement with most electrophiles. With increased temperature and lowered concentration of substrate, the rearranged product that was formed *via* a 1,2-migration from the primary radical to a tertiary radical intermediate prior to the trapping with the electrophile, is dominantly observed. These

two factors (concentration and temperature) allowed to control the regioisomeric ratio, while the exact distributions are very different depending on the trapping reagent.

Focusing on linear or cyclic aliphatic alkanes, Duan and co-workers explored carbon-carbon bond formations with electron-deficient alkenes and the formation of carbon-nitrogen bonds with azodicarboxylates as trapping reagents (**Figure 7c**).[185] In this case, the investigated unfunctionalized alkanes or (hetero)cyclic substrates are structurally unable to rearrange and selectivity with substrates bearing primary, secondary and tertiary carbon-hydrogen bonds mostly depends on the stability of the generated radical and the amount of corresponding hydrogen atoms. While some differences in the substrates' choice for the scope of Michael acceptors and alkanes were evident, the most interesting change compared to the work of the group of Rovis was the lowered catalyst loading to only 1 mol% for activated acceptors like electron-deficient diazenes or benzylidenemalonitriles, which led to the desired products in good to excellent yields. Specifically, the nature of the Michael acceptor seemed important here, as increased catalyst loadings of 10-20 mol% were needed with less activated acceptors like acrylate-based trapping reagents.

In 2022, a C–H functionalization with gaseous alkanes for methylation, ethylation, propylation and butylation of electron-deficient alkenes with good yields under UV light irradiation was published (**Figure 7d**).[186] Mechanistic analysis revealed a positive impact of increased $FeCl_3$ catalyst loading and a linear relationship between the gas pressure and the product formation at the beginning of the reaction. Theoretical calculations of the UV-vis absorption spectra were used to conclude that an octahedral iron complex with three coordinated acetonitrile and three coordinated chlorides was the actual photoactive species that release a $Cl^{\bullet}$ upon excitation.[186]

Next to the direct C–H bond activation from a $Cl^{\bullet}$, alcoholic substrates were also considered for this step, especially for a remote C–H activation reactivity.[132, 187] $FeCl_3$ and tetra-*n*-butylammonium bromide or chloride as additional ligand were successfully used for a photoinduced amination of unactivated carbon-hydrogen bonds of aliphatic alcohols. Similar concepts were previously investigated with other photocatalysts,[164, 188-190] and in the present case, trapping with diazenes enabled the functionalization of δ-C(sp^3)–H to the alcoholic group in an overall redox-neutral reaction (**Figure 7e**).[191] The group of Zhang illustrated that different functional groups were tolerated next to the newly formed carbon-nitrogen bond and different diazenes were tested as trapping reagents with good to moderate yields. In analogy to the literature, a 1,5-HAT from an alkoxy radical to selectively activate the desired bond is proposed as key step for the remote functionalization approach. As mechanistic

pathways for substrate activation, a LMCT excitation with alkoxides or chlorides as ligands was proposed to directly or indirectly generate the proposed alkoxy radical. In a thematically related study (**Figure 7f**),[187] the group of Hu investigated various substrates including primary, secondary and tertiary alcohols. Slightly decreased product formation was found for secondary and tertiary alcohols in comparison to primary alcohols, likely due to the steric hindrance for 1,5-HAT activation as well as through a potential competition from carbon bond cleavage *via* β-scission from the alkoxy radical intermediate. Interestingly, late-stage functionalization of structurally complex substrates like a dihydroartemisinic acid derivative were also possible using this protocol with reasonable selectivity and 61% product yield (**Figure 7f**).

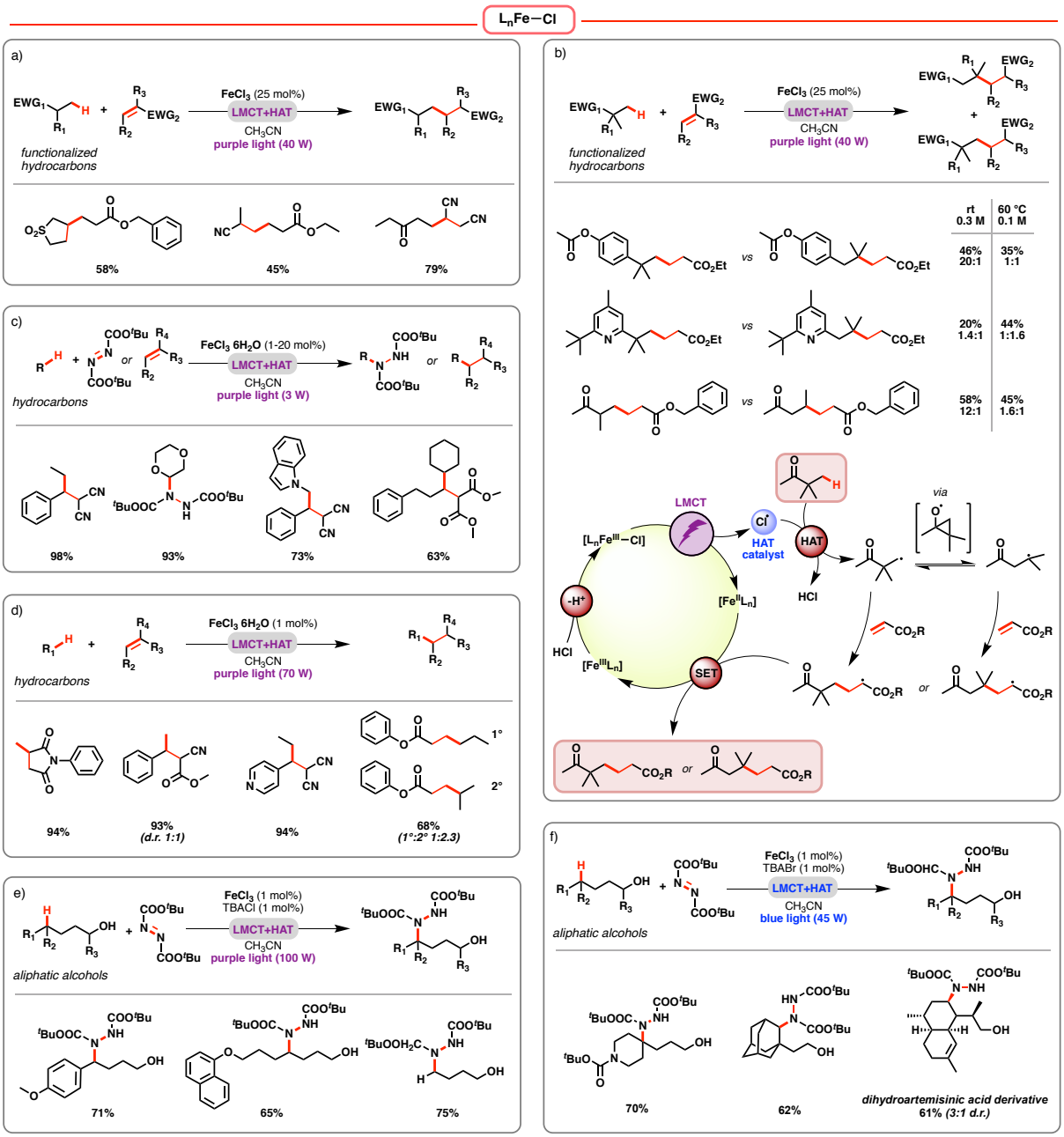


Figure 7. Transformations using ligand-to-metal charge-transfer activation of coordinated chloride with Fe^{III} precursors for substrate activation *via* hydrogen atom transfer. The focus is placed on the activation of hydrocarbons especially and subsequent trapping with Michael acceptors and electron-deficient diazenes for carbon-carbon and carbon-nitrogen bond formation respectively. [183-187, 191-196] TBACl = tetra-*n*-butylammonium chloride. TBABr = tetra-*n*-butylammonium bromide.

The examples in **Figure 7** focused on the formation of carbon-carbon and carbon-nitrogen bonds *via* the interception of a carbon-centered radical, itself generated *via* HAT using Cl•, with electron-deficient Michael acceptors and diazenes, like the commonly used Boc-protected diazene. Several other functional groups have also been successfully introduced by intercepting carbon-centered radicals with other reagents (**Figure 8**) and these examples are discussed hereafter.

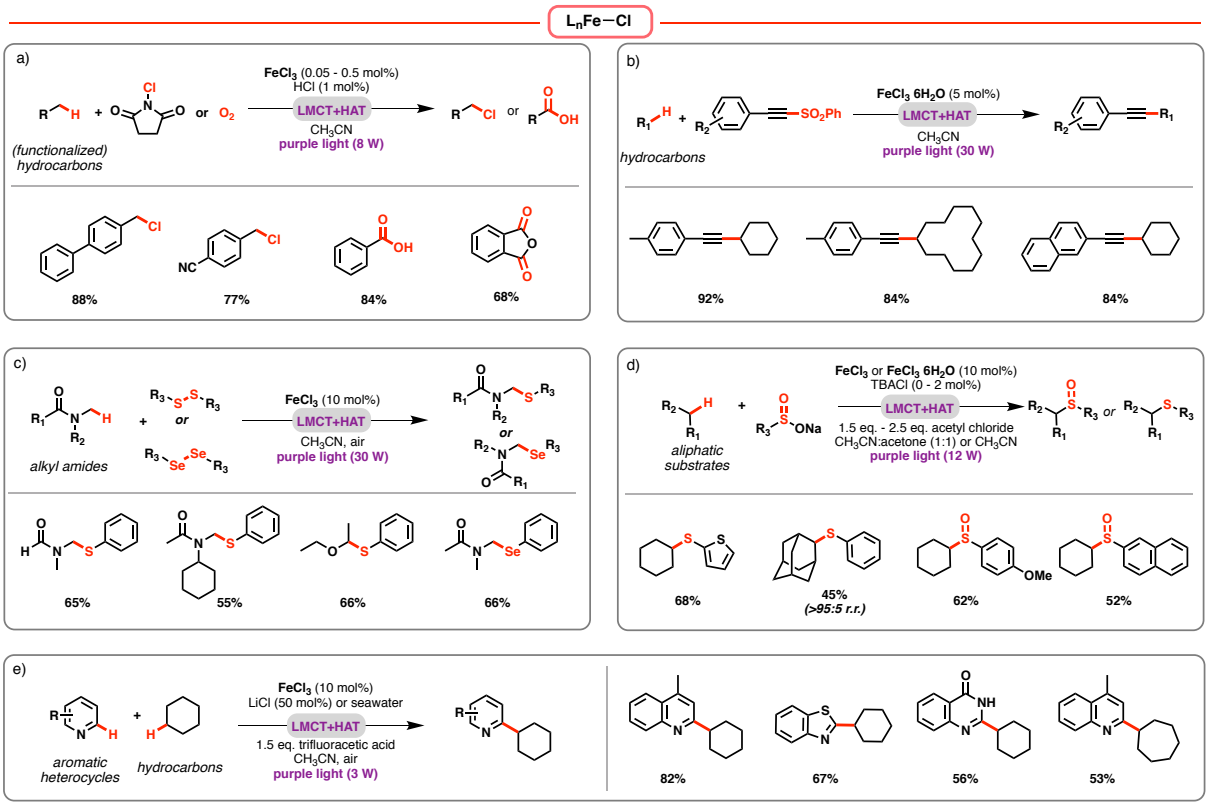


Figure 8. Transformations using ligand-to-metal charge-transfer activation of coordinated chloride with Fe^{III} precursors for substrate activation *via* hydrogen atom transfer. The focus is here on the introduction of new functional groups apart from Michael acceptors and electron-deficient diazenes. [183-186, 191-196] TBACl = tetra-*n*-butylammonium chloride.

In their work with different aliphatic and benzylic substrates for a HAT reactivity initiated by $FeCl_3$ as catalyst precursor, Gong and coworkers investigated the introduction of different functional groups using reactants different from electron-deficient double bonds to react with the radical intermediate (**Figure 8a**).[192] In this case, the extensive substrate scope for trapping the aliphatic and benzylic alkanes by electrophiles like 2-benzylidenemalononitrile was complemented with several examples for chlorinations (using *N*-chlorosuccinimide) or aerobic oxidations (using oxygen). Overall, good to excellent yields were achieved in this light-driven photocatalysis using low catalyst loadings (0.05-0.5 mol%) in the presence of additional hydrogen chloride (1 mol%) and in most cases large excess of aliphatic substrates. Screening of the reaction conditions for the aliphatic C–H activation revealed that the absence of hydrogen chloride or the addition of water resulted in a decreased product formation. UV-vis titration measurements and comparison to a reference suggested that $[FeCl_4]^-$ was the actual photoactive iron complex. Detailed mechanistic analysis including deuteration and radical trapping experiments were performed to propose a catalytic cycle involving a photoactive iron tetrachloride intermediate, HAT substrate activation by $Cl^{\bullet}$ and single electron transfer to the Fe^{II} catalyst after radical addition of the substrate to the trapping reagent. Interestingly, with

prolonged reaction times and an even lower catalyst loading of 0.01% $FeCl_3$, turnover numbers of 9900 with respect to the iron salt for the light-driven C–H functionalization were determined using 390 nm irradiation.

Expanding the achievable transformations of HAT catalysis with iron catalysts, a direct alkynylation of different alkanes with arylethynyl phenyl sulfones using $FeCl_3$ as catalyst has been investigated with $Cl^{\bullet}$ initiated C–H functionalization (**Figure 8b**).[193] Good to excellent yields were reported for linear and branched cyclic and acyclic alkanes with different chain lengths and the functional group tolerance was shown with a series of substituents on the aryl alkyne that included halides, methoxy, or esters groups. As most mechanisms in this section, the proposed pathway includes a HAT activation of the alkane with the chlorine radical formed upon excitation of the iron halide photocatalyst. A radical addition of the carbon-centered radical on the triple bond and subsequent elimination of a phenyl sulfonyl radical was suggested for product formation. The Fe^{III} chloride precursor was then regenerated through subsequent single-electron transfer to the phenyl sulfonyl radical, forming the corresponding sulfinate anion as by-product, and chloride addition. This reaction was also developed in a continuous-flow setup, which facilitates the reaction upscaling up to several hundreds of milligram.

In addition to the purely aliphatic or benzylic substrates used for the C–H bond activation *via* hydrogen atom transfer (**Figure 7c-f**), other classes of substrates with accessible hydrogen atoms were also targeted. For example, a light-driven functionalization of amides, sulfonamides, and carbamates as well as aliphatic ethers was reported using $FeCl_3$ as photocatalyst (**Figure 8c**).[194] In the presence of disulfides with 10 mol% catalyst loading, a thiolation of amides to access amido-*N,S*-acetals was developed with moderate yields under aerobic conditions. Apart from the unchanged steps of $Cl^{\bullet}$ formation and HAT catalyst activation, the thiyl radical generated from the disulfide was proposed as reactive intermediate to regenerate the iron photocatalyst.

In a very recent paper, Guo, Xia and coworkers reported the undirected C(sp^3)–H borylation, thiolation and sulfinylation of simple hydrocarbons with $FeCl_3$ using purple irradiation (**Figure 8d**)[196] The reaction exhibited broad functional group tolerance, with over 150 examples reported. In particular, the borylation reaction was applicable to alkanes, silanes, ketones, esters and amides resulting in moderate to good yields with 20 mol% of iron catalyst and 1 equivalent of *N*-fluorobenzensulfonimide as oxidant. The reaction was shown to proceed with an unconventional regioselectivity for the distal methyl position. Interestingly, silanes were also suitable substrate for the borylation reaction. Thiolation and sulfinylation were both realized with sodium sulfinate salt as sulfur source in the presence of 1.5 equivalents of acetyl

chloride for the activation of the sulfinate providing the desired products in moderate to good yields. While the overall conditions were quite similar for these two types of reactions, control experiments revealed that the presence of water for the thiolation or anhydrous conditions for sulfinylation were of key importance. The initial activation of sulfinate with acetyl chloride was detected as decisive step between these two transformations. The general mechanism was studied through a series of control experiments. Kinetic isotope experiments gave ratios of 1 for the borylation, thiolation and sulfinylation reactions. This indicated that the hydrogen atom transfer process was not rate-determining. It was proposed that LMCT excitation led to the release of $Cl^{\bullet}$ and the formation of the corresponding Fe^{II} center. The chlorine radical could then perform hydrogen atom abstraction with the desired substrate to generate the corresponding radical that could engage in the subsequent borylation, thiolation or sulfinylation reaction. Interestingly, for the thiolation and sulfination, control experiments with acetic anhydride and additional sodium chloride highlighted the importance of acetyl chloride, which was suggested as a Cl source in this specific case.

The formation of $Cl^{\bullet}$ for C–H activation with an LMCT excitation of an iron chloride catalyst was also considered as a key step for a HAT abstraction from cyclic and acyclic aliphatic alkanes for a Minisci-type reaction with protonated quinolones and benzothiazoles as trapping reagents (**Figure 8e**).[195] Overall moderate yields were obtained when the reaction was performed with various substitutions on the heteroaromatic structure and different ring sizes. Interestingly, experiments were also performed with seawater and similar yields as with 50 mol% lithium chloride as additive were reported. In comparison to the decarboxylative approach for similar transformations discussed earlier (**Figure 5b**),[143] where the LMCT directly guides the selectivity based on the position of the carboxylate, in this case the hydrogen atom transfer step from the substrate by the chlorine radical is determining the selectivity.[197, 198] Mechanistically, a pronounced isotope effect for the homocleavage of the aliphatic carbon-hydrogen bond indicated that this step was rate-determining and the measured reaction quantum yield of about 24% implied no significant contribution from radical chain processes.

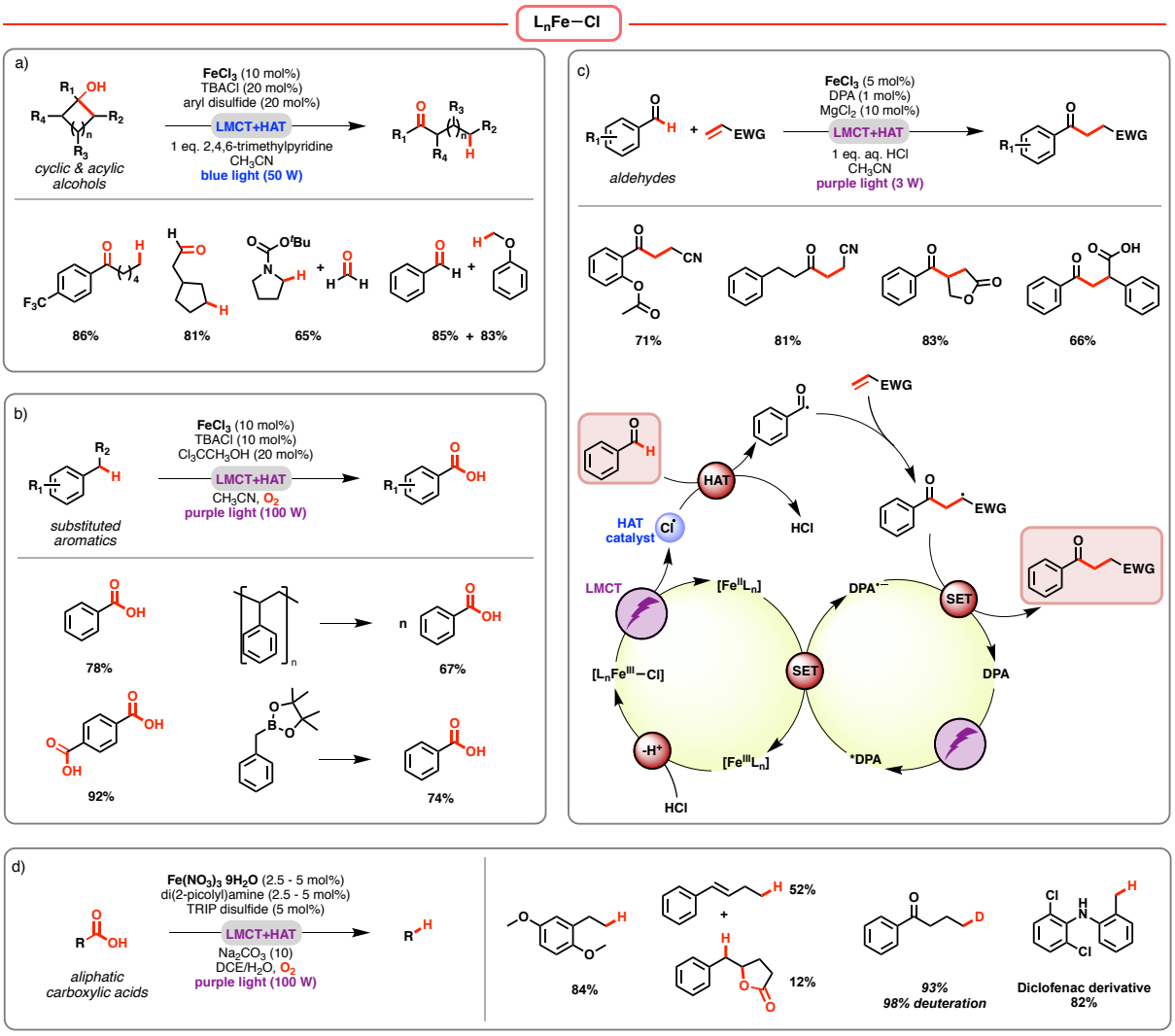


Figure 9. Transformations using ligand-to-metal charge-transfer activation of coordinated chloride with Fe^{III} precursors for substrate activation *via* hydrogen atom transfer in combination with a cocatalyst.[199-204] TBACl = tetra-*n*-butylammonium chloride, DPA = 9,10-diphenylanthracene. TRIP disulfide = 2,4,6-tri-isopropyldisulfide.

In the examples discussed up to now for light-induced iron-based HAT catalysis, the catalytic system typically consisted of Fe^{III} chloride as (pre)catalyst and in some cases additional chloride ions as ligands were added (**Figure 7-8**). In addition to these comparably simple systems, more complex and sophisticated systems consisting of catalyst combinations of Fe^{III} salts together with a cocatalyst have been investigated in recent years (**Figure 9**).

A first example from 2021 involved the ring opening of cyclic alcohols to obtain aliphatic ketones (**Figure 9a**).[199] Different ring sizes of secondary and tertiary alcohols were investigated and examples with primary alcohols to synthesize the corresponding aldehyde were presented. Good yields were reported in most cases for a catalyst combination of Fe^{III} chloride (10 mol%), *tetra-n*-butylammonium chloride (20 mol%) and aryl disulfide (20 mol%).

The proposed mechanism involved two hydrogen atom transfer steps. After photoexcitation of Fe^{III} chloride, a hydrogen atom transfer from the alcohol to the chlorine radical was proposed, followed by β-scission to form a carbon-centered radical and a ketone or aldehyde. A second HAT from aryl sulfide was proposed to yield the final product and the thiyl radical, which in turn regenerated the iron catalyst.

As abundant and inexpensive catalysts, iron salts are also very attractive for light-driven degradation of waste or pollutants. In 2021, $FeCl_3$ in combination with 2,2,2-trichloroethanol as cocatalyst and additional *tetra-n*-butylammonium chloride was explored as catalytic system for the degradation of polystyrene (**Figure 9b**).[200] The study was centered on model reactions such as the light-driven conversion of alkylated aromatics to benzoic acids under an oxygen atmosphere. Primary and secondary benzylic groups or ethers as well as tertiary alkenyls or alkynyls resulted in the formation of the corresponding benzoic acid and in the latter cases the corresponding substituent was cleaved off. In addition, degradation of polystyrene under air or oxygen atmosphere was possible with 54% yield of benzoic acid after several days of irradiation with a near-UV LED. The 2,2,2-trichloroethanol cocatalyst was not necessary for the reaction to proceed, but its addition increased the reaction yields. It was proposed that this could offer an additional way to generate alkoxy radicals that could then perform hydrogen atom abstraction in a similar fashion as chlorine radicals. Similar investigations without cocatalyst and more focus on polystyrene degradation have been published in recent years.[205, 206]

Lately, the group of Reiser presented a dual photocatalytic approach using HAT catalysis initiated by $FeCl_3$ in combination with 9,10-diphenylanthracene (DPA) as second photocatalyst. In this case, hydrogen atom transfer from aldehydes was explored for a hydroacylation of alkenes *via* the formation of acyl radicals and subsequent trapping with alkenes (**Figure 9c**).[201] Good and in some cases excellent yields were achievable with various aldehydes and alkenes. Similar to earlier work from the group of Zuo with cerium photocatalysts,[165] after photoinduced substrate activation and trapping with an intermediate, an interplay between the two photoactive catalysts is proposed to facilitate the catalyst recovery from the Fe^{II} intermediate in a photoinduced electron transfer cascade *via* reductive quenching of DPA (**Figure 9c**). Electron transfer from the DPA radical anion to the alkyl radical intermediate generates the final ketone product and closes the catalytic cycle. The approach of combining two photocatalysts was crucial for an effective product formation as the presence the DPA increased the yield from 30% to 94% and similar concepts might become more important in the future to expand the scope of applications with iron photocatalysts.

Very recently Lu and West reported a light-driven decarboxylative protonation and deuteration method using an iron catalyst in combination with a disulfide cocatalyst (**Figure 9d**).[207] Iron nitrate in combination with a di(2-picolyl)amine ligand in the presence of a base enabled the chemoselective decarboxylation under UV light irradiation with a 390 nm LED, while the HAT cocatalyst closed the catalytic cycle and introduced the hydrogen atom to release the final product. This reactivity was explored for different aliphatic carboxylic acids including late-stage modification of drugs and complex natural products with good to excellent yields (**Figure 9d**).[207] In contrast to the decarboxylative outer-sphere oxidation *via* electron transfer with highly oxidizing catalysts - for example acridinium salts - the substrate coordination for inner-sphere electron transfer with first row-transition metal complexes like iron allowed for the chemoselective activation of the carboxylate in the presence of other potentially oxidizable groups like electron-rich arenes, olefins or amines. This concepts elegantly illustrates the potential advantages of *in situ* generated photoactive substrate-catalyst complexes in comparison to well-defined catalysts relying on outer-sphere mechanisms, and this conceptual idea will likely obtain further attention in the future.[96, 103, 141]

2.4) Miscellaneous

Next to the plethora of reports for the *in situ* generation of different photoactive complexes with coordinated carboxylates (section 2.1), alkoxides (section 2.2) and chlorides (section 2.3) there are also several examples where different approaches are followed that do not perfectly fit within these abovementioned categories. This includes examples of different coordinated substrates like nitrogen-containing reactants, combinations of light-driven iron catalysis with transition metal cross-coupling approaches (**Figure 10**) and reports where an excited state electron transfer from iron salts is suggested (**Figure 11**).

In 2021, the groups of Yamamoto and Bao presented light-driven nitrene transfer reactions with dioxazolones using Fe^{III} precursors (**Figure 10a**).[202] In their very extensive study, over one hundred reactions were investigated, among which the intermolecular amidation of 1,3-dicarbonyl compounds and diphenylmethane substrates as well as the imidization of sulfoxides, sulfides and phosphines. Iron bromide or chloride was used as precatalyst under blue light irradiation, which led to good to excellent yields for the different transformations. The first mechanistic step involved the formation of a photoactive iron catalyst through the coordination of the dioxazolone to the iron center. This was proposed based on UV-vis absorption experiments while further mechanistic steps were suggested based on computational studies. The proposed key step was the intersystem crossing from sextet excited

state to the quartet excited state, which facilitated the stepwise extrusion of carbon dioxide to form a radical acylnitrene iron intermediate (**Figure 10a**). This radical was then engaged in the subsequent amidations and imidizations reactions.

The formation of a photoactive nitrogen-binding iron complex was also proposed as a key prerequisite for the light-driven 1,2-diazidation of alkenes using trimethylsilyl azide and LMCT activation of iron complexes that was recently investigated independently by two groups (**Figure 10b-c**).[208, 209] In both studies, good yields were accessible with styrene and unactivated alkenes using blue light irradiation and, based on control experiments, the photo-induced generation of an azide radical was proposed as key mechanistic step in both studies. After radical addition of one azide to the alkene, the carbon-centered radical was intercepted by a second equivalent of iron azide to finally release the 1,2-diazidation products. In line with this proposed mechanism and other literature reports for (non-irradiated) iron-based azidation of alkenes,[210-212] no hints for carbocation formation were observed with suitable model compounds to trap this possible ionic intermediate. Overall, this reaction sequence allowed the introduction of two azides in one synthetic step and diversification for example to free 1,2-diamines seems easily possible.[213] Interestingly, Shi and coworkers found that copper as well as other salts based on earth-abundant metals like manganese or cobalt were unsuccessful as metal to form photoactive reagents for this light-driven reaction and iron nitrate was identified as ideal photosensitizer. In contrast to other light-driven and thermal approaches with metal complexes that operate with catalytic amounts of catalyst,[214-216] the transformations here used stoichiometric amounts of iron nitrate (1.0 or 1.2 equivalents). This also circumvents the need for additional chemical oxidants. Looking at the main differences between both studies, West and coworkers additionally included the diazidation of drugs and natural product-derived substrates with moderate to good yields (**Figure 10b**).[209] Furthermore, selected examples were examined for a synthesis with continuous flow photoreactors.

The light-driven formation of carbon-nitrogen bonds was recently reported to proceed *via* an electrophilic amidation using *N*-methoxyamides and arylboronic acids in concert with Fe^{II} salts (**Figure 10c**).[203] In this report from 2022, moderate to good yields with various substituents on the (hetero)aryl *N*-methoxyamides derivative as well as on the arylboronic acid side were obtained under blue light irradiation. Surprisingly, in contrast to all proposed mechanisms described in this section where Fe^{III} halides were considered as photoactive complex or precatalyst for LMCT activation, the present report proposed a MLCT excitation from the Fe^{II} intermediate. This would generate an Fe^{III} center that could then undergo transmetalation with the boronic acid followed by a radical attack from the nitrogen centered

radical. Electron transfer from the radical intermediate to the Fe^{III} is expected to close the catalytic cycle and release the product. This reaction would benefit from additional investigations to elucidate the mechanism using time-resolved techniques and reaction quantum yield determination as propagation or different parallel pathways occurring at once cannot be ruled out based on the provided on/off experiments.

The desire to replace rare and precious transition metals is not only present in the field of photoredox catalysis but is also gaining momentum in the field of cross-coupling reactions where research endeavors are centered on substituting palladium for first row transition metals. Several transformations have already been studied in that regard.[217-219] In the last years, the merging of photocatalysis with transition metal catalysis, so called metallaphotoredox catalysis, received considerable attention.[124] While copper and nickel are well-studied for cross-coupling transformations with assisting photocatalysts present, iron has not received much attention up to now.[220-222]

In 2019, the group of Noël investigated an iron-catalyzed Kumada-Corriu coupling under blue light irradiation in continuous flow (**Figure 10d**).[204] Different aryl chlorides and heteroaryl chlorides were successfully coupled to aliphatic Grignard reagents with good to excellent yields. Interestingly, depending on the substrate, some product formation was also observed without irradiation, indicating that light most probably facilitated the rate-determining step of the reaction. Time dependent batch reactions revealed a clear beneficial effect from additional irradiation and UV-vis studies pointed towards an acceleration of the oxidative addition step. Overall, this study nicely illustrates that iron catalyst can have a dual role and serve both as cross-coupling catalyst while also exhibiting photoactive properties that potentially allowed a photo-activated step to accelerate the transformations.

Moving away from iron as cross-coupling catalyst, examples combining iron photoredox catalysis with other transition-metal complexes have recently been published (**Figure 10e-f**). Under irradiation with near-UV light, decarboxylative aminations, olefinations and alkylations of aliphatic acids were successfully performed using a combination of Fe^{III} and Cu^{II} catalysts in the presence of substoichiometric amounts of base and, when needed, di-*tert*-butyl peroxide as terminal oxidant for net oxidative transformations.[223] The extensive substrate scope revealed good to moderate yields for different substitution patterns on the substrate as well as on the respective trapping reagents. The proposed mechanism (**Figure 10e**) involved a light-induced decarboxylation followed by trapping of the radical intermediate by the copper complex bearing a coordinated amine substrate and reductive elimination for the formation of a carbon-nitrogen bond.[224]

Following a similar mechanistic idea, the combination of an iron photocatalyst with a cobalt cocatalyst ([Co(dmgH)$_2$(4-CN-Py)Cl], dmgH$_2$ = dimethylglyoxime, 4-CN-py = 4-cyano-pyridine) was investigated for the decarboxylative styrene formation under irradiation with purple light (**Figure 10f**).[225] In the presence of catalytic amounts of base, good to moderate yields of alkenes were reported with different cyclic aliphatic substrates. Interestingly, in the absence of cocatalyst under aerobic conditions, the formation of a ketone and an aldehyde upon ring-opening of tertiary cycloalkane carboxylic acids was possible with the same iron catalyst and stoichiometric amounts of base. In contrast to many other systems relying on earth-abundant transition metals in combination with photocatalysts based on precious metal complexes,[124] the use of iron photocatalysts or other earth-abundant catalysts for metallaphotoredox catalysis seems very attractive and will likely receive more attention in the future.

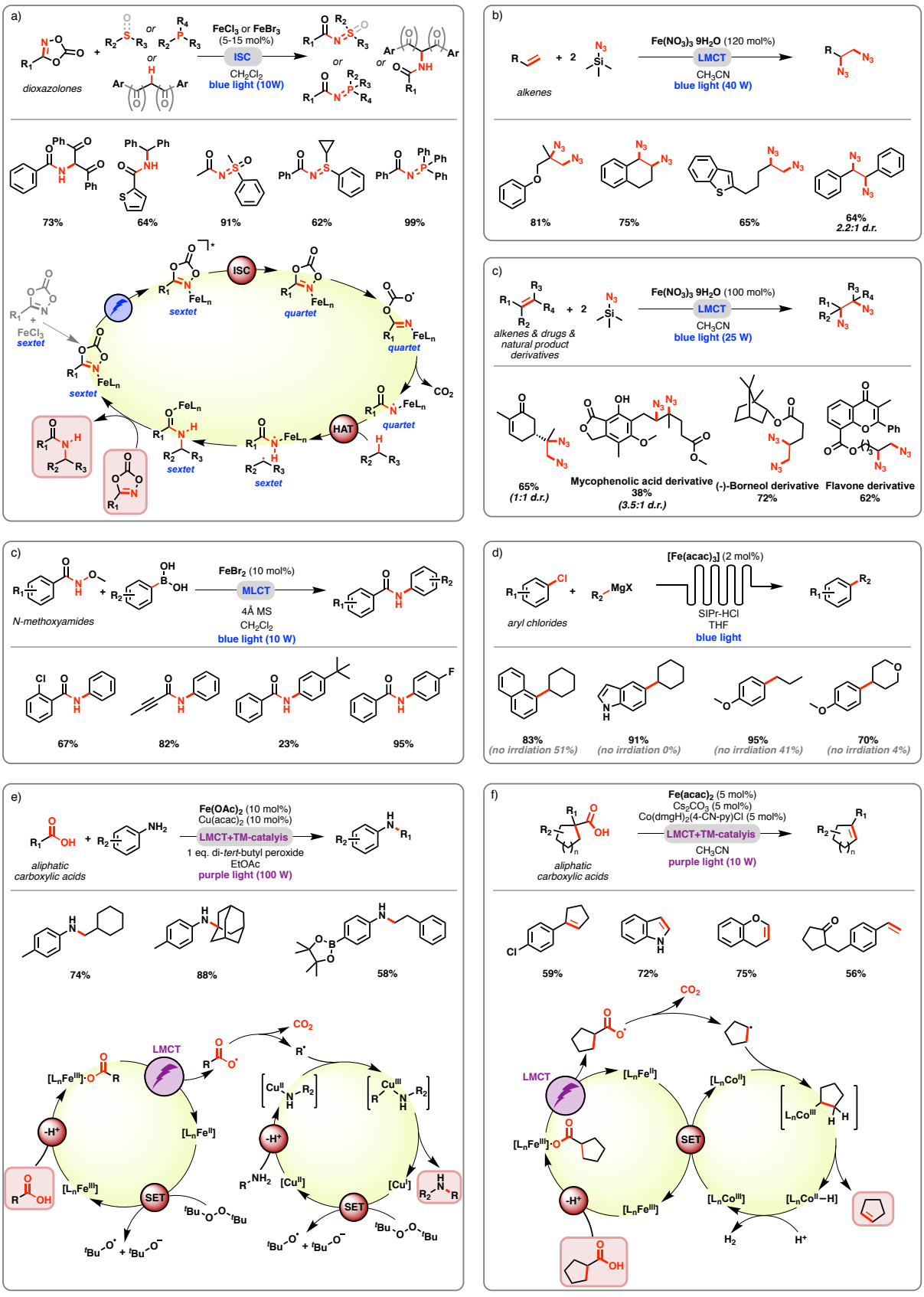

a)
dioxazolones
FeCl3 or FeBr3
(5-15 mol%)
ISC
CH2Cl2
blue light (10W)
73%
64%
91%
62%
99%
sextet
quartet
ISC
HAT
CO2
b)
alkenes
Fe(NO3)3 9H2O (120 mol%)
LMCT
CH3CN
blue light (40 W)
81%
75%
65%
64%
2.2:1 d.r.
c)
alkenes & drugs & natural product derivatives
Fe(NO3)3 9H2O (100 mol%)
LMCT
CH3CN
blue light (25 W)
65%
(1:1 d.r.)
Mycophenolic acid derivative
38%
(3.5:1 d.r.)
(-)-Borneol derivative
72%
Flavone derivative
62%
c)
N-methoxyamides
FeBr2 (10 mol%)
MLCT
4Å MS
CH2Cl2
blue light (10 W)
67%
82%
23%
95%
d)
aryl chlorides
[Fe(acac)3] (2 mol%)
SIPr-HCl
THF
blue light
83%
(no irrdiation 51%)
91%
(no irrdiation 0%)
95%
(no irrdiation 41%)
70%
(no irrdiation 4%)
e)
aliphatic carboxylic acids
Fe(OAc)2 (10 mol%)
Cu(acac)2 (10 mol%)
LMCT+TM-catalysis
1 eq. di-tert-butyl peroxide
EtOAc
purple light (100 W)
74%
88%
58%
LMCT
SET
f)
aliphatic carboxylic acids
Fe(acac)2 (5 mol%)
Cs2CO3 (5 mol%)
Co(dmgH)2(4-CN-py)Cl (5 mol%)
LMCT+TM-catalysis
CH3CN
purple light (10 W)
59%
72%
75%
56%
LMCT
SET

Figure 10. Transformations using ligand-to-metal charge-transfer activation of Fe^{III} catalysts for specific examples with nitrogen-containing substrates as ligands as well as systems for metallaphotoredox catalysis with carboxylic acids.[208, 223, 225-228] SIPr-HCl = 3-bis(2,6-diisopropylphenyl)-imidazolinium chloride, acac = acetylacetone, dmgH = dimethylglyoxime, 4-CN-py = 4-cyanopyridine. ISC = intersystem crossing. MS = Molecular sieves.

A relatively early example of the light-driven catalysis with iron photocatalysts, when put in perspective to the currently fast increasing amount of reports in the last years, is the oxidative methylation of arylacrylamides (**Figure 11a**).[126] Dimethylsulfoxide (DMSO) simultaneously serves as solvent and methyl donor for the synthesis of oxindoles, while 3 equivalents of hydrogen peroxide are added as sacrificial oxidant. Good yields are found with various substituents on the aryl ring and some substitutions on the amide nitrogen were also tolerated. Scavenging experiments with TEMPO indicated the presence of methyl radicals in solution and deuteration experiments with DMSO-d_6 confirmed that the methyl group was transferred from the solvent. Overall, a hydrogen peroxide degradation by oxidation of Fe^{II} and formation of the hydroxy radical is suggested, which initiates a radical cascade with the solvent and radical attack of a methyl radical is expected to lead to the formation of two new carbon-carbon bonds. Photo-initiated electron transfer hydroperoxyl radical formation from Fe^{III} is suggested to close the catalytic cycle and lead to the formation of the final product. This light-driven enhancement for the hydrogen peroxide degradation - that is proposed to enable this reaction - is sometimes also described as a photo-Fenton process.[229-233]

Earlier in this review, the extensive studies on HAT catalysis using photoactive iron halides as catalyst were discussed (section 2.3). In contrast to this very broadly investigated reactivity of halogen radicals, a radical attack and/or overall aliphatic halogenation is not often reported with light-driven iron catalysis. In 2020, the group of Zhu utilized Fe^{III} halides as photocatalysts for the light-driven synthesis of α-bromo- and α-chloroketones from styrenes (**Figure 11b**).[234] Moderate to good yields were reported using potassium halides in stochiometric conditions in the presence of molecular oxygen. In general, chlorinations often performed with smaller yields compared to analogous bromination reactions. Mechanistically, it was proposed that, after light-induced iron-halide bond cleavage, a radical attack of the halogen atom on the styrene took place and that molecular oxygen served as terminal oxidant to generate the desired α-halogenated ketones.

In comparison to the processes with well-defined iron-based photocatalysts, excited-state electron transfer is hardly considered for iron halide and iron halide anion catalysts, presumably due to the very short excited state lifetimes and competition with the very fast ligand bond dissociation.[100] Nevertheless, several publications suggest a sequence of electron transfer steps with less defined iron catalysts.

Inspired by the reactivity of iron-sulfur proteins in Nature, Yu and coworkers investigated a thiocarboxylation of styrenes and acrylates with CO_2 (**Figure 11c**).[235] A three-component system consisting of styrene, thiophenol and carbon dioxide together with iron chloride and a base allowed the formation of the desired products with, in most cases, good to excellent yields under blue light irradiation. Different electron-withdrawing and electron-donating substituents were tolerated on the aryl rings of the arylthiol as well as on the styrene. The mechanism was not analyzed in detail, but the deprotonation of the thiol was found to be important to presumably form an iron sulfur complex as photoredox catalyst and/or electron transfer intermediate. The reduction step for CO_2 to generate the carbon dioxide radical anion was suggested by excited-state quenching from the Fe/S complex.

In 2020, another three-component system was investigated in a light-driven aminoselenation of alkenes with iron bromide as catalyst (**Figure 11e**).[228] The substrate scope for substituted styrenes, anilines and aryl diselenides derivatives was investigated with good to moderate yields. Interestingly, the functional group tolerance on the aniline was greater than for the other two components. An iron center with a coordinated aniline substrate was proposed as photoactive catalyst for this three-component coupling reaction. Reductive quenching of the excited catalyst by the diselenide was proposed to initiate the addition from the selenyl radical or the selenyl cation to the alkene. Introduction of the aniline was proposed for the formation of the final product. It should be mentioned that, although very interesting, this transformation would warrant additional mechanistic information. Indeed, whereas the reaction used blue LED (440-480 nm) to initiate the reaction, the emission quenching experiments were performed monitoring the emission at 332 nm, which cannot be attributed to the presumed *in situ* generated photoactive catalyst. Mechanistic insights might be challenging to obtain with such multi-component systems and *in situ* catalyst formation, but a clearer picture of the actual roles of the different components would be highly desirable to expand the scope of these transformations.

Under aerobic conditions, photo-oxygenations of styrene-based vinyl halides have been reported already in 2018 for the formation of α-halogenated acetophenones (**Figure 11d**).[227] Different alkyl chains and substitutions of the aromatic ring were examined with iron halide anionic catalysts under blue light irradiation. In addition, selective benzylic oxygenations of arylated alkanes were shown with the same catalytic system with good yields.

Degradation of polystyrene has been discussed earlier (**Figure 9b**), but the formation of polymeric structures was also rendered possible *via* light-driven initiation with an iron catalyst (**Figure 11f**).[226] Analysis of different iron halides, additional halide ions as ligands and

initiators with different halides indicated an improved polymerization process for polymethylacrylate formation with bromide compared to chloride-based systems. In related studies, polymerizations of alkylated or semifluorinated methylacrylates were achieved with similar iron-ligand combinations.[236, 237] Interestingly, iron concentrations going down to 100 ppm with respect to the monomer were used and the absence of additional halide ligands resulted in decreased conversion of the monomers. Electrochemical and spectroscopic analyses were presented to enhance the understanding of the differences between the iron-based initiators. A lower dispersity of the resulting polymer was rationalized by the faster deactivation with $FeBr_3$ precursors and consequently better control over the polymerization process. Similar to LMCT excitation strategies discussed in the previous sections (section 2.3), a light-induced generation of halogen radicals from iron halides was proposed for these transformations. Notably, a photoinitiation mechanism including electron transfer has been discussed in earlier reports with Fe^{II} polypyridyl complexes, indicating that the ligand plays an important role on the actual mechanism.[238, 239]

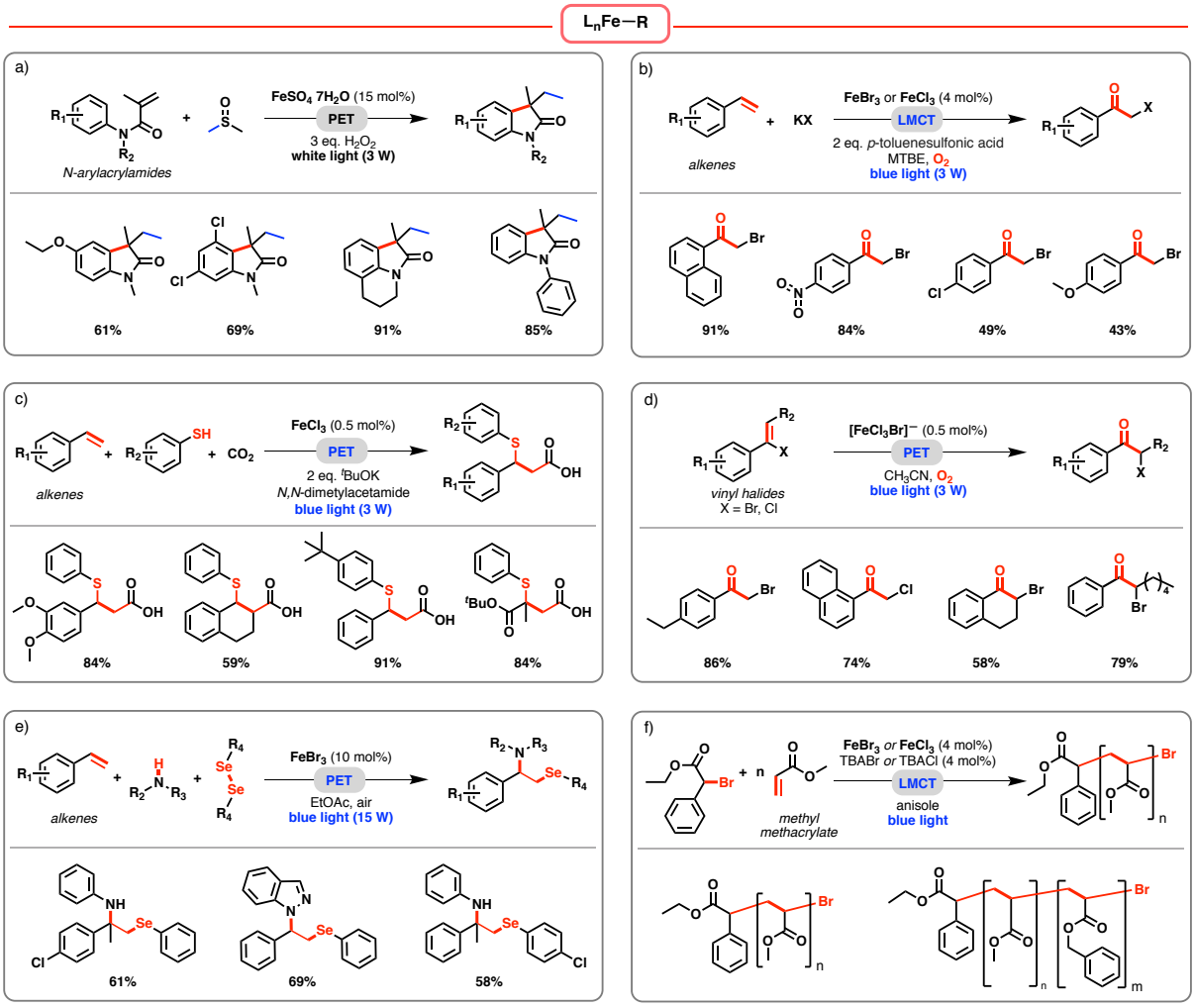


Figure 11. Transformations using photoinduced electron transfer (PET) and ligand-to-metal charge-transfer activation with chloride ligands apart from HAT substrate activation. MTBE = methyl-*tert*-butyl ether, EtOAc = ethyl acetate, TBACl = tetra-*n*-butylammonium chloride, TBABr = tetra-*n*-butylammonium bromide.

Overall, these versatile examples presented herein showcase that *in situ* generated radicals can be explored with iron salts and generally offer broad applicability and functional group tolerance. While the generation of Cl$^{\bullet}$ received the highest attention within the last years (**section 2.3**), the selectivity can limit their applications for challenging structures with very similar C–H bonds present. In this regard, the defined coordination side with carboxylates (**section 2.1**) and alkoxides (**section 2.2**) which generates clearly localized radicals and/or bond cleavages after excitation offers a higher degree of control over the reactivity. Together with the exploration of currently less investigated light-induced reactivities with iron catalysts (e.g. **Figure 10a-d**) and in combination with TM catalysis, these aspects are currently still underexplored and will likely receive more attention in the future.

3) Photoredox catalysis using well defined photosensitizers

The photoredox transformation using the *in situ* formation of iron photosensitizers presented before showed an impressively broad range of achievable transformations. However, these photosensitizers are often structurally less defined which can sometimes limit a detailed mechanistic investigation using spectroscopic tools and limit the tunability. The present section is dedicated to structurally well-defined photosensitizers that have been used for photoredox catalysis applications. A selected series of well-defined iron photosensitizers, not all used for photoredox catalysis applications, alongside their corresponding excited-state lifetime and excited-state nature is presented in **Figure 12**. It is easily visible that different types of excited states (LMCT, MLCT, CT, MC) are accessible with iron photocatalysts depending on the iron oxidation state and the coordinated ligand. The concept, trends and design principles have been summarized in excellent review articles[46, 47, 52, 56, 65, 81-85] and is not further discussed here, while the focus is placed on the application in photoredox catalysis. The reason why many of these photosensitizers were not used in photoredox catalysis stems from their usually extremely short excited-state lifetime within the picosecond or short nanosecond time scale that prevents diffusional reactivity in most cases. Indeed, a photosensitizer with an excited state lifetime of 650 ps would only be able to travel a distance of 18 Å using a diffusion coefficient of $2.5 \cdot 10^{-5}$ $cm^2\,s^{-1}$, whereas a photosensitizer with an excited-state lifetime of 1 µs would travel distances of ~700 Å. Such short excited-state lifetime and travelled distances render the encounter between the excited state and the quencher less probable. Solution to remediate these

limitations often consists in using near molar concentrations of quencher or using prolonged irradiation times.

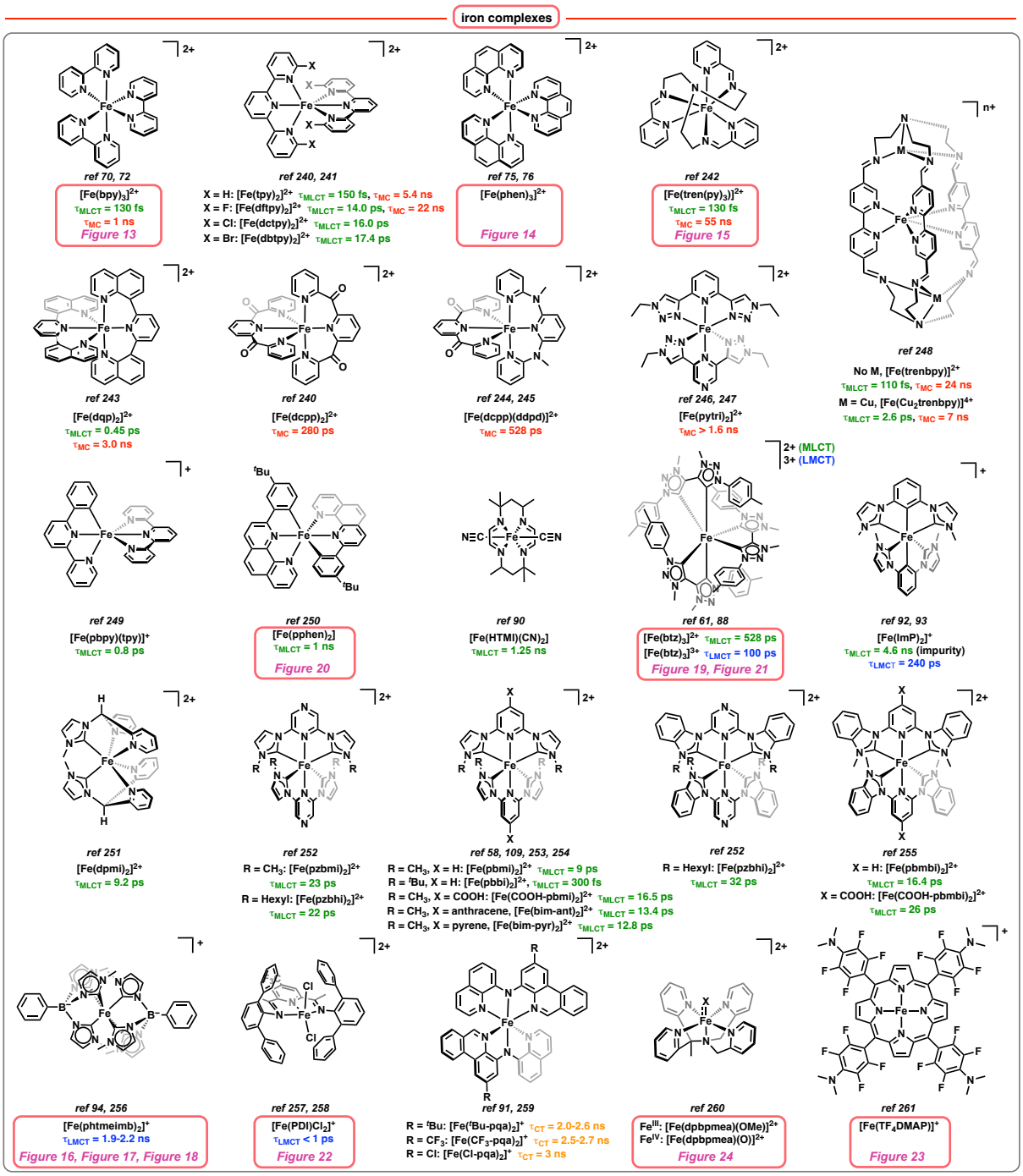


Figure 12. Overview of selected iron complexes and their excited state nature and corresponding lifetimes. Excited states are color-coded (MLCT: green, LMCT: blue, MC: red, CT: orange). Complexes explicitly discussed for their light-induced reactivity are highlighted in red boxes and the corresponding figures covering transformations with these catalysts are indicated. First row: Structure of $[Fe(bpy)_3]^{2+}$ (ref [70, 72]), $[Fe(tpy)_2]^{2+}$ (ref [240]), $[Fe(dftpy)_2]^{2+}$ (ref [241]), $[Fe(dctpy)_2]^{2+}$ (ref [241]), $[Fe(dbtpy)_2]^{2+}$ (ref [241]), $[Fe(phen)_3]^{2+}$ (ref [75, 76]), $[Fe(tren(py)_3)]^{2+}$ (ref [242]), Second row: Structure of $[Fe(dqp)_2]^{2+}$ (ref [243]), $[Fe(dcpp)_2]^{2+}$ (ref [240]), $[Fe(dcpp)(ddpd)]^{2+}$ (ref [244, 245]), $[Fe(pytri)_2]^{2+}$ (ref [246, 247]), $[Fe(trenbpy)]^{2+}$ (ref [248]), $[Fe(Cu_2trenbpy)]^{4+}$ (ref [248]), Third row: Structure of $[Fe(pbpy)(tpy)]^{+}$ (ref [249]), $[Fe(pphen)_2]$ (ref [250]), $[Fe(HTMI)(CN)_2]$ (ref [90]), $[Fe(btz)_3]^{2+}$ (ref [88]), $[Fe(btz)_3]^{3+}$ (ref [61]), $[Fe(ImP)_2]^{+}$ (ref [92] and proof of impurity ref [93]), Fourth row: Structure of $[Fe(dpmi)_2]^{2+}$ (ref [251]), $[Fe(pzbmi)_2]^{2+}$ (ref [252]), $[Fe(pzbhi)_2]^{2+}$ (ref [252]), $[Fe(pbmi)_2]^{2+}$ (ref [58, 253]), $[Fe(pbbi)_2]^{2+}$ (ref [58]), $[Fe(COOH\text{-}pbmi)_2]^{2+}$ (ref [109]), $[Fe(bim\text{-}ant)_2]^{2+}$ (ref [254]), $[Fe(bim\text{-}pyr)_2]^{2+}$ (ref [254]), $[Fe(pzbhi)_2]^{2+}$ (ref [252]), $[Fe(pbmbi)_2]^{2+}$ (ref [255]), $[Fe(COOH\text{-}pbmbi)_2]^{2+}$ (ref [255]), Fifth row: Structure of

[Fe(phtmeimb)$_2$] (ref [94, 256]), [Fe(DPI)Cl$_2$]$^+$ (ref [257, 258]) [Fe(^{t}Bu-pqa)$_2$] (ref [91]), [Fe(CF$_3$-pqa)$_2$] (ref [91]), [Fe(Cl-pqa)$_2$] (ref [259]), [Fe(dpbpmea)(OMe)]$^{2+}$ (ref [260]),[Fe(dpbpmea)(O)]$^{2+}$ (ref [260]), [Fe(TF$_4$DMAP)]$^+$ (ref [261]).

3.1) The case of [Fe(bpy)$_3$]$^{2+}$ and its derivatives

The closest analogue structure from well-known [Ru(bpy)$_3$]$^{2+}$ with the same ligands is the photocatalyst with iron instead of ruthenium. As mentioned in the introduction, there are significant differences in the excited-state deactivation pathways and a very short lifetime for the MLCT excited state is observed with the Fe^{II} catalyst. Nevertheless, Cozzi *et al.* successfully used [Fe(bpy)$_3$]$^{2+}$ as photosensitizer for the enantioselective α-alkylation of aldehydes with α-bromo-malonate derivatives in the presence of an organocatalyst.[262] This reaction was initially reported by Macmillan and coworkers, using [Ru(bpy)$_3$]$^{2+}$ as photosensitizer irradiated by visible light.[38] The utilization of [Fe(bpy)$_3$]$^{2+}$ gave surprisingly high reaction yields and enantioselectivities comparable to those obtained with [Ru(bpy)$_3$]$^{2+}$ (**Figure 13a**). The reaction was performed on various aldehydes and α-bromo-malonate derivatives, showing broad functional group tolerance and this methodology was further expanded to the preparation of enantio-enriched lactones, as depicted in **Figure 13b**.

Classical steady-state photoluminescence quenching experiments could not be performed since [Fe(bpy)$_3$]$^{2+}$ is not luminescent but additional mechanistic investigations were carried out to better understand the reaction pathway. The formation of radical species was initially demonstrated *via* spin trapping experiments with the addition of *N*-*tert*-butyl-α-phenylnitrone, which formed a radical species, confirmed by EPR analysis. The addition of a radical scavenger, i.e. (2,2,6,6-tetramethylpiperidin-1-yl)oxyl (TEMPO), completely inhibited product formation. These results contributed to the hypothesis that the reaction proceeded *via* the [Fe(bpy)$_3$]$^{2+}$ mediated photoinduced radical generation (**Figure 13e**). Light/dark experiments revealed that the reaction progressed faster under irradiation than in the dark, suggesting that the photosensitizer acted as a radical photo-initiator and that the dehalogenated radical-malonate species introduces a radical chain propagation pathway.[263]

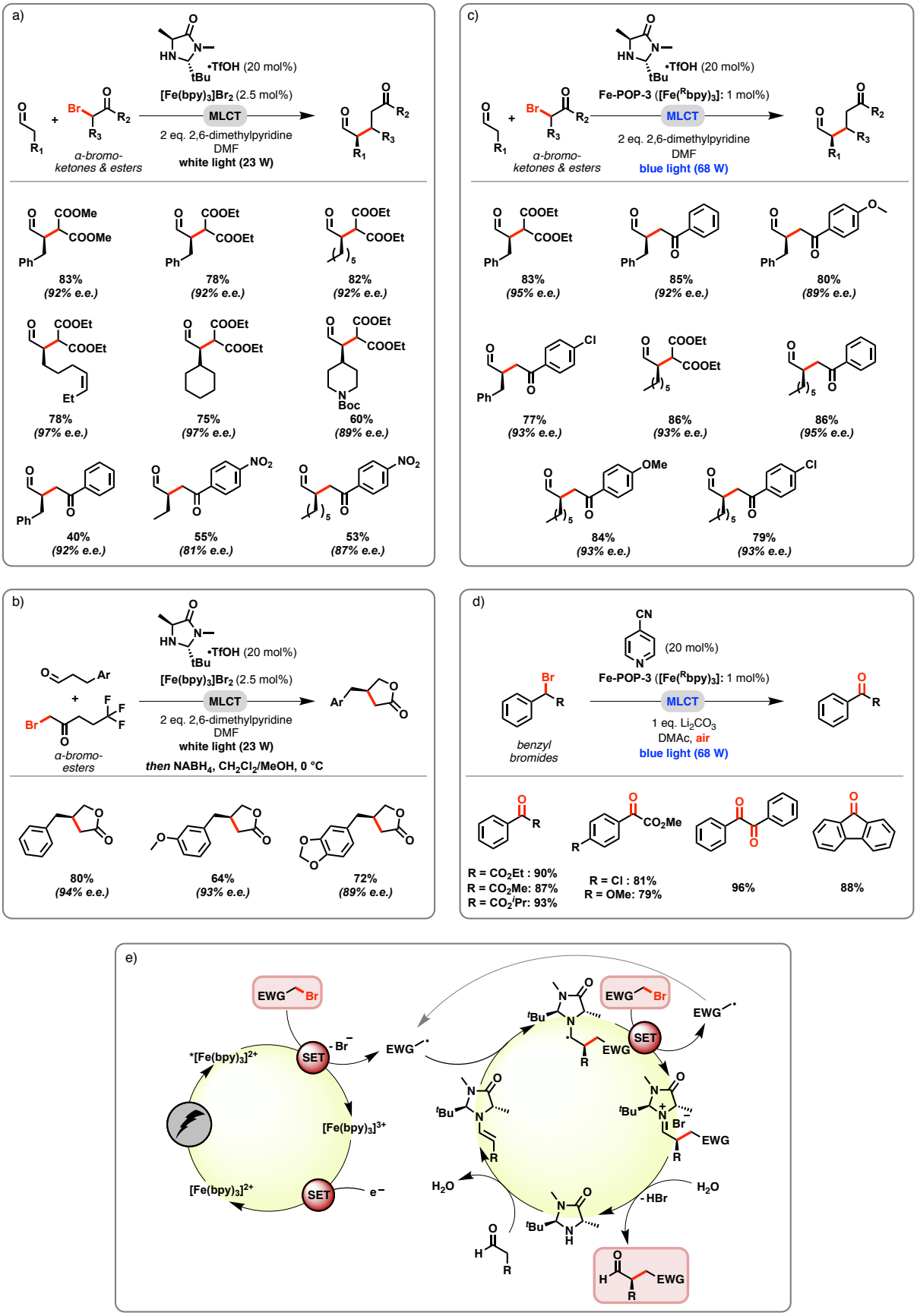

a)
•TfOH (20 mol%)
[Fe(bpy)3]Br2 (2.5 mol%)
MLCT
2 eq. 2,6-dimethylpyridine
DMF
white light (23 W)
α-bromo-ketones & esters
83% (92% e.e.)
78% (92% e.e.)
82% (92% e.e.)
78% (97% e.e.)
75% (97% e.e.)
60% (89% e.e.)
40% (92% e.e.)
55% (81% e.e.)
53% (87% e.e.)
c)
•TfOH (20 mol%)
Fe-POP-3 ([Fe(Rbpy)3]: 1 mol%)
MLCT
2 eq. 2,6-dimethylpyridine
DMF
blue light (68 W)
α-bromo-ketones & esters
83% (95% e.e.)
85% (92% e.e.)
80% (89% e.e.)
77% (93% e.e.)
86% (93% e.e.)
86% (95% e.e.)
84% (93% e.e.)
79% (93% e.e.)
b)
•TfOH (20 mol%)
[Fe(bpy)3]Br2 (2.5 mol%)
MLCT
2 eq. 2,6-dimethylpyridine
DMF
white light (23 W)
then NABH4, CH2Cl2/MeOH, 0 °C
α-bromo-esters
80% (94% e.e.)
64% (93% e.e.)
72% (89% e.e.)
d)
(20 mol%)
Fe-POP-3 ([Fe(Rbpy)3]: 1 mol%)
MLCT
1 eq. Li2CO3
DMAc, air
blue light (68 W)
benzyl bromides
R = CO2Et : 90%
R = CO2Me: 87%
R = CO2iPr: 93%
R = Cl : 81%
R = OMe: 79%
96%
88%
e)
EWG Br
SET
- Br−
EWG•
*[Fe(bpy)3]2+
[Fe(bpy)3]3+
[Fe(bpy)3]2+
e−
tBu
R
H2O
- HBr
EWG

Figure 13. Stereoselective α-alkylation (a+c), preparation of enantioriched lactone (b) and debromination (d) using $[Fe(bpy)_3]^{2+}$ and derivatives thereof as photosensitizer under visible light.[262, 264] e) Proposed mechanism for the visible light mediated stereoselective alkylation using $[Fe(bpy)_3]^{2+}$. EWG = electron-withdrawing group. POP = porous organic polymers, DMAc = dimethylacetamide.

Transient absorption spectroscopy displayed the characteristic bleach of $^{*}[Fe(bpy)_3]^{2+}$ centered at 535 nm, corresponding to the $^5T_{2g}$ excited state. The addition of bromomalonate or enamine reaction intermediate did not change the spectrum features and the underlying lifetime.[262] Hence, in the proposed mechanism, $^{*}[Fe(bpy)_3]^{2+}$ acts as an excited-state reductant that reduces the bromomalonate derivative to yield free bromide and the corresponding radical, which subsequently adds to the enamine part of the organo-catalytic cycle subsequently resulting in the formation of the enantioriched α-alkylated aldehyde (**Figure 13e**). The aminoalkyl radical intermediate acts as a strong reductant that can also induce the reduction of bromomalonate to engage in a radical chain propagation pathway.

Similar reactions for enantioselective functionalization of aldehydes were carried out by the group of Zhang in 2021, using porous organic polymers (POP) composed of an octahedral $[Fe(bpy)_3]^{2+}$ core that was connected *via* condensation to aromatic diamines bearing one, two or three aromatic rings.[264] The corresponding POP were obtained in high yields and were used to perform the visible-light mediated oxidation of benzyl halide derivatives (**Figure 13d**) as well as for the enantioselective α-alkylation of aldehydes (**Figure 13c**).

In addition to the work of Cozzi and coworkers, Collins *et al.* reported the use of $[Fe(phen)_3]^{2+}$ as photocatalyst for the formation of carbazoles from di- and triarylamines using flow chemistry and oxygen as a sacrificial oxidant (**Figure 14)**.[265] Yields between 63% and 91% were obtained with $[Fe(phen)_3]^{2+}$ depending on the substituents of the individual aryl rings. Interestingly, the yields decreased drastically with other Fe^{II} photosensitizers, i.e. like $[Fe(bpy)_3]^{2+}$ or $[Fe(tpy)_2]^{2+}$ (tpy = 2,2';6',2''-terpyridine) and substituted analogues thereof, as well as with more prototypical photosensitizers such as $[Ru(bpy)_3]^{2+}$, $[Ir(ppy)_3]$ (ppy = 2-phenylpyridine) and Eosin Y. Control experiments using catalytic or stoichiometric amounts of $[Fe(phen)_3]^{3+}$ confirmed that the reaction did not proceed *via* electron transfer with triphenylamine. Rather, it seems that the oxidation of triphenylamines to the corresponding carbazoles occurs *via* the formation of superoxide anion (**Figure 14**). A similar mechanism has previously been proposed using iodine or oxygen as sacrificial electron acceptor.[266] The flow tube-in-tube system likely helped accelerate the reaction rate by improving mixing of O_2. In batch, the yields of 9-phenylcarbazole only reached 15% in 50 hours of irradiations whereas yields of 91% were obtained using a residence time of 200 minutes in the flow reactor.

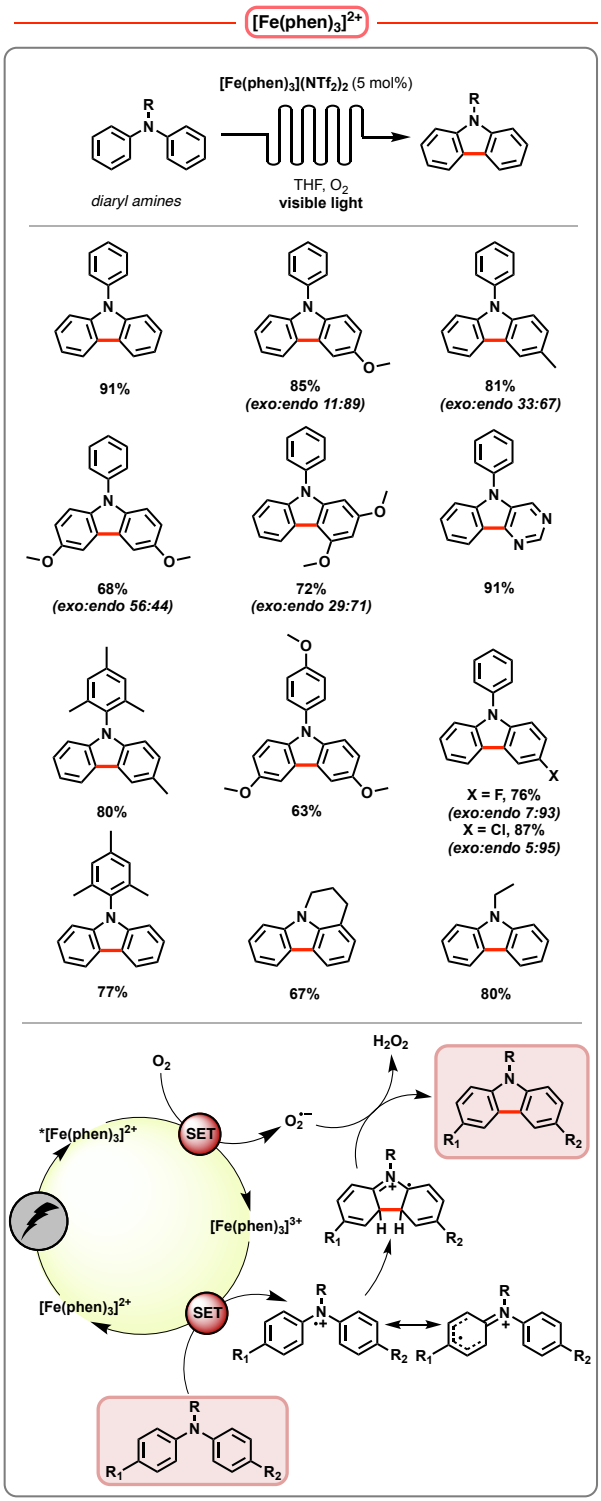


Figure 14. Scope of carbazoles obtained using $[Fe(phen)_3](NTf_2)_2$ as photosensitizer.[265] Incorporation of the substituted aryl group is defined as the *endo* product, while exclusion of the substituted aryl is defined as the *exo* substituent. Values in parenthesis correspond to *exo:endo* distribution.

Very recently, McCusker and coworkers studied another Fe^{II}-based polypyridyl complex by ultrafast time-resolved electronic absorption spectroscopy on a ~100 fs time scale.[73, 267] The structure of $[Fe(tren(py)_3)]^{2+}$ ($tren(py)_3$ = tris(2-pyridyl-methyliminoethylamine) is presented in **Figure 15**. They observed novel absorption features

above 600 nm within the first 100 fs after photoexcitation which were attributed, by comparison with spectroelectrochemical measurement, to a transient charge transfer species $^{*}[Fe^{III}(tren(py^{\bullet-})(py)_2)]^{2+}$, i.e. the ^{1}MLCT state, with a lifetime of 80 ± 20 fs. Afterwards, this absorption feature was converted into a characteristic bleach of the ligand-field excited-state with a long excited-state lifetime of 55 ns. This excited-state lifetime is suitable for bimolecular reactivity and as such, this photosensitizer was thus investigated for the excited-state reduction of benzoquinones derivatives, covering a range of redox potentials.[242] Consequently, Stern-Volmer experiments by investigating the excited-state lifetimes of the bleach upon successive addition of different quenchers were performed. A systematic decrease of the $^{5}T_{2g}$ excited-state lifetime with increasing concentration of 2,3-dichloro-5,6-dicyano-1,4-benzoquinone (DDQ) was observed, which is a clear indication of dynamic quenching of the excited state. Similar effects were observed with 2,3-dicyano-1,4-benzoquinone (DCBQ) and 3,4,5,6-tetrachloro-1,2-benzoquinone (*o*-TCBQ) where quenching rate constants between 2.1 and $2.7 \cdot 10^5$ $M^{-1}s^{-1}$ were determined. A closer inspection of the reported data seems to indicate that the quenching rate constant might actually be three orders of magnitude larger, *i.e.* between 2.1 and $2.7 \cdot 10^8$ $M^{-1}s^{-1}$. In contrast, similar experiments with 2,3,5,6-tetrachloro-1,4-benzoquinone (*p*-TCBQ) and 3,4,5,6-tetrabromo-1,2-benzoquinone (*o*-TBBQ) did not result in significant excited-state quenching. A correlation between the redox potentials and the Stern-Volmer quenching rate constant suggested an excited-state quenching mechanism proceeding *via* electron transfer from the excited photosensitizer to the quinone.[268] The absence of quenching with *o*-TBBQ and *p*-TCBQ was indicative of a transition between exergonic and endergonic reaction, which led to the estimation of the $^{5}T_2$ excited-state reduction potential for $E_{1/2}([Fe^{III}]/^{*}[Fe^{II}])$ of ~ –0.35 ± 0.05V *vs* Fc/Fc^+ in acetone and ~ –0.25 ± 0.05V *vs* Fc/Fc^+ in acetonitrile. Transient absorption spectroscopy to prove that the quenching process occurred *via* excited-state electron transfer to form the corresponding oxidized photosensitizer and semiquinone was complicated due to overlapping features of the $^{5}T_{2g}$ state and the semiquinone. This does not represent a photoredox catalytic example *per se* but constitutes the first direct evidence that Fe^{II} based photosensitizer can be used for bimolecular reactivity even from the metal-centered ligand-field excited-state.

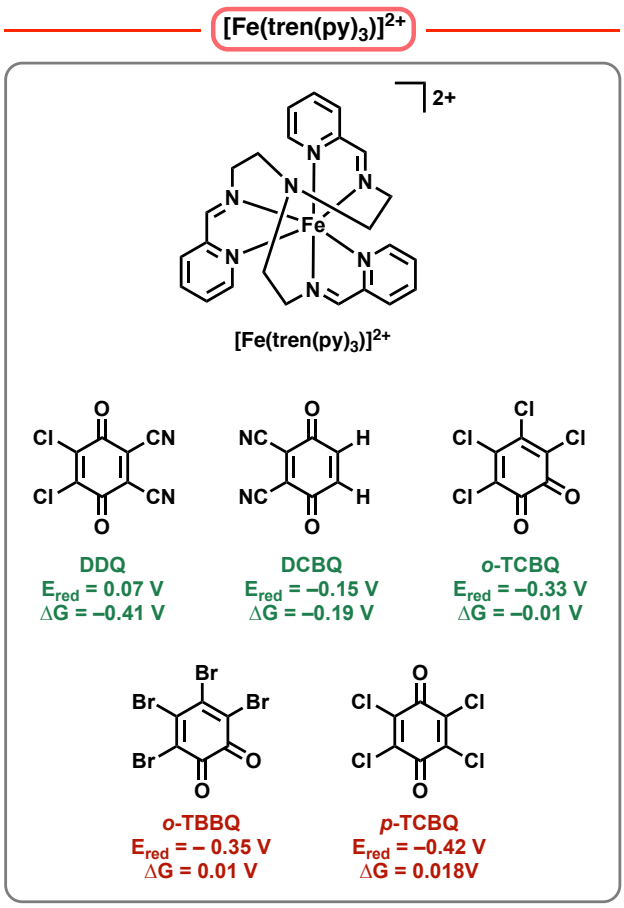


Figure 15. Series of benzoquinones used for the bimolecular quenching experiments with $[Fe(tren(py)_3)]^{2+}$.[242] DDQ = 2,3-dichloro-5,6-dicyano-1,4-benzoquinone, DCBQ = 2,3-dicyano-1,4-benzo-quinone, *o*-TCBQ = 3,4,5,6-tetrachloro-1,2-benzoquinone, *o*-TBBQ = 3,4,5,6-tetrabromo-1,2-benzoquinone, and *p*-TCBQ = 2,3,5,6-tetrachloro-1,4-benzoquinone. The color-code indicates successful (green) and unsuccessful (red) excited-state quenching.

3.2) Photoredox catalysis using LMCT excited states

Ligand-to-metal chare transfer excited states represent a unique opportunity to drive light activated processes. Simple photosensitizers, such as $[Fe(acac)_3]$ (acac = acetylacetone), have been shown to populate a ^{4}LMCT excited state upon illumination. That state was used to perform efficient oxidative ring opening of cyclic ethers and acetals.[269] Although the author proposed a mechanism occurring via electron transfer and propagation, they also noted that uncertainties remain and that additional in-depth experiments would be required to investigate the light induced reaction. Indeed, such bimolecular reactivity is particularly surprising given the 60 ps excited-state lifetime of $[Fe(acac)_3]$.[270]

In 2019, the field of iron photosensitizer experienced a massive breakthrough with the continuous efforts of pioneers such as Wärnmark, Lomoth, Persson, Sundström and Yartsev amongst others, that reported the synthesis of $[Fe(phtmeimb)_2]^+$ (phtmeimb = phenyl[tris(3-methyl-imidazolin-2-ylidene]borate).[94] This is a Fe^{III}-based photosensitizer with outstanding

photophysical and photochemical properties that, due to its $3d^5$ valence electronic configuration, exhibits an unconventional low-lying luminescent doublet ligand-to-metal charge transfer (^{2}LMCT) excited-state with an excited-state lifetime of 2.2 ns in aerated and deareated acetonitrile and an emission quantum yield of 2.1%. Excited-state potential of +1.34 V *vs* SCE and –1.50 V *vs* SCE were calculated for the $E_{1/2}(^*[Fe^{III}]/[Fe^{II}])$ and $E_{1/2}([Fe^{IV}]/^*[Fe^{III}])$ respectively, using a zero-zero energy ($E_{0\text{-}0}$) of 2.13 eV. Most importantly, its excited state is able to undergo diffusional electron transfer with different quenchers like diphenylamine as electron donor or methylviologen as electron acceptor. This was confirmed by nanosecond transient absorption spectroscopy. The outstanding properties of this homoleptic complex rely on the ligand structure and the coordinating approach of the chelating sites. Indeed, the phtmeimb$^-$ ligand is composed of three NHCs imidazolinylidene attached to a borate center. In addition, the six coordinated NHCs adopt a nearly perfect octahedral structure around the iron center. Therefore, the combination of six strong σ-donating NHCs ligands having an octahedral coordination around the iron center, in addition to the negative charge on the borate increases consequently the electron density of the iron core. These perturbations to the σ-bonding network have a huge impact in terms of modulating the energy of ligand field states. Recently, additionally substituted derivatives bearing methoxy, carboxylic acid or bromide substituents were reported and similar excited state properties with nanosecond excited-state lifetimes were found.[94, 271]

Following these first reports on the photophysical properties of this Fe^{III} complex, the relatively long excited-state lifetime of $^{2*}[Fe(phtmeimb)_2]^+$ was deemed sufficient to investigate excited-state reactivity. Hence, additional studies on the photocycle of charge separation and recombination down to ultra-short time scales were carried out at room temperature in acetonitrile.[272] The unconventional ^{2}LMCT photoactive excited state exhibits donor-dependent charge separation rates of up to 1.25 ps^{-1} that exceed the rates found for typical Ru^{II}-based systems and are instead more similar to those reported for organic sensitizers.[273, 274] Surprisingly, even with a very fast charge separation rate the overall cage escape yield was very small. The poor photoproduct yields were explained by a fast charge recombination with rates of 0.2 ps^{-1}, limiting the cage escape yield and the photoproduct formation in acetonitrile.

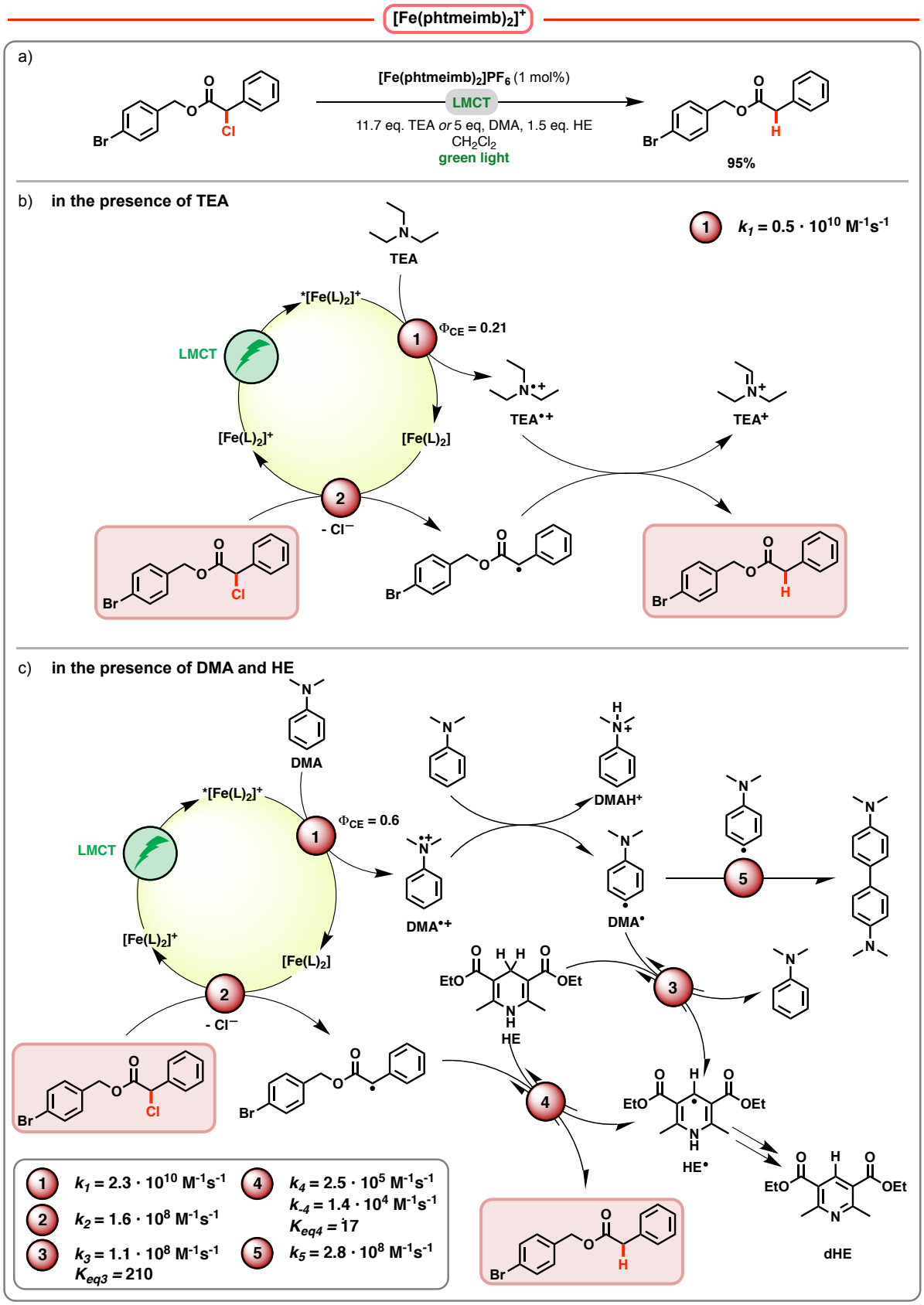


Figure 16. a) Investigated reaction for green-light driven dehalogenation with an iron photocatalyst. Proposed mechanism for the visible-light mediated dehalogenation of 4-bromobenzyl-2-chloro-2-phenylacetate in CH_2Cl_2 using $[Fe(phtmeimb)_2]^+$ as photosensitizer in the presence of b) triethylamine (TEA) as sacrificial electron donor or c) in the presence of dimethylaniline (DMA) as a sacrificial electron donor and Hantzsch ester (HE).[256] L = phtmeimb.

In a comprehensive study, an extended analysis of the parameters that control excited-state reactivity of $^{2*}[Fe(phtmeimb)_2]^+$ were investigated with a series of ten different sacrificial electron donors as quenchers to subsequently perform green-light induced dehalogenation reactions.[256] Excited-state quenching with all quenchers was close to the diffusion limit (10^9-10^{10} $M^{-1}s^{-1}$) in various different solvents that were investigated, *i.e.* dichloromethane, acetone, butyronitrile, acetonitrile and dimethylformamide. Despite these large quenching rate constants, yields of dehalogenation of 4-bromobenzyl-2-chloro-2-phenylacetate were very small in all solvents with the exception of dichloromethane, where dehalogenation yields over 90% were determined with either triethylamine or *N,N*-dimethylaniline as sacrificial electron donors in combination with Hantzsch ester (**Figure 16a**). Femtosecond and nanosecond transient absorption spectroscopy corroborated that the excited-state quenching proceeded *via* electron transfer from the sacrificial electron donor to $^{2*}[Fe(phtmeimb)_2]^+$. More interestingly, it was found that the cage-escape yields, *i.e.* the efficiency with which the geminate radical pair $\{PS^{\bullet -}, Q^{\bullet +}\}$ escapes the solvent cage was strongly influenced by the nature of the solvent. In acetonitrile and dimethylformamide as solvent, the cage-escape yields were extremely low (below 0.10), in line with the results of Wärnmark and coworkers mentioned earlier.[94] However, in dichloromethane, these cage-escape yields were much higher, i.e. close to 0.60 with aniline derivatives like *N,N*-dimethylaniline, *N,N*-dimethyltoluidine and tri-*p*-tolylamine. These changes in cage-escape yields could explain the difference in isolated yields, as previously described.

Time-resolved infrared spectroscopy (TRIR) was further used to gain additional information on the mechanism (**Figure 16b-c**). These measurements confirmed that the mono-reduced iron complex was able to transfer an electron to 4-bromobenzyl-2-chloro-2-phenylacetate, with a kinetic rate constant of $1.6 \cdot 10^8$ $M^{-1}s^{-1}$, which irreversibly induced heterolytic C–Cl bond breaking to yield the corresponding radical and Cl^-. The sacrificial behavior of *N,N*-dimethylaniline (DMA) as an irreversible electron donor requires a deprotonation of the radical cation intermediate ($DMA^{\bullet +}$) - generated upon reductive quenching of the excited iron catalyst – by a suitable base, e.g. a second DMA molecule to generate a $DMA^{\bullet}$ radical.[275, 276] The subsequent encounter of two $DMA^{\bullet}$ radicals results in the dimerization of the sacrificial reagent. This dimerization reaction, studied in great detail by Bard and coworkers, occurs in acetonitrile with a rate constant of $2.5 \cdot 10^8$ $M^{-1}s^{-1}$.[276] Time resolved IR data revealed that the Hantzsch ester and $DMA^{\bullet}$ also introduce an additional reactivity *via* hydrogen atom transfer (HAT). This leads to an unwanted consumption of Hantzsch ester that competes with the desired pathway for product formation. These results are

in line with ^{1}H NMR observations that revealed the need of an excess of Hantzsch ester to ensure complete conversion of 4-bromobenzyl-2-chloro-2-phenylacetate into 4-bromobenzyl-2-phenylacetate. The mechanism by which the HE$^{\bullet}$ reacts to form the corresponding pyridine core was not investigated but is thermodynamically favorable. Overall, a first example for a dehalogenation with an iron photocatalyst together with a detailed mechanistic study to examine the mechanism has been outlined in this pioneering study.

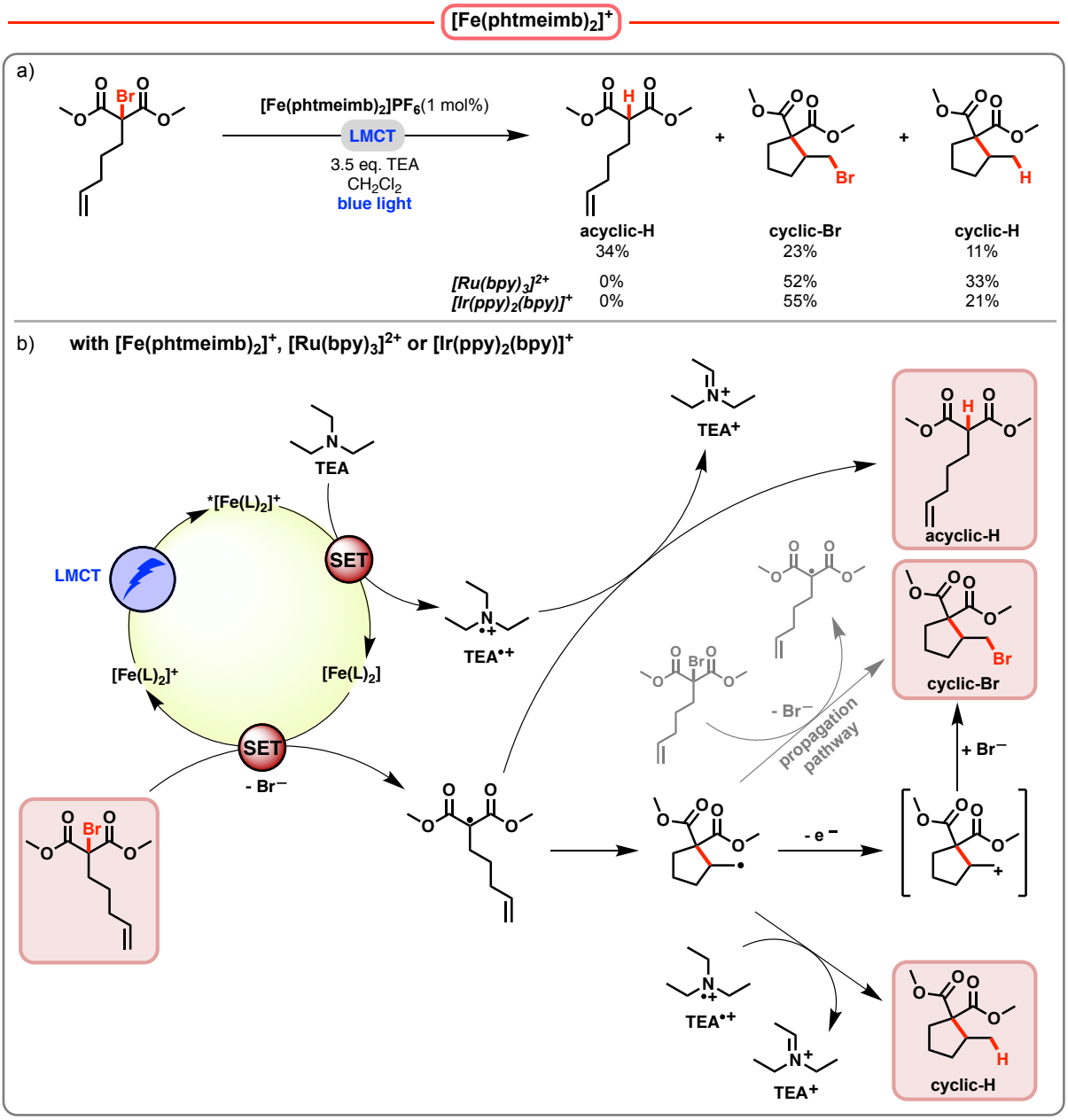


Figure 17. a) Investigated reaction for green-light driven dehalogenation with an iron photocatalyst. b) Proposed mechanism for the visible-light mediated dehalogenation with different photocatalysts.[277] L = phtmeimb, TEA = triethylamine.

In a second study,[278] a comparison between $[Fe(phtmeimb)_2]^{+}$ as photocatalyst and prototypical Ru^{II} and Ir^{III} photosensitizers, i.e $[Ru(bpy)_3]^{2+}$ and $[Ir(ppy)_2(bpy)]^{+}$ was carried out

(**Figure 17**). The light-driven reaction of 2-bromo-2-(pent-4-en-1-yl)malonate leads to significantly different results depending on the photocatalyst. While with $[Fe(phtmeimb)_2]^+$ 34% of dehalogenated product (acylic-H), 23% of the formal atom-transfer product (cyclic-Br) and 11% of cyclized dehalogenated product (cyclic-H) were found, a change to $[Ru(bpy)_3]^{2+}$ changed the distribution exclusively to 52% of cyclic product with bromide and 33% of the dehalogenated analogue (**Figure 17a**). Several spectroscopic techniques were utilized to gain insights into the different mechanisms. In this case, TRIR measurements could not be performed using $[Fe(phtmeimb)_2]^+$ and triethylamine as quencher due to an insufficient signal intensity to analyze the subsequent reactivity between the reduced complex and the substrate. With $[Ru(bpy)_3]^{2+}$ as photocatalyst, the reaction with triethylamine could be studied due to the longer excited-state lifetime, even with a low cage-escape yield. In experiments performed using concentrations relevant to photoredox catalysis, pulsed light excitation of a solution containing $[Ru(bpy)_3]^{2+}$, triethylamine and 2-bromo-2-(pent-4-en-1-yl)malonate resulted in changes detected *via* TRIR that were consistent with the consumption of 2-bromo-2-(pent-4-en-1-yl)malonate. The kinetics measured with $[Ru(bpy)_3]^{2+}$ as the photosensitizer comprised several steps corresponding to the reaction pathway of the substrate 2-bromo-2-(pent-4-en-1-yl)malonate: 1) electron transfer from the reduced photocatalyst to the substrate 2) cyclization of the formed radical intermediate and 3) bromine atom transfer from a second substrate to give the final product. The spectroscopic measurements indicate that the initial transformation of 2-bromo-2-(pent-4-en-1-yl)malonate is to the acyclic dehalogenated radical intermediate, a common mechanistic step for all photosensitizers studied here. This common denominator naturally sparks an intriguing question – *why is the chemoselectivity for product distribution different when the iron-based photocatalyst drives the catalytic reaction?* Even though cyclization of the radical to produce the final product is an intramolecular step, it occurs on early microsecond time scales. Hence, depending on the respective rate constant of other competitive reaction pathways can potentially occur. A conversion to the acyclic dehalogenated product requires a hydrogen-atom transfer competing with the cyclization, presumably from a radical intermediate of the sacrificial electron donor ($TEA^{\bullet+}$). As such, the rate for hydrogen-atom transfer is strongly dependent on the concentration of the intermediate $TEA^{\bullet+}$ generated under steady-state illumination conditions. While similar rate constants ($\sim 1.5 \cdot 10^8\ M^{-1}s^{-1}$) were found for the electron transfer from the mono-reduced photocatalyst to the substrate, the excited-state quenching of $^{2*}[Fe(phtmeimb)_2]^+$ by triethylamine is two to three orders of magnitude larger than for $^{3*}[Ru(bpy)_3]^{2+}$ and $^{3*}[Ir(ppy)_2(bpy)]^+$. Hence, a much higher steady-

state concentration of $TEA^{\bullet+}$ is present under synthetic conditions that can potentially favor hydrogen-atom transfer over the cyclization step.

Overall, the data presented herein allow a plausible mechanism to be proposed for the three photosensitizers (**Figure 17b**). Light excitation of the photocatalyst yields an excited state that is reductively quenched by triethylamine. The reduced photosensitizer transferred an electron to the substrate, which induced heterolytic C–Br bond breaking to yield the corresponding acyclic radical intermediate. In the case of $[Ru(bpy)_3]^{2+}$ and $[Ir(ppy)_2(bpy)]^+$, the product distribution is consistent with a pathway where intramolecular cyclisation follows the bond breaking event leading to the cyclic radical intermediate, while for $[Fe(phtmeimb)_2]^+$ the HAT reactivity seems to be competing with the cyclisation (**Figure 17b**).

Due to its high photostability and very favorable excited-state redox potentials, $[Fe(phtmeimb)_2]^+$ was also used for hydrogen photo-production applications (**Figure 18**).[279] The group of Wärnmark recently used this photosensitizer in combination with Pt-colloids or $[Co(dmgH)_2(py)Cl]$ as proton reduction catalysts, $[HNEt_3][BF_4]$ as proton donor and triethanolamine or triethylamine as sacrificial electron donor to produce hydrogen in acetonitrile solutions. In contrast to earlier investigations with Fe^{II} photocatalysts and molecular dyads containing iron sensitizers with limited turnover numbers,[280-282] $[Fe(phtmeimb)_2]^+$ allowed turnover numbers above 1000 without significant catalyst degradation. Quenching rate constants of $7.8 \cdot 10^9\ M^{-1}s^{-1}$ and $1.3 \cdot 10^9\ M^{-1}s^{-1}$ were determined for the reductive quenching by triethylamine and triethanolamine, respectively. The cage-escape yields in acetonitrile were very small (0.02 and 0.03) and attempts to improve hydrogen photo-production using a solvent leading to larger cage-escape yields (i.e. dichloromethane) were unsuccessful. Although oxidative electron transfer from the excited iron photosensitizer to $[Co(dmgH)_2(py)Cl]$ is thermodynamically favorable,[283] no evidence for the formation of any reduced or oxidized species was detected by nanosecond transient absorption spectroscopy. Hence, the mechanism was mostly consistent with reductive quenching of the excited state by triethanolamine (**Figure 18**). The proton reduction catalyst can then be reduced *via* electron transfer either from the reduced photosensitizers or by the generated α-amino alkyl radical originating from the initial electron donor. To close the catalytic cycle the reduction of $Co^{II/I}$ *via* a strongly reducing radical is suggested. As alternative pathway, it was proposed that the subsequent protonation of Co^{I} results in a Co^{III} hydride that is reduced by the Fe^{II} intermediate and would finally lead to the formation of hydrogen *via* a bimetallic route (not explicitly shown in **Figure 18**).

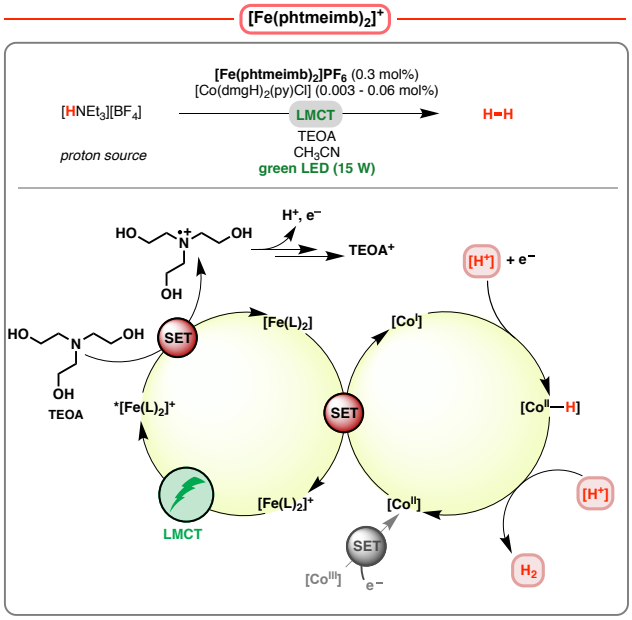


Figure 18. Hydrogen production using $[Fe(phtmeimb)_2]^+$ as photosensitizer and a cobalt cocatalyst together with the proposed mechanism. [279] L = phtmeimb, TEOA = triethanolamine.

Finally, $[Fe(phtmeimb)_2]^+$ was also shown to be amongst the rare example of compounds capable of undergoing photoinduced symmetry-breaking charge separation, i.e. single photon excitation would lead to an excited-state capable of undergoing electron transfer with a ground-state photosensitizer to generate a singly oxidized and a singly reduced photosensitizer according to PS* + PS → PS^+ + PS^-.[284, 285] The driving force for bimolecular symmetry-breaking charge separation resulting in disproportionation to $[Fe^{II}(phtmeimb)_2]$ and $[Fe^{IV}(phtmeimb)_2]^{2+}$ was calculated as –0.7 eV. Given the short excited-state lifetime, it was estimated that concentration smaller than 5 mM would not allow the observation of this effect and hence concentration of 70 mM in acetonitrile in 25 µm path length cells were investigated. Transient absorption experiments provided unambiguous proof that pulse light excitation resulted in the formation of $[Fe^{II}(phtmeimb)_2]$ and $[Fe^{IV}(phtmeimb)_2]^{2+}$ in equimolar amount with a total product yield of 4% followed by a charge recombination on the microsecond timescale. Hence, this approach allows the generation of two potentially active catalytic species from one excited photosensitizer. Photophysical measurements in different solvents at variable temperatures revealed that charge separation to form $[Fe^{II}(phtmeimb)_2]$ and $[Fe^{IV}(phtmeimb)_2]^{2+}$ can be obtained at very low concentrations below 0.5 µM, if the temperature was decreased close to the freezing point of the solvent (i.e. 140-180 K).[284] This effectively enabled a temperature dependent aggregation and thus a local increase in concentration of $[Fe^{III}(phtmeimb)_2]^+$. This photoinduced symmetry-breaking charge separation using a single excited state is unique to $^{2*}[Fe(phtmeimb)_2]^+$ and cannot be achieved using

prototypical Ru^{II} and Ir^{III} photosensitizer. This unique reactivity could open interesting novel pathways for iron-mediated photoredox catalysis.

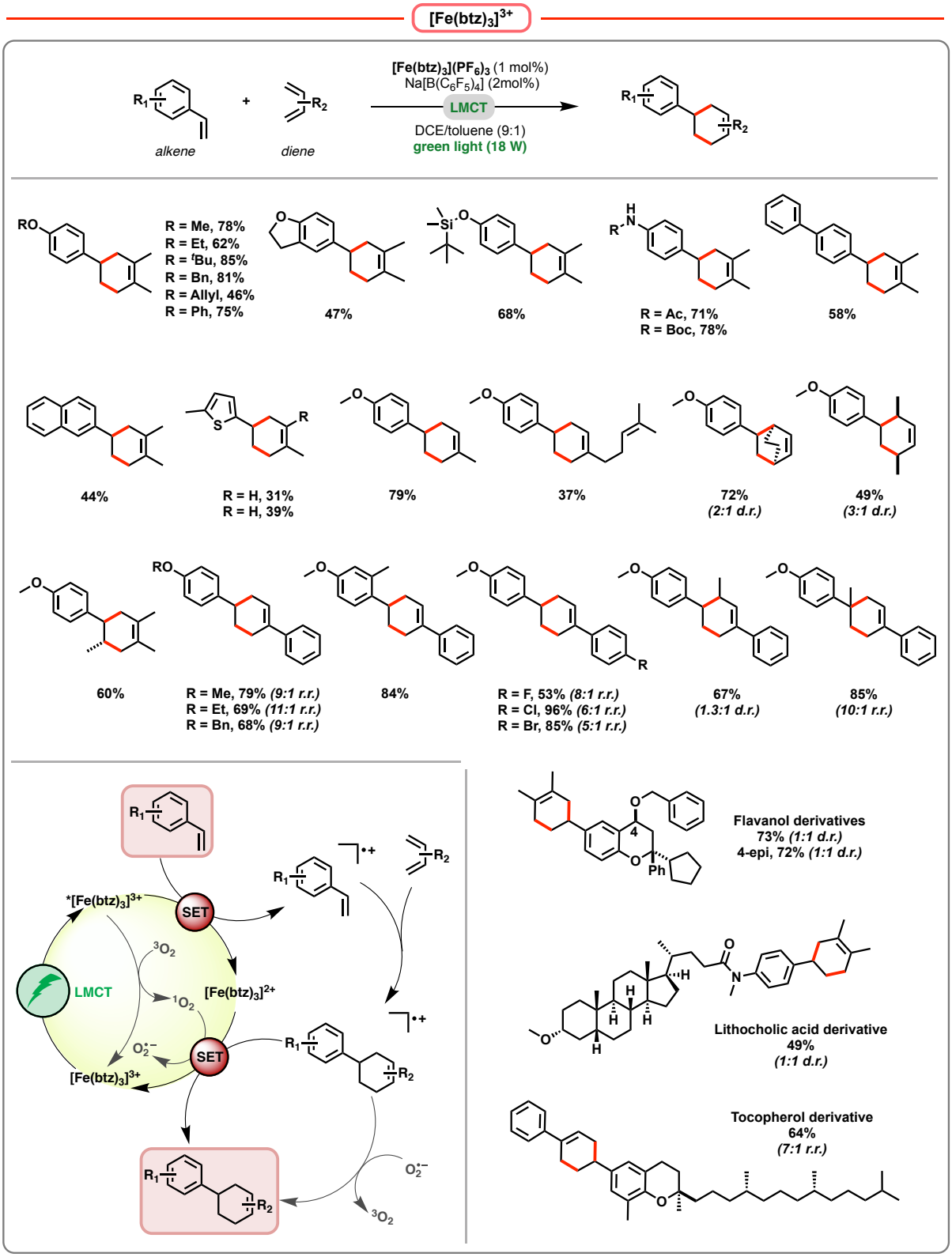


Figure 19. Substrate scope for the photocatalyzed radical cationic [4+2] cycloaddition using $[Fe(btz)_3]^{3+}$ as photosensitizer.[286] Inset: Proposed mechanism. DCE = dichloroethane.

Another iron-based photocatalyst with a ^{2}LMCT excited state has been successfully used in photoredox catalysis. Recently, Kang and coworkers reported the green-light driven radical cationic [4+2] cycloaddition using a photoactive Fe^{III} complex with three bidentate NHC ligands (**Figure 19**).[286] This photosensitizer, another photosensitizer pioneered by the group of Wärnmark in 2017, exhibits a ^{2}LMCT excited state with corresponding lifetime of 100 ps. The structure of $[Fe(btz)_3]^{3+}$ (btz = 3,3'-dimethyl-1,1'-bis(p-tolyl)-4,4'-bis(1,2,3-triazol-5-ylidene)) is presented in **Figure 12**. Green-light excitation of $[Fe(btz)^3]^{3+}$ enabled the radical cationic [4+2] cycloaddition of 4-methoxy styrene and 2,3-dimethylbuta-1,3-diene in 47% yield (**Figure 19**), alongside several side products including a 1,2-dioxane, cyclobutane and tetrahydronaphthalene cores (not shown). The use of toluene as co-solvent allowed to increase the yield to 62% while the introduction of non-coordinating counterions such as 2 mol% sodium tetrakis(pentafluorophenyl)borate ($Na[B(C_6F_5)_4]$). increased the yields to 78% while decreasing the reaction time by a factor of three. Similar counterion effects have earlier been observed by the group of Yoon with ruthenium catalysts.[287] The reaction scope was then extended (**Figure 19**), and it was found that the methoxy substituent on the styrene could be replaced with various alkoxy substituents, including allyloxy, fused tetrahydrofuranyl, and silyloxy groups, which implies that an electron-donating substituent is beneficial for the reaction to proceed in high yields. Cyclization of styrenes bearing amido substituents yielded the corresponding cyclohexene products. Phenyl and naphthyl groups were compatible with such photo-induced transformation whereas moderate yields were obtained when thiophene was used. In addition, the dioxane side product resulting from the [2+2+2] cyclooxygenation reaction was also obtained in 24% yield with thiophene as substrate. The use of isoprene or myrcene instead of 2,3-dimethylbutadiene led to the exclusive formation of 1,4-disubstituted cyclohexene derivatives as a single regioisomer. Several cyclic and acyclic dienes were also used to form the corresponding tri- and tetra-substituted cyclohexenes as diastereomeric mixtures with moderate selectivity. Larger substrates like lithocholic acid, flavanol and tocopherol derivatives were successfully used as substrates with yields of 49%, 73% and 64% respectively (**Figure 19**).

Mechanistically, the reaction was proposed to be initiated by excited-state electron transfer from the styrene to $^{2*}[Fe(btz)_3]^{3+}$ (**Figure 16**). Indeed, with an excited-state reduction potential $E_{1/2}(^*[Fe^{III}]/[Fe^{II}])$ = 1.94 V *vs* SCE, a favorable driving force of nearly 0.7 eV is expected for oxidation of styrene ($E_{1/2}$ = 1.27 V *vs* SCE). Photolysis experiments of 1 mM $[Fe(btz)_3]^{3+}$ in the presence of 100 mM 4-methoxy-styrene led to the gradual decrease of absorption bands corresponding to $^{2*}[Fe(btz)_3]^{3+}$ concomitant with the appearance of novel

absorption bands of $[Fe(btz)_3]^{2+}$ that are in line with electrochemically generated reference spectra. Additional X-band EPR experiments of the same solution revealed a transition from an octahedral low-spin d^5 Fe^{III} species to a diamagnetic low-spin d^6 Fe^{II} species, in line with the proposed reduction of the metal center. A quantum yield of 0.49 was determined for the cycloaddition reaction through control experiments at various irradiation time intervals, which pointed towards a potential (minor) contribution from a radical chain mechanism. Hence, it appeared that after light-induced electron transfer, the styrene radical cation was able to undergo cyclization with the diene to yield the corresponding cyclohexene radical cation, which was subsequently reduced by electron transfer from the reduced photosensitizer (**Figure 19**). Performing the reaction under argon decreased the efficiency of the entire reaction and therefore the higher yields obtained under normal air conditions were rationalized by the generation of $^1O_2$ *via* energy transfer from $^{2*}[Fe(btz)_3]^{3+}$. *In fine*, $^1O_2$ is proposed to oxidize the reduced photosensitizer back to its ground-state product and generate $O_2^{\bullet-}$ that could oxidize the cyclohexene radical cation to form the desired product. Although the importance of oxygen is undoubtful, a mechanism proceeding *via* energy transfer with such a short excited-state lifetime is likely rather inefficient and the oxygen might have additional roles.

3.3) Photoredox catalysis using MLCT excited states

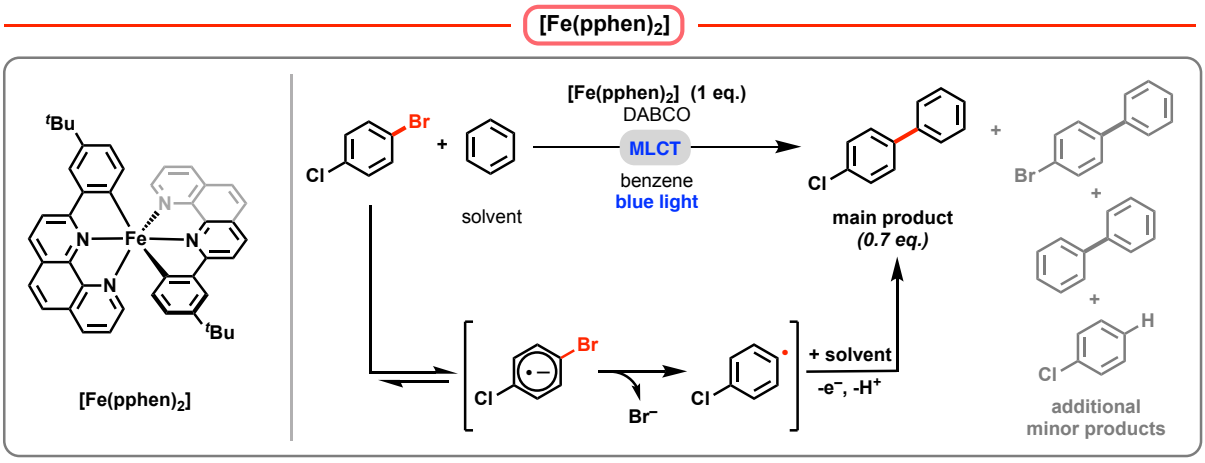


Figure 20. Visible light mediated transformation of 4-chlorobromobenzene to 4-chlorobiphenyl using stoichiometric amounts of $[Fe(pphen)_2]$.[250] Minor products are provided in grey. DABCO = 1,4-diazabicyclo[2.2.2]octane.

Metal-to-ligand charge transfer excited-state of iron complexes have been scarcely used in photoredox applications thus far. The reason, as discussed in the introduction, is the ultrafast deactivation of MLCT excited states to lower energy metal-centered ligand field states. Density functional theory calculations on modified $[Fe(tpy)_2]^{2+}$ type photosensitizers with one or several

cyclometalating units at different chelating positions indicate that it is possible to switch the relative ^{3}MLCT and ^{3}MC position in Fe^{II} complexes which could potentially lead to luminescent complexes.[87, 288, 289] The combination of 2,2'-bipyridine coordination scaffold with a σ-donating phenyl leading to an overall tridentate ligand scaffold was forecasted to render the ^{3}MLCT state more stable than the metal-centered ones in a homoleptic Fe^{II} complex.[87, 288, 289] Very recently, Berkefeld and coworkers used this approach using a 1,10-phenanthroline backbone which led to the formation of $[Fe(pphen)_2]$ as blue-purple crystals.[89] Strikingly, near-infrared photoluminescence (λ = 1170–1230 nm) of the ^{3}MLCT was observed in the solid form and in solutions of 1,2-difluorobenzene, benzene, tetrahydrofuran and acetonitrile. This luminescent excited state had a characteristic mono-exponential decay with excited-state lifetime of 2.4 ns in the solid state and ~1 ns in solution, which matched with the value obtained by transient absorption spectroscopy. To the best of our knowledge, this complex is the first example of a luminescent Fe^{II}-based complex. On the one hand, the ground-state oxidation potential of $E_{1/2}([Fe^{II}]/[Fe^{III}])$ = –0.88V *vs* Fc/Fc^+ makes this compound prone to oxidation by air, while on the other hand this results in an excited-state redox potential $E_{1/2}(^*[Fe^{II}]/[Fe^{III}])$ of –2.0V *vs* Fc/Fc^+. This potential is sufficient to induce dehalogenation reaction of aromatic compounds. Hence, light-induced cross-coupling of 4-chlorobromobenzene and benzene in presence of a stoichiometric amount of iron sensitizer was performed (**Figure 20**). This transformation led to the formation of 4-chlorobiphenyl (0.7 equiv. with respect to the photosensitizer) as well as chlorobenzene, 4-bromobiphenyl, and biphenyl as additional side products. The reaction was proposed to proceed *via* reductive quenching of the excited Fe^{II} catalyst and electron transfer to 4-chlorobromobenzene, which induced the fragmentation of the C–Br bond (**Figure 20**). The corresponding aryl radical is proposed to be trapped by the solvent, *i.e.* benzene, to generate the corresponding 4-chlorobiphenyl. Contrary to most other examples discussed here with iron sensitizers, it should be noted that the iron complex is used in stoichiometric amounts, likely due to the very low oxidation potential, hampering the recovery of the oxidized catalyst with commonly used sacrificial electron donors[290] to allow the use of sub-stoichiometric concentrations.

3.4) Photoredox catalysis using a multi-photon excitation pathway

In addition to the catalytic cycles discussed before in this section of well-defined catalysts that all rely on mono-photonic mechanisms, a consecutive photo-induced electron transfer (conPET) was recently also considered with iron photocatalysts. This mechanistic

sequence was investigated by the group of Wärnmark using $[Fe(btz)_3]^{3+}$ as photosensitizer for an atom transfer radical addition (ATRA) reaction.[291] The addition of alkyl halides to alkenes and alkynes was investigated using green light irradiation. The reaction rational was that the ^{2}LMCT excited state could be efficiently reductively quenched to generate the corresponding $[Fe(btz)_3]^{2+}$ that exhibits a ^{3}MLCT excited state. This triplet excited state is a stronger reductant than the ^{2}LMCT of $[Fe(btz)_3]^{3+}$ and therefore it is possible to envision a consecutive ^{2}LMCT-^{3}MLCT excitation of $[Fe(btz)_3]^{3+}$ to activate challenging substrates (inset in **Figure 21**). The reaction of 5-hexen-1-ol with 1-iodoperfluorooctane in the presence of triethylamine (TEA) reached full conversion within 8 minutes of 530 nm irradiation using a 3 W LED array. Optimal reaction condition used a photosensitizer loading of 0.5 mol% and substoichiometric amounts (0.34 eq) of sacrificial electron donor (**Figure 21**).

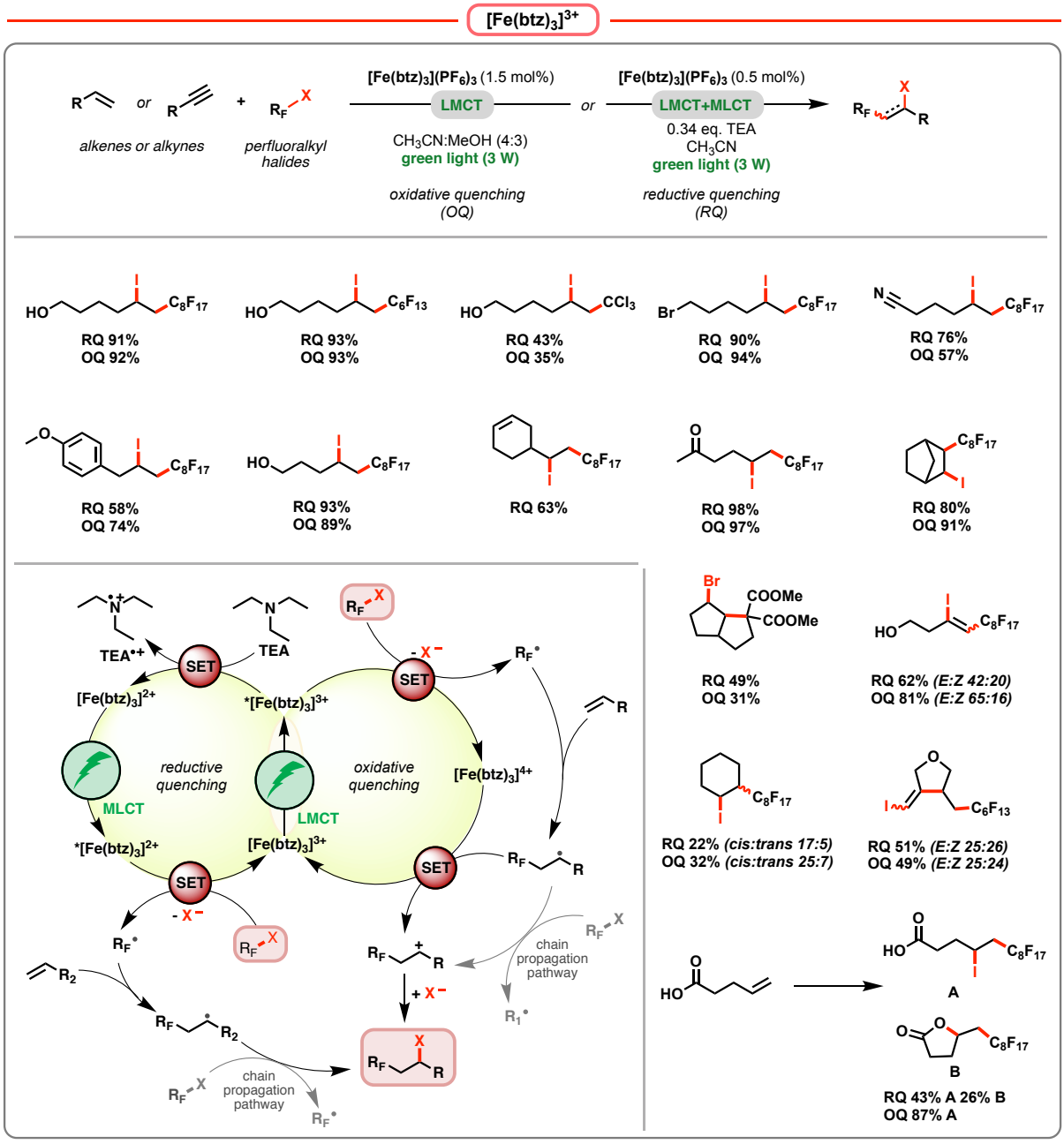


Figure 21. Scope of the visible light-mediated atom transfer radical addition reaction through reductive (RQ) and oxidative (OQ) quenching of $[Fe(btz)_3]^{3+}$.[292] Inset: Proposed mechanism. R_F = iodoperfluoroalkanes, TEA = triethylamine, btz = 3,3'-dimethyl-1,1'-bis(p-tolyl)-4,4'-bis(1,2,3-triazol-5-ylidene).

The reaction mechanism was investigated by means of transient absorption spectroscopy and Stern-Volmer experiments. Diffusion limited quenching rate constants were determined when triethylamine was used as electron donor. Excited-state oxidation of triethylamine by $^{2*}[Fe(btz)_3]^{3+}$ was confirmed by transient absorption spectroscopy, where the formation of $[Fe(btz)_3]^{2+}$ was unambiguously detected. Cage-escape yields greater than 0.20 were determined in 4:3 acetonitrile:methanol mixtures, greatly exceeding those previously determined in acetonitrile.[94, 256, 277] $[Fe(btz)_3]^{2+}$ was unable to react with $C_8F_{17}I$ in dark

conditions, but the gradual conversion of $[Fe(btz)_3]^{2+}$ to $[Fe(btz)_3]^{3+}$ was observed upon exposure to ambient light, suggesting that the photo-oxidation of $^{2*}[Fe(btz)_3]^{2+}$ is thermodynamically favorable. Furthermore, this step was investigated by transient absorption spectroscopy of $[Fe(btz)_3]^{2+}$ and an irreversible transformation of Fe^{II} to Fe^{III} *via* oxidative quenching by 1-iodoperfluorooctane was observed, in line with a consecutive photoinduced electron transfer (conPET) mechanism for the ATRA reaction in the presence of a sacrificial electron donor.

An oxidative route *via* excited-state quenching by perfluoroalkyl halides in the absence of sacrificial electron donors was also investigated (**Figure 21**). It was shown that full conversion could be obtained *via* this route, albeit with a longer irradiation time (40 minutes), an increased catalyst loading of 1.5 mol% and the use of acetonitrile rather than the above-mentioned solvent mixture. Indeed, no excited-state quenching was observed in the solvent mixture with methanol present, but weak emission quenching of the ^{2}LMCT state was detected in neat acetonitrile. In both the oxidative and reductive routes, the large reaction quantum yields also highlight that radical chain propagation is occurring once the initial perfluoroalkyl radical has been generated. The two proposed mechanisms for the initial reductive and oxidative excited-state quenching of $^{2*}[Fe(btz)_3]^{3+}$ are presented in the inset of **Figure 21**. Both the oxidative and reductive routes were useful for the investigated ATRA transformations and yielded overall similar yields. An exception lies in the reaction of pentenoic acid that solely produced the desired product in 87% yield according to an atom transfer radical addition pathways whereas, in the presence of base (triethylamine), the reaction produced 43% of the desired product and 26% of the corresponding lactone.

Finally, as mentioned in the introduction, Bauer *et al.* recently reported the synthesis of $[Fe(ImP)_2](PF_6)_2$, a Janus-type dual emitter with ^{2}LMCT and ^{2}MLCT excited-state lifetime of 240 ps and 4.6 ns, respectively.[92] This dual emission violated Kasha's rule and led to excited-state reduction potential of $E_{1/2}([Fe^{II}]/^*[Fe^{III}]) = 1.12$ V *vs* SCE and $E_{1/2}(^*[Fe^{III}]/[Fe^{IV}]) = -1.44$ V *vs* SCE for the ^{2}LMCT state. Excited-state reduction potential of $E_{1/2}([Fe^{II}]/^*[Fe^{III}]) = 1.94$ V *vs* SCE and $E_{1/2}(^*[Fe^{III}]/[Fe^{IV}]) = -3.02$ V *vs* SCE for the ^{2}MLCT state were determined. These potentials render this excited state an extremely potent photo-oxidant and photo-reductant. In fact, these potentials are sufficient to drive toluene or bromide oxidation or reduce lithium cations as well as several solvents.[293, 294] Reductive excited-state quenching was however solely investigated with molar concentrations of typical sacrificial electron donors such as triethylamine and triethanolamine. With 1 M of the latter electron donor, the excited-state lifetime was quenched from 4.6 ns to 0.7 ns. Oxidative quenching was also attempted with

benzonitrile (1.6 M, E_{red} = –2.76 V) where a decrease of the excited-state lifetime to 1.0 ns was observed. No transient absorption spectroscopy to confirm excited-state electron transfer was performed. Note that it was very recently shown that this relatively long-lived excited state originated from the presence of an impurity and the quenching behavior could not be reproduced when pristine $[Fe^{III}(ImP)_2]^+$ was used.[93]

Overall, the examples of photoredox catalysis with MLCT excited states of iron catalysts are presently much more limited than those using LMCT excited states (section 3.2). Recent developments that have led to an excited-state lifetime increase as well as to the use of these well-defined iron photosensitizers in photoredox catalysis will undoubtedly lead to the report of numerous novel applications in the near future.

3.5) Photoredox catalysis using dissociative excited states

The activation modes of iron catalysts discussed up to this point essentially consisted either in the excited-state quenching of well-defined complexes in an outer-sphere process (section 3) or the *in situ* substrate activation *via* an inner-spere process with coordinated substrates formed with iron precatalysts (section 2). Obviously, a combination of well-defined ligand structures *together with* a free coordination site to reversibly bind an additional ligand would in principle still allow the exploitation of inner-sphere substrate activation, while possibly introducing opportunities to modify the properties of the photoactive iron catalyst through judicious ligand design. The approach to use dissociative excited states with well-defined iron catalysts are still rare.

As already discussed in the section of *in situ* generated photocatalysts (section 2.3), chlorine radicals are extremely active radicals and tend to easily react with C–H bonds.[294] While the high reactivity allows the activation of various bonds, the selectivity is not necessarily controllable. Indeed, with a thermodynamically favorable H–Cl bond formation (BDE = 103 kcal/mol), chlorine radical reacts efficiently with primary carbons (BDE = 105.0 kcal/mol) and even more efficiently with weaker secondary and tertiary C–H bonds. Furthermore, these radicals also undergo ast back-electron transfer. To tackle these issues, Nocera and coworkers recently attempted to control the excited-state release of chlorine radicals using a series of Fe^{III} chloride pyridine diimine complexes.[257, 258] The structure of a representative $[Fe(PDI)Cl_2]^+$ complex (PDI = 2,6-bis((2,6-diphenylphenyl)imino)ethyl)-4-(trifluoromethyl)-pyridine) is presented in **Figure 12**. The same authors had elegantly shown in the past that such chorine radicals could be stabilized through secondary coordination effect with a suitable ligand

scaffold by forming a Cl•|arene complex that could be observed by transient absorption spectroscopy.[295, 296] In the present series of iron photosensitizers, the pyridine diimine ligand (PDI) is decorated with aromatic groups that bear electron withdrawing or donating substituents which immediately impacts C–H activation. Substituents bearing electron-donating groups are expected to increase selectivity for the weakest C–H bond while electron withdrawing groups would decrease selectivity. Femtosecond transient absorption spectroscopy revealed that LMCT excitation of these iron photosensitizers led to the cleavage of the Fe–Cl bond, leading to a reduced iron center and a chlorine radical (Cl•). A clear peak at 435 nm was observed which matched well with the reported Cl•|arene adduct[295] and hence with the formation of reduced Fe^{II}. Two recombination processes were monitored by transient absorption spectroscopy. The first one, with a lifetime of 1.1 ps, was attributed to the rapid recombination for Fe^{II} and Cl•. A second, slower process was attributed to the decay of the Cl•|arene adduct with a lifetime of 70 ps. The stabilization of the Cl•|arene adduct was then taken advantage of to drive several halogenation reactions. The reaction was first investigated with 3-methylpentane, *i.e.* a substrate bearing primary, secondary and tertiary C–H bonds (**Figure 22a**). Without any stabilization, the selectivity would have matched the thermodynamic requirement related to the C–H bond energy, *i.e.* with site selectivity that follows the trend tertiary > secondary > primary. With arene stabilization and the steric constraint that the ligand imposes, the selectivity was expected to be higher for primary and secondary C–H bonds.

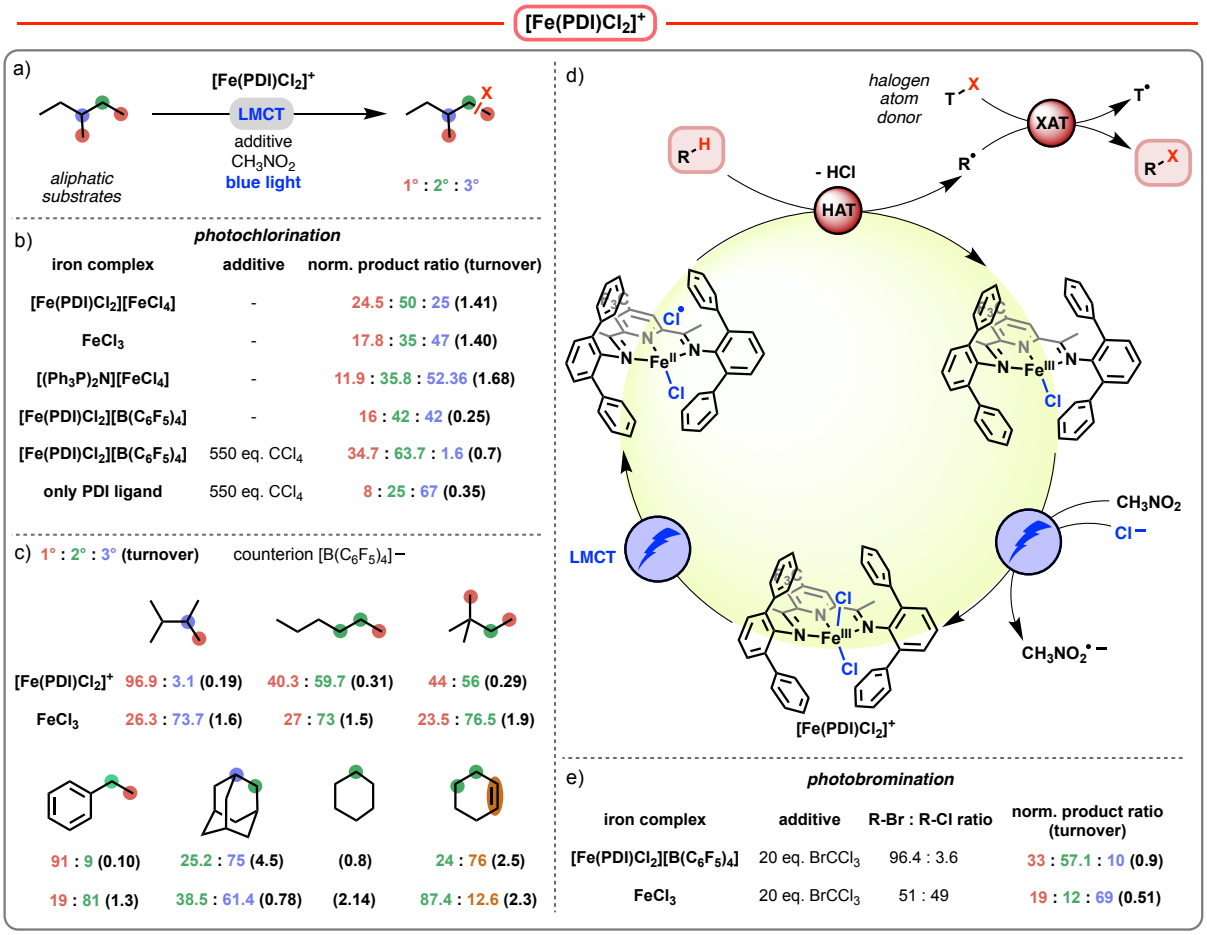


Figure 22. a) Overall approach towards the functionalization of aliphatic substrate using $[Fe(PDI)Cl_2]^+$.[258] Photochlorination of b) 3-methylpentane and c) substrate scope investigation under blue light irradiation. d) Proposed reaction mechanism. e). Photobromination of 3-methylpentane under blue light irradiation.

Indeed, the $[Fe(PDI)Cl_2]^+$ photosensitizers exhibited higher selectivity for secondary and primary positions compared to the reference system with $FeCl_3$ (**Figure 22c**). Hence, this approach seems to induce steric selectivity for less hindered C–H bonds. It was furthermore shown that the $[FeCl_4]^-$ counterion could also lead to undesired chlorine radical elimination, which overall decreased the photochlorination selectivity. To circumvent these limitations, photochlorination reactions were carried out using the tetrakis(pentafluorophenyl)borate counterion ($[B(C_6F_5)_4]^-$). Under otherwise identical conditions, the $[B(C_6F_5)_4]^-$ photosensitizer only showed low activity and low selectivity. However, upon the addition of carbon tetrachloride as halogen atom donor, a highly selective C–H photochlorination was observed (**Figure 22b-c**). Different unsubstituted aliphatic substrates with primary, secondary and tertiary C–H bonds were studied (**Figure 22c**) and the $[Fe(PDI)Cl_2]^+$ complexes appear to shift the reactivity towards primary C–H bond functionalization compared to $FeCl_3$. Furthermore, in the case of cyclohexene, chlorine addition was favored compared to C–H activation.

The reaction scope was then further expanded by replacing the halogen atom donor carbon tetrachloride (CCl_4) by bromotrichloromethane ($BrCCl_3$) (**Figure 22e**). When $[Fe(PDI)Cl_2]^+$ was used as photosensitizer, C–H bromination was favored over chlorination, with an enhanced selectivity for more accessible C–H bonds. Control experiments using $FeCl_3$ led to significantly higher proportion of chlorinated products. This further highlighted that the main role of PDI photosensitizers was to generate an active Cl$^{\bullet}$|arene adduct whose purpose is to perform C–H activation of the substrate to give the corresponding radical that can be engaged in subsequent reactions. Overall, the proposed mechanism for selective C–H functionalization was suggested to involve the light-induced apical Fe–Cl bond cleavage to generate the reduced Fe^{II} center and chlorine radical, which is stabilized through a charge-transfer complex with the secondary coordination scaffold (**Figure 22d**). The chlorine radical is then able to perform C–H activation, yielding HCl and a hydrocarbon radical which is finally halogenated using a radical trap. The ground-state photosensitizer is then recuperated *via* a light-induced oxidation of Fe^{II} by the solvent (nitromethane) along with the addition of a chloride ligand. While the turnover numbers close to 1 imply a stoichiometric rather than a catalytic use of the Fe^{III} complex, this unique reactivity due to the formation of Cl$^{\bullet}$|arene adducts might serve as inspiration to tune the reactivity of radicals in light-driven photoredox catalysis not only with iron complexes.[297]

Finally, Fe^{III} porphyrins in combination to organic azides were recently used for the C(sp^3)–H amination and alkene aziridination with chemo- and regio- selectivity under blue light irradiation.[261] The work is based on seminal work by Newcomb and coworkers that focused on the generation of reactive iron-oxo species for C–H hydroxylation using visible light irradiation of porphyrin in the presence of perchlorate.[298] It was surmised that iron porphyrins with labile axial coordination sites could promote the nitrene C–H insertion and aziridination using organic azides. For that, the iron porphyrins are expected to serve both as photosensitizer as well as scavengers to capture free nitrene forming a reactive metal–nitrene / imido intermediate.

This challenging approach was first investigated using a series of iron porphyrins based on the archetypical tetraphenyl porphyrin ligand structure and introducing modifications on the four phenyl rings. The light driven C–H amination of indane with 3,5-bis(trifluoromethyl)phenyl azide proceeded at 25-35°C under blue LED irradiation with yields that ranged from 12 to 99% after 24 hours, with a fluorinated methylated aniline substituted iron porphyrin being the most effective catalyst (**Figure 23a**). The structure of this catalyst is shown as $[Fe(TF_4DMAP)]^+$ in **Figure 12**. The aziridination of *cis*- and *trans*-alkenes using 3,5-bis(trifluoromethyl)phenyl azide under photocatalytic conditions in the presence of molecular

sieves showed good stereoselectivity, giving *cis*-aziridines and *trans*-aziridines in 60% and 90% yield, respectively. This retention of the relative configuration points towards a mechanism occurring *via* a metal-nitrene intermediate rather that a free triplet nitrene.

A very comprehensive substrate scope was investigated and only a subset on this scope is presented herein (**Figure 23**). Using indane as substrate (**Figure 23a**), it was shown that multiple electron-withdrawing substituents (-CF_3, -F and -Cl) of aryl azides facilitated the intermolecular C–H amination with yields above 90%. Yields decreased when only one withdrawing substituent was introduced and reached less than 5% yield when electron-donating methoxy substituents were introduced. Using azide as the nitrene source, the reaction scope was extended to hydrocarbons such as ethylbenzene, tetralin, diphenylmethane, fluorene, xanthene, and isochromane to give the amination products in good to excellent yields (**Figure 23b**). When isopentylbenzene, was used as the substrate, the reaction took place regioselectively at the benzylic C–H bond over the tertiary C–H bond. This photochemical C–H amination was also applicable to allylic C–H bonds and enabled the photocatalytic C–H amination of tetrahydrofuran, unactivated C–H bonds and α-C–H bond of ketones. The intramolecular C–H amination of alkyl azides and the intramolecular C–H amination of α-azidoketones was also investigated with yields above 80% with cyclic substrates larger than azidocycloheptanone (**Figure 23d**). Finally, the versatility of this light-driven iron-catalyzed reaction was demonstrated in the late-stage functionalization of bioactive compounds (**Figure 23e**).

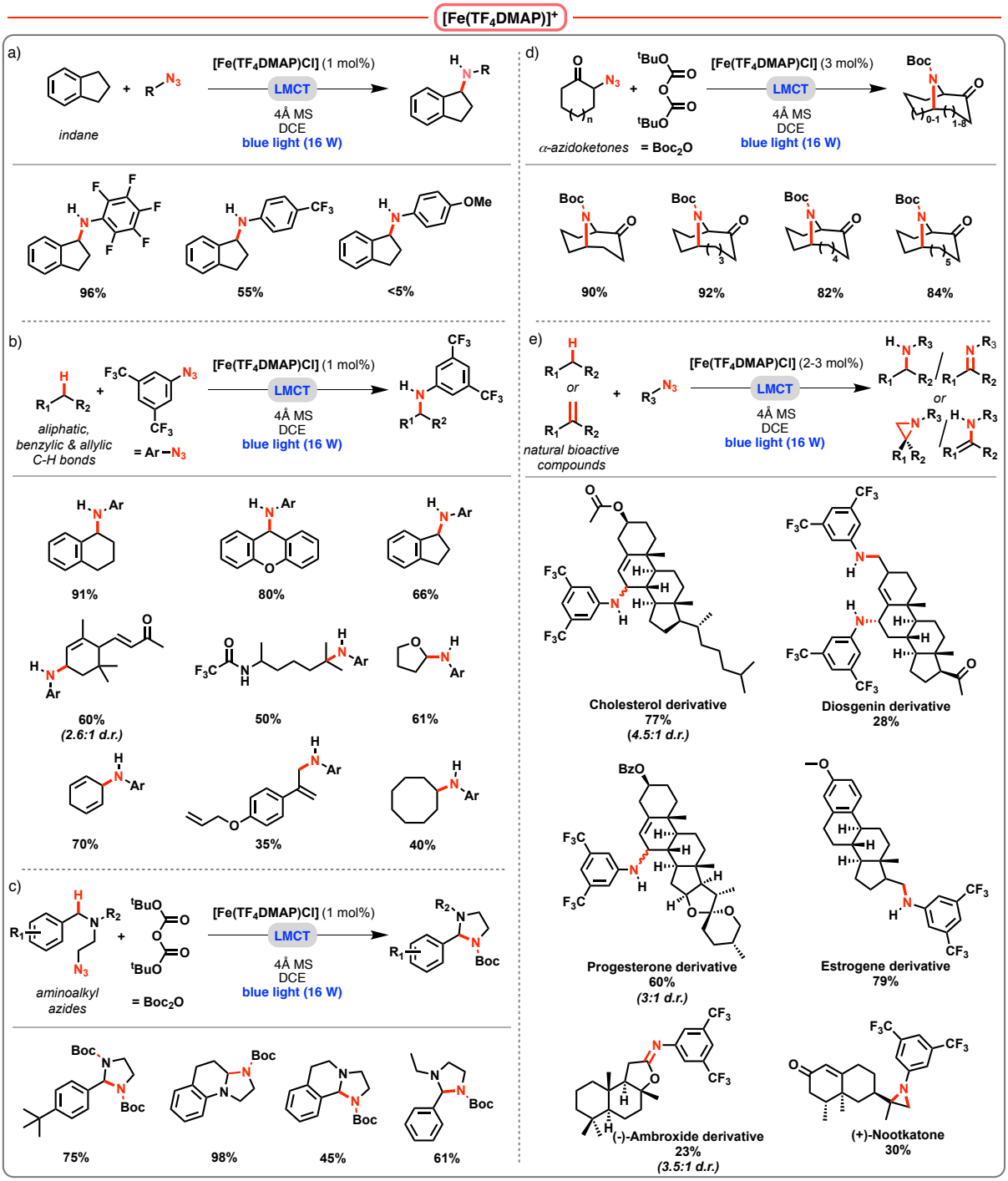


Figure 23. Light-driven functionalization with azides using an iron porphyrin photocatalyst.[261] a) Reaction of organic azides under photocatalytic conditions with indane derivatives. b) C–H amination with an organic azide under photocatalytic conditions. Intramolecular C–H amination of aminoalkyl azides (c) and a-azodoketones (d). e) Late stage functionalization of complex molecules. DCE = 1,2-dichloroethane, 4Å MS = molecular sieves.

Dissociative excited-states of hemes/non-hemes photosensitizers have also been widely used.[299-303] For example, Karlin and Meyer showed that a μ-oxo bridged heme/non-heme diiron complex was capable, under irradiation, to undergo photo-reduction and produce triphenylphosphine oxide by oxo-transfer.[300] The system could perform ~28 turnovers before degradation of the μ-oxo bridged diiron complex. This complex was also competent for

aromatic C–Cl bond cleavage. Nocera used bis-iron^{II}-μ-oxo Pacman porphyrin to perform the photocatalytic oxidation of hydrocarbons using oxygen. Upon visible light irradiation under an oxygen atmosphere, the Pacman porphyrin was able an oxidize fluorene, dihydroanthracene, diphenylmethane, cumene and toluene with turnover numbers between 76 and 287. Recently, Browne, Gruden and Drakshaprapu developed a non-Heme iron photocatalyst that was competent for the light-driven oxidation of methanol to formaldehyde.[260] The proposed mechanism for that transformation is represented in **Figure 24**. Through a series of spectroscopic measurements and density functional theory calculations, it was proposed that the irradiation of the (L)Fe^{III}-μO-Fe^{III}(L) non-heme complex led to the charge-transfer state that formed the corresponding (L)Fe^{IV}=O and (L)Fe^{II} species (L = 1,1-di(pyridine-2-yl)-*N,N*-bis(pyridine-2-ylmethyl)-ethan-1-amine). Under continuous irradiation in aerobic conditions, the (L)Fe^{IV}=O species was capable to perform methanol oxidation to formaldehyde with over 50 turnover in 150 minutes. The presence of O_2 was also shown to be crucial to close the catalytic cycle where light-induced oxidation of the Fe^{II} to the corresponding Fe^{III} state was achieved. The (L)Fe^{III}–OMe state undergo solvent exchange with water to form the (L)Fe^{III}–OH that was in equilibrium with (L)Fe^{III}-μO-Fe^{III}(L) to close the catalytic cycle. In contrast to the other examples with Fe^{II} and Fe^{III} discussed in this review, here an Fe^{IV} was suggested as photoactive catalyst for the substrate activation. Furthermore, this is a rare example for a formally overall three-photonic mechanism for one catalytic turnover.[18]

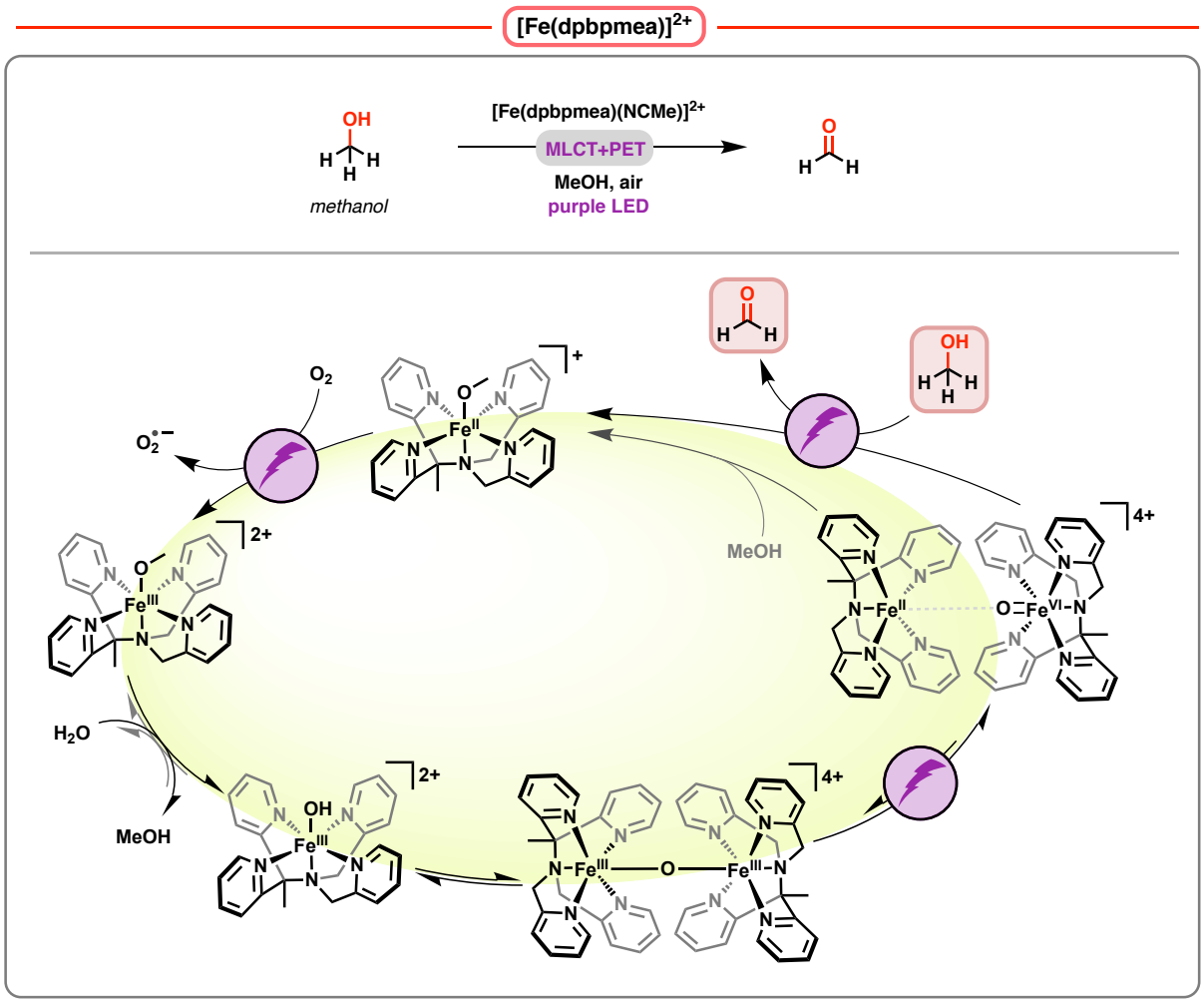


Figure 24. Light-driven aerobic oxidation of methanol to formaldehyde together with the proposed mechanism using a non-heme iron photocatalyst.[260]

4) Conclusions and Perspectives

This review presented the recent developments in the field of photoredox catalysis using *in situ* generated and well-defined iron photosensitizers. While early investigations with iron catalysts mainly focused on iron as transition-metal catalyst as well as light-induced or sensitized (pre)catalyst activation, in recent years, iron salts for the *in situ* generation of the photosensitizers are currently more employed than structurally well-defined photosensitizers.[220, 222, 238, 239, 304-311] Given the operational simplicity, cheap and straightforward possibilities to screen different precursors, it is unsurprising that this approach especially attracted the attention of synthetically oriented research groups within the photoredox community where the focus has mostly been placed on substrate scope and functional group tolerance (**section 2**), while the mechanistic details are often underexplored. More detailed mechanistic insights might help provide a better understanding of the elemental

steps at stake for these reactions and will undoubtedly guide further advances in the field. This could potentially help expand the applications beyond the dominant Giese-type reactions with different substrates to new classes of transformations. Hydrogen atom transfer catalysis initiated by $FeCl_3$ has received a lot of attention in recent years and first examples to combine iron photocatalysts with (photo-inactive) cocatalysts have already pointed out possible ways to broaden the scope of light-driven catalysis with iron salt precursors. As pointed out earlier, carboxylates or alkoxides as coordinated substrates can offer ways to generate radical intermediates with a better control over the spatial location of carbon-centered radicals compared to indirect C–H activation with chlorine radicals (section 2.1-2.2).[158-160, 187, 191, 204] A better mechanistic understanding would also be beneficial for the further development of metallaphotoredox and dual photocatalysis approaches, which offer synthetically great opportunities. Similar to investigations with nickel or cerium catalysis in photoredox catalysis,[124, 312] combined efforts of organic and spectroscopically oriented research groups could potentially help provide a good understanding of the synthetic opportunities and limitations as well as the essential steps of the reaction mechanism(s).

Note that several reports of photoredox catalysis using *in situ* generated iron photosensitizers have been published over the course of the reviewing process. These include light-induced decarboxylation reactions with ferrocene,[313] light-driven methane to ethane conversion,[314] dehydrogenative amidation,[315] reductive amidation,[316] aerobic propane oxidation,[317] enantioselective C-H amination,[318] photoelectrochemical hydrosilane and hydrogermane functionalization,[319] decarboxylative azidation with *in situ* generated iron catalyst,[320] enantioselective radical cation [2+2] and [4+2] cycloadditions,[321-323] new iron chloride induced HAT catalysis,[321, 322] dye-sensitized solar cells,[324] radical depolymerization[325] and are thus not detailed in the present review, but highlight the very vibrant field that is iron photoredox catalysis.

Using well-defined iron photosensitizers, the field is only at its infancy as progress in that area has only been possible through pioneering work that has allowed extending the excited-state lifetime of photosensitizer in the nanosecond timescale. Hence, only a handful of examples have been published since, where the emphasis has mostly been placed on mechanistic information rather than large substrate scope and functional group tolerance. Once again, the field might benefit from further collaborations between spectroscopy-oriented groups and synthetically oriented ones. At any rate, it is undoubtful that scientists active in the field and newcomers will continue their research endeavors dedicated to extending the excited-state lifetime of iron photosensitizers and tune their excited-state properties accordingly. Even if this

is highly desired for numerous mechanistic investigations, amongst others, seminal reports presented herein have established that even with sub-nanosecond charge transfer excited-state lifetimes, iron photosensitizers can operate as photosensitizers in diffusional reactivity for photoredox application in organic chemistry and solar fuel production. A key parameter to further extend the scope of targeted transformations will be to find ways to decrease geminate charge recombination and favor cage-escape in a variety of solvents. Hence, even if Ru^{II} and Ir^{III} photosensitizers are considered as photochemical warheads in the field of photoredox catalysis, the currently available $iron^{II/III}$ photosensitizers can already be considered as possible attractive alternatives. Similar to other first row transition metals,[51, 52, 96, 326-329] photoactive complexes in different oxidation states together with complementary photophysical properties and the very different possible activation modes investigated up to now – in the case of iron LMCT excited states, MLCT excited states and dissociative excited states and *in situ* substrate activation – indicate possibly even more versatile scope of applications for these metals in comparison to second and third row analogues thereof. Hence, there is no doubt that the development of iron photosensitizers in photoredox catalysis and solar fuel production will experience a drastic development in the coming decade and many will join on the way to the "holy grail".

Declaration of Competing Interest

The authors declare that they have no known competing financial interests or personal relationships that could have appeared to influence the work reported in this paper.

Acknowledgments

Financial support was provided to A.A. by the F.R.S.-FNRS (FRIA fellowship). L.T.-G. is a Chercheur Qualifié of the Fonds de la Recherche Scientifique – FNRS. A.A., B.E. and L.T.-G. gratefully acknowledge the UCLouvain for financial support. We also thank our diverse group of lab members for creating an environment that supports our scientific endeavors. F. G. thanks his (former) mentors O.S. Wenger and C. Kerzig for their support.

References

[1] G. Ciamician, Science, 36 (1912) 385-394.
[2] N.E.S. Tay, D. Lehnherr, T. Rovis, Chem. Rev., 122 (2022) 2487-2649.
[3] F. Strieth-Kalthoff, M.J. James, M. Teders, L. Pitzer, F. Glorius, Chem. Soc. Rev., 47 (2018) 7190-7202.
[4] M.D. Kärkäs, J.A. Porco, C.R.J. Stephenson, Chem. Rev., 116 (2016) 9683-9747.
[5] M.J. Genzink, J.B. Kidd, W.B. Swords, T.P. Yoon, Chem. Rev., 122 (2022) 1654-1716.
[6] P. Bellotti, H.-M. Huang, T. Faber, F. Glorius, Chem. Rev., (2023).
[7] M. Uji, T.J.B. Zähringer, C. Kerzig, N. Yanai, Angew. Chem. Int. Ed., n/a e202301506.
[8] C.B. Larsen, O.S. Wenger, Chem-Eur. J., 24 (2018) 2039-2058.
[9] F. Glaser, O.S. Wenger, Coord. Chem. Rev., 405 (2020) 213129.
[10] F. Glaser, C. Kerzig, O.S. Wenger, Angew. Chem. Int. Ed., 59 (2020) 10266-10284.
[11] B. Xu, L. Troian-Gautier, R. Dykstra, R.T. Martin, O. Gutierrez, U.K. Tambar, J. Am. Chem. Soc., 142 (2020) 6206-6215.
[12] A. Ripak, S. De Kreijger, R.N. Sampaio, C.A. Vincent, É. Cauët, I. Jabin, U.K. Tambar, B. Elias, L. Troian-Gautier, Chem Catal., (2023) 100490.
[13] G. Ciamician, P. Silber, Ber. Dtsch. Chem. Ges., 41 (1908) 1071-1080.
[14] A. Srikrishna, S.S.V. Ramasastry, Tetrahedron Lett., 46 (2005) 7373-7376.
[15] A. Srikrishna, S.S.V. Ramasastry, Tetrahedron Lett., 47 (2006) 335-339.
[16] J.D. Winkler, R.D. Scott, P.G. Williard, J. Am. Chem. Soc., 112 (1990) 8971-8975.
[17] J.D. Winkler, J.M. Axten, J. Am. Chem. Soc., 120 (1998) 6425-6426.
[18] L. Næsborg, C. Jandl, A. Zech, T. Bach, Angew. Chem. Int. Ed., 59 (2020) 5656-5659.
[19] Z. Lu, T.P. Yoon, Angew. Chem. Int. Ed., 51 (2012) 10329-10332.
[20] D. Sarkar, N. Bera, S. Ghosh, Eur. J. Org. Chem., 2020 (2020) 1310-1326.
[21] C.K. Prier, D.A. Rankic, D.W.C. MacMillan, Chem. Rev., 113 (2013) 5322-5363.
[22] L. Marzo, S.K. Pagire, O. Reiser, B. König, Angew. Chem. Int. Ed., 57 (2018) 10034-10072.
[23] S. Zhang, X. Yang, Y. Numata, L. Han, Energ. Environ. Sci., 6 (2013) 1443-1464.
[24] E.S. Andreiadis, M. Chavarot-Kerlidou, M. Fontecave, V. Artero, Photochem. Photobiol., 87 (2011) 946-964.
[25] B. Elias, A. Kirsch-De Mesmaeker, Coord. Chem. Rev., 250 (2006) 1627-1641.
[26] F.E. Poynton, S.A. Bright, S. Blasco, D.C. Williams, J.M. Kelly, T. Gunnlaugsson, Chem. Soc. Rev., 46 (2017) 7706-7756.
[27] H. Cano-Yelo, A. Deronzier, J. Chem. Soc. Perk. T. 2, (1984) 1093-1098.
[28] H. Cano-Yelo, A. Deronzier, J. Photochem., 37 (1987) 315-321.
[29] H. Hennig, D. Rehorek, De Gruyter, Berlin, Boston, 1987.
[30] A. Juris, V. Balzani, F. Barigelletti, S. Campagna, P. Belser, A. von Zelewsky, Coord. Chem. Rev., 84 (1988) 85-277.
[31] F. Barigelletti, A. Juris, V. Balzani, P. Belser, A. Von Zelewsky, Inorg. Chem., 22 (1983) 3335-3339.
[32] J.R. Lakowicz, Principles of Fluorescence Spectroscopy, Springer US, New York, 2006.
[33] D. Rehm, A. Weller, Berich. Bunsen. Gesell., 73 (1969) 834-839.
[34] J.W. Verhoeven, Pure Appl. Chem., 68 (1996) 2223-2286.
[35] J.-H. Shon, T.S. Teets, Comment. Inorg. Chem., 40 (2020) 53-85.
[36] R. Bevernaegie, S.A.M. Wehlin, B. Elias, L. Troian-Gautier, ChemPhotoChem, 5 (2021) 217-234.
[37] N.A. Romero, D.A. Nicewicz, Chem. Rev., 116 (2016) 10075-10166.
[38] D.A. Nicewicz, D.W.C. MacMillan, Science, 322 (2008) 77-80.

[39] I.A. MacKenzie, L. Wang, N.P.R. Onuska, O.F. Williams, K. Begam, A.M. Moran, B.D. Dunietz, D.A. Nicewicz, Nature, 580 (2020) 76-80.
[40] A. Joshi-Pangu, F. Lévesque, H.G. Roth, S.F. Oliver, L.-C. Campeau, D. Nicewicz, D.A. DiRocco, J. Org. Chem., 81 (2016) 7244-7249.
[41] C.A. Vincent, M.I. Chiriac, L. Troian-Gautier, U.K. Tambar, ACS Catal., (2023) 3668-3675.
[42] A. Tlili, S. Lakhdar, Angew. Chem. Int. Ed., 60 (2021) 19526-19549.
[43] C. Fischer, C. Kerzig, B. Zilate, O.S. Wenger, C. Sparr, ACS Catal., 10 (2020) 210-215.
[44] E. Speckmeier, T.G. Fischer, K. Zeitler, J. Am. Chem. Soc., 140 (2018) 15353-15365.
[45] O.S. Wenger, Nature Chem., 12 (2020) 323-324.
[46] C. Förster, K. Heinze, Chem. Soc. Rev., 49 (2020) 1057-1070.
[47] O.S. Wenger, J. Am. Chem. Soc., 140 (2018) 13522-13533.
[48] L.A. Büldt, O.S. Wenger, Angew. Chem. Int. Ed., 56 (2017) 5676-5682.
[49] Y. Zhang, J.L. Petersen, C. Milsmann, J. Am. Chem. Soc., 138 (2016) 13115-13118.
[50] Y. Zhang, T.S. Lee, J.M. Favale, D.C. Leary, J.L. Petersen, G.D. Scholes, F.N. Castellano, C. Milsmann, Nature Chem., 12 (2020) 345-352.
[51] J. Beaudelot, S. Oger, S. Peruško, T.-A. Phan, T. Teunens, C. Moucheron, G. Evano, Chem. Rev., 122 (2022) 16365-16609.
[52] N. Sinha, O.S. Wenger, J. Am. Chem. Soc., 145 (2023) 4903-4920.
[53] W. Zhang, K.S. Kjær, R. Alonso-Mori, U. Bergmann, M. Chollet, L.A. Fredin, R.G. Hadt, R.W. Hartsock, T. Harlang, T. Kroll, K. Kubiček, H.T. Lemke, H.W. Liang, Y. Liu, M.M. Nielsen, P. Persson, J.S. Robinson, E.I. Solomon, Z. Sun, D. Sokaras, T.B. van Driel, T.-C. Weng, D. Zhu, K. Wärnmark, V. Sundström, K.J. Gaffney, Chem. Sci., 8 (2017) 515-523.
[54] H. Tatsuno, K.S. Kjær, K. Kunnus, T.C.B. Harlang, C. Timm, M. Guo, P. Chàbera, L.A. Fredin, R.W. Hartsock, M.E. Reinhard, S. Koroidov, L. Li, A.A. Cordones, O. Gordivska, O. Prakash, Y. Liu, M.G. Laursen, E. Biasin, F.B. Hansen, P. Vester, M. Christensen, K. Haldrup, Z. Németh, D. Sárosiné Szemes, É. Bajnóczi, G. Vankó, T.B. Van Driel, R. Alonso-Mori, J.M. Glownia, S. Nelson, M. Sikorski, H.T. Lemke, D. Sokaras, S.E. Canton, A.O. Dohn, K.B. Møller, M.M. Nielsen, K.J. Gaffney, K. Wärnmark, V. Sundström, P. Persson, J. Uhlig, Angew. Chem. Int. Ed., 59 (2020) 364-372.
[55] O. Prakash, P. Chábera, N.W. Rosemann, P. Huang, L. Häggström, T. Ericsson, D. Strand, P. Persson, J. Bendix, R. Lomoth, K. Wärnmark, Chem-Eur. J., 26 (2020) 12728-12732.
[56] Y. Liu, P. Persson, V. Sundström, K. Wärnmark, Acc. Chem. Res., 49 (2016) 1477-1485.
[57] Y. Liu, K.S. Kjær, L.A. Fredin, P. Chábera, T. Harlang, S.E. Canton, S. Lidin, J. Zhang, R. Lomoth, K.-E. Bergquist, P. Persson, K. Wärnmark, V. Sundström, Chem-Eur. J., 21 (2015) 3628-3639.
[58] Y. Liu, T. Harlang, S.E. Canton, P. Chábera, K. Suárez-Alcántara, A. Fleckhaus, D.A. Vithanage, E. Göransson, A. Corani, R. Lomoth, V. Sundström, K. Wärnmark, Chem. Commun., 49 (2013) 6412-6414.
[59] S. Kaufhold, N.W. Rosemann, P. Chábera, L. Lindh, I. Bolaño Losada, J. Uhlig, T. Pascher, D. Strand, K. Wärnmark, A. Yartsev, P. Persson, J. Am. Chem. Soc., 143 (2021) 1307-1312.
[60] T.C.B. Harlang, Y. Liu, O. Gordivska, L.A. Fredin, C.S. Ponseca Jr, P. Huang, P. Chábera, K.S. Kjaer, H. Mateos, J. Uhlig, R. Lomoth, R. Wallenberg, S. Styring, P. Persson, V. Sundström, K. Wärnmark, Nature Chem., 7 (2015) 883.
[61] P. Chábera, Y. Liu, O. Prakash, E. Thyrhaug, A.E. Nahhas, A. Honarfar, S. Essén, L.A. Fredin, T.C.B. Harlang, K.S. Kjær, K. Handrup, F. Ericson, H. Tatsuno, K. Morgan, J. Schnadt, L. Häggström, T. Ericsson, A. Sobkowiak, S. Lidin, P. Huang, S. Styring, J. Uhlig, J. Bendix, R. Lomoth, V. Sundström, P. Persson, K. Wärnmark, Nature, 543 (2017) 695-699.
[62] T.H. Bürgin, F. Glaser, O.S. Wenger, J. Am. Chem. Soc., 144 (2022) 14181-14194.

[63] S. Otto, M. Grabolle, C. Förster, C. Kreitner, U. Resch-Genger, K. Heinze, Angew. Chem. Int. Ed., 54 (2015) 11572-11576.
[64] F. Reichenauer, C. Wang, C. Förster, P. Boden, N. Ugur, R. Báez-Cruz, J. Kalmbach, L.M. Carrella, E. Rentschler, C. Ramanan, G. Niedner-Schatteburg, M. Gerhards, M. Seitz, U. Resch-Genger, K. Heinze, J. Am. Chem. Soc., 143 (2021) 11843-11855.
[65] O.S. Wenger, Chem-Eur. J., 25 (2019) 6043-6052.
[66] D.W. Fink, W.E. Ohnesorge, J. Am. Chem. Soc., 91 (1969) 4995-4998.
[67] J.P. Paris, W.W. Brandt, J. Am. Chem. Soc., 81 (1959) 5001-5002.
[68] C. Creutz, M. Chou, T.L. Netzel, M. Okumura, N. Sutin, J. Am. Chem. Soc., 102 (1980) 1309-1319.
[69] S. Decurtins, P. Gutlich, K.M. Hasselbach, A. Hauser, H. Spiering, Inorg. Chem., 24 (1985) 2174-2178.
[70] A. Hauser, Chem. Phys. Lett., 173 (1990) 507-512.
[71] C. Brady, J.J. McGarvey, J.K. McCusker, H. Toftlund, D.N. Hendrickson, Time-Resolved Relaxation Studies of Spin Crossover Systems in Solution, in: P. Gütlich, H.A. Goodwin (Eds.) Spin Crossover in Transition Metal Compounds III, Springer Berlin Heidelberg, Berlin, Heidelberg, 2004, pp. 1-22.
[72] J.K. McCusker, K.N. Walda, R.C. Dunn, J.D. Simon, D. Magde, D.N. Hendrickson, J. Am. Chem. Soc., 114 (1992) 6919-6920.
[73] A.L. Smeigh, M. Creelman, R.A. Mathies, J.K. McCusker, J. Am. Chem. Soc., 130 (2008) 14105-14107.
[74] H.R. Chang, J.K. McCusker, H. Toftlund, S.R. Wilson, A.X. Trautwein, H. Winkler, D.N. Hendrickson, J. Am. Chem. Soc., 112 (1990) 6814-6827.
[75] M.A. Bergkamp, B.S. Brunschwig, P. Gütlich, T.L. Netzel, N. Sutin, Chem. Phys. Lett., 81 (1981) 147-150.
[76] M.A. Bergkamp, C.K. Chang, T.L. Netzel, J. Phys. Chem, 87 (1983) 4441-4446.
[77] E.A. Juban, A.L. Smeigh, J.E. Monat, J.K. McCusker, Coord. Chem. Rev., 250 (2006) 1783-1791.
[78] A. Cannizzo, C.J. Milne, C. Consani, W. Gawelda, C. Bressler, F. van Mourik, M. Chergui, Coord. Chem. Rev., 254 (2010) 2677-2686.
[79] R. Englman, J. Jortner, Mol. Phys., 18 (1970) 145-164.
[80] J.K. McCusker, Science, 363 (2019) 484-488.
[81] L. Lindh, P. Chábera, N.W. Rosemann, J. Uhlig, K. Wärnmark, A. Yartsev, V. Sundström, P. Persson, Catalysts, 10 (2020) 315.
[82] S. Kaufhold, K. Wärnmark, Catalysts, 10 (2020) 132.
[83] P. Chábera, L. Lindh, N.W. Rosemann, O. Prakash, J. Uhlig, A. Yartsev, K. Wärnmark, V. Sundström, P. Persson, Coord. Chem. Rev., 426 (2021) 213517.
[84] P. Dierks, Y. Vukadinovic, M. Bauer, Inorg. Chem. Front., 9 (2022) 206-220.
[85] L.H.M. de Groot, A. Ilic, J. Schwarz, K. Wärnmark, J. Am. Chem. Soc., 145 (2023) 9369-9388.
[86] A.K. Pal, G.S. Hanan, Chem. Soc. Rev., 43 (2014) 6184-6197.
[87] I.M. Dixon, F. Alary, M. Boggio-Pasqua, J.-L. Heully, Dalton Trans., 44 (2015) 13498-13503.
[88] P. Chábera, K.S. Kjaer, O. Prakash, A. Honarfar, Y. Liu, L.A. Fredin, T.C.B. Harlang, S. Lidin, J. Uhlig, V. Sundström, R. Lomoth, P. Persson, K. Wärnmark, J. Phys. Chem. Lett., 9 (2018) 459-463.
[89] W. Leis, M.A. Argüello Cordero, S. Lochbrunner, H. Schubert, A. Berkefeld, Journal of the American Chemical Society, (2022).
[90] J.T. Malme, R.A. Clendening, R. Ash, T. Curry, T. Ren, J. Vura-Weis, J. Am. Chem. Soc., 145 (2023) 6029-6034.

[91] J.D. Braun, I.B. Lozada, C. Kolodziej, C. Burda, K.M.E. Newman, J. van Lierop, R.L. Davis, D.E. Herbert, Nature Chem., 11 (2019) 1144-1150.
[92] J. Steube, A. Kruse, O.S. Bokareva, T. Reuter, S. Demeshko, R. Schoch, M.A. Argüello Cordero, A. Krishna, S. Hohloch, F. Meyer, K. Heinze, O. Kühn, S. Lochbrunner, M. Bauer, Nature Chem., (2023).
[93] C.E. Johnson, J. Schwarz, M. Deegbey, O. Prakash, K. Sharma, P. Huang, T. Ericsson, L. Häggström, J. Bendix, A.K. Gupta, E. Jakubikova, K. Wärnmark, R. Lomoth, Chem. Sci., (2023).
[94] K.S. Kjær, N. Kaul, O. Prakash, P. Chábera, N.W. Rosemann, A. Honarfar, O. Gordivska, L.A. Fredin, K.-E. Bergquist, L. Häggström, T. Ericsson, L. Lindh, A. Yartsev, S. Styring, P. Huang, J. Uhlig, J. Bendix, D. Strand, V. Sundström, P. Persson, R. Lomoth, K. Wärnmark, Science, 363 (2019) 249-253.
[95] N.W. Rosemann, L. Lindh, I. Bolaño Losada, S. Kaufhold, O. Prakash, A. Ilic, J. Schwarz, K. Wärnmark, P. Chábera, A. Yartsev, P. Persson, Chem. Sci., 14 (2023) 3569-3579.
[96] F. Juliá, ChemCatChem, 14 (2022) e202200916.
[97] N.W. Dow, P.S. Pedersen, T.Q. Chen, D.C. Blakemore, A.-M. Dechert-Schmitt, T. Knauber, D.W.C. MacMillan, J. Am. Chem. Soc., 144 (2022) 6163-6172.
[98] S.K. Kariofillis, A.G. Doyle, Acc. Chem. Res., 54 (2021) 988-1000.
[99] S.I. Ting, S. Garakyaraghi, C.M. Taliaferro, B.J. Shields, G.D. Scholes, F.N. Castellano, A.G. Doyle, J. Am. Chem. Soc., 142 (2020) 5800-5810.
[100] R. Fayad, S. Engl, E.O. Danilov, C.E. Hauke, O. Reiser, F.N. Castellano, J. Phys. Chem. Lett., 11 (2020) 5345-5349.
[101] Y. Abderrazak, A. Bhattacharyya, O. Reiser, Angew. Chem. Int. Ed., 60 (2021) 21100-21115.
[102] C. Li, X.Y. Kong, Z.H. Tan, C.T. Yang, H.S. Soo, Chem. Phys. Rev., 3 (2022) 021303.
[103] A. Hossain, A. Bhattacharyya, O. Reiser, Science, 364 (2019) eaav9713.
[104] S. Ferrere, Chem. Mater., 12 (2000) 1083-1089.
[105] T.C. Motley, G.J. Meyer, NPG Asia Mater., 8 (2016) e261-e261.
[106] T.C.B. Harlang, Y. Liu, O. Gordivska, L.A. Fredin, C.S. Ponseca, P. Huang, P. Chábera, K.S. Kjaer, H. Mateos, J. Uhlig, R. Lomoth, R. Wallenberg, S. Styring, P. Persson, V. Sundström, K. Wärnmark, Nature Chem., 7 (2015) 883-889.
[107] S. Mukherjee, D.N. Bowman, E. Jakubikova, Inorg. Chem., 54 (2015) 560-569.
[108] S. Ferrere, B.A. Gregg, J. Am. Chem. Soc., 120 (1998) 843-844.
[109] T. Duchanois, T. Etienne, C. Cebrián, L. Liu, A. Monari, M. Beley, X. Assfeld, S. Haacke, P.C. Gros, Eur. J. Inorg. Chem., 2015 (2015) 2469-2477.
[110] T. Duchanois, L. Liu, M. Pastore, A. Monari, C. Cebrián, Y. Trolez, M. Darari, K. Magra, A. Francés-Monerris, E. Domenichini, M. Beley, X. Assfeld, S. Haacke, P.C. Gros, Inorganics, 6 (2018) 63.
[111] A.R. Marri, E. Marchini, V.D. Cabanes, R. Argazzi, M. Pastore, S. Caramori, C.A. Bignozzi, P.C. Gros, Chem-Eur. J., 27 (2021) 16260-16269.
[112] E. Marchini, M. Darari, L. Lazzarin, R. Boaretto, R. Argazzi, C.A. Bignozzi, P.C. Gros, S. Caramori, Chem. Commun., 56 (2020) 543-546.
[113] A. Reddy Marri, E. Marchini, V.D. Cabanes, R. Argazzi, M. Pastore, S. Caramori, P.C. Gros, J. Mater. Chem. A, 9 (2021) 3540-3554.
[114] X. Wu, Z. Ma, T. Feng, C. Zhu, Chem. Soc. Rev., 50 (2021) 11577-11613.
[115] L. Pitzer, F. Sandfort, F. Strieth-Kalthoff, F. Glorius, J. Am. Chem. Soc., 139 (2017) 13652-13655.
[116] P.S. Engl, A.P. Häring, F. Berger, G. Berger, A. Pérez-Bitrián, T. Ritter, J. Am. Chem. Soc., 141 (2019) 13346-13351.
[117] J.W. Beatty, J.J. Douglas, K.P. Cole, C.R.J. Stephenson, Nature Comm., 6 (2015) 7919.

[118] J.P. Barham, B. König, Angew. Chem. Int. Ed., 59 (2020) 11732-11747.
[119] S. Wu, J. Kaur, T.A. Karl, X. Tian, J.P. Barham, Angew. Chem. Int. Ed., 61 (2022) e202107811.
[120] J. Liu, L. Lu, D. Wood, S. Lin, ACS Cent. Sci., 6 (2020) 1317-1340.
[121] L. Capaldo, D. Ravelli, Eur. J. Org. Chem., 2017 (2017) 2056-2071.
[122] F. Juliá, T. Constantin, D. Leonori, Chem. Rev., 122 (2022) 2292-2352.
[123] D. Birnthaler, R. Narobe, E. Lopez-Berguno, C. Haag, B. König, ACS Catal., 13 (2023) 1125-1132.
[124] A.Y. Chan, I.B. Perry, N.B. Bissonnette, B.F. Buksh, G.A. Edwards, L.I. Frye, O.L. Garry, M.N. Lavagnino, B.X. Li, Y. Liang, E. Mao, A. Millet, J.V. Oakley, N.L. Reed, H.A. Sakai, C.P. Seath, D.W.C. MacMillan, Chem. Rev., 122 (2022) 1485-1542.
[125] Y. Qiao, E.J. Schelter, Acc. Chem. Res., 51 (2018) 2926-2936.
[126] Z. Xie, P. Li, Y. Hu, N. Xu, L. Wang, Org. Biomol. Chem., 15 (2017) 4205-4211.
[127] Y. Ma, H. Luo, L. Lin, Org. Lett., 25 (2023) 3492-3496.
[128] A. Hossain, A. Bhattacharyya, O. Reiser, Science, 364 (2019) eaav9713.
[129] T.P. Nicholls, A.C. Bissember, Tetrahedron Lett., 60 (2019) 150883.
[130] P. Xu, P. López-Rojas, T. Ritter, J. Am. Chem. Soc., 143 (2021) 5349-5354.
[131] J.-J. Guo, A. Hu, Y. Chen, J. Sun, H. Tang, Z. Zuo, Angew. Chem. Int. Ed., 55 (2016) 15319-15322.
[132] L. Chang, Q. An, L. Duan, K. Feng, Z. Zuo, Chem. Rev., 122 (2022) 2429-2486.
[133] S. Gavelle, M. Innocent, T. Aubineau, A. Guérinot, Adv. Synth. Catal., 364 (2022) 4189-4230.
[134] R.C. Paul, R.C. Narula, S.K. Vasisht, Trans. Metal Chem., 3 (1978) 35-38.
[135] J. Catterick, P. Thornton, Structures and Physical Properties of Polynuclear Carboxylates, in: H.J. Emeléus, A.G. Sharpe (Eds.) Advances in Inorganic Chemistry and Radiochemistry, Academic Press, 1977, pp. 291-362.
[136] R.K. Cannan, A. Kibrick, J. Am. Chem. Soc., 60 (1938) 2314-2320.
[137] J.D. Griffin, M.A. Zeller, D.A. Nicewicz, J. Am. Chem. Soc., 137 (2015) 11340-11348.
[138] L. Candish, M. Freitag, T. Gensch, F. Glorius, Chem. Sci., 8 (2017) 3618-3622.
[139] H. Yang, C. Tian, D. Qiu, H. Tian, G. An, G. Li, Org. Chem. Front., 6 (2019) 2365-2370.
[140] X.-Q. Hu, Z.-K. Liu, Y.-X. Hou, Y. Gao, iScience, 23 (2020) 101266.
[141] Q.Y. Li, S.N. Gockel, G.A. Lutovsky, K.S. DeGlopper, N.J. Baldwin, M.W. Bundesmann, J.W. Tucker, S.W. Bagley, T.P. Yoon, Nature Chem., 14 (2022) 94-99.
[142] G. Feng, X. Wang, J. Jin, Eur. J. Org. Chem., 2019 (2019) 6728-6732.
[143] Z. Li, X. Wang, S. Xia, J. Jin, Org. Lett., 21 (2019) 4259-4265.
[144] S. Xia, K. Hu, C. Lei, J. Jin, Org. Lett., 22 (2020) 1385-1389.
[145] Y. Zhang, J. Qian, M. Wang, Y. Huang, P. Hu, Org. Lett., 24 (2022) 5972-5976.
[146] S. Akira, Y. Tetsuo, Chem. Lett., 15 (1986) 409-412.
[147] S. Akira, Y. Tetsuo, B. Chem. Soc. Jpn., 59 (1986) 3911-3915.
[148] S.-F. Wang, X.-P. Cao, Y. Li, Angew. Chem. Int. Ed., 56 (2017) 13809-13813.
[149] F.-F. Tan, X.-Y. He, W.-F. Tian, Y. Li, Nature Comm., 11 (2020) 6126.
[150] I.B. Seiple, S. Su, R.A. Rodriguez, R. Gianatassio, Y. Fujiwara, A.L. Sobel, P.S. Baran, J. Am. Chem. Soc., 132 (2010) 13194-13196.
[151] T.Q. Chen, P.S. Pedersen, N.W. Dow, R. Fayad, C.E. Hauke, M.C. Rosko, E.O. Danilov, D.C. Blakemore, A.-M. Dechert-Schmitt, T. Knauber, F.N. Castellano, D.W.C. MacMillan, J. Am. Chem. Soc., 144 (2022) 8296-8305.
[152] J. Chateauneuf, J. Lusztyk, K.U. Ingold, J. Am. Chem. Soc., 110 (1988) 2886-2893.
[153] J.W. Hilborn, J.A. Pincock, J. Am. Chem. Soc., 113 (1991) 2683-2686.
[154] A. Fawcett, J. Pradeilles, Y. Wang, T. Mutsuga, E.L. Myers, V.K. Aggarwal, Science, 357 (2017) 283-286.

[155] W.-M. Cheng, R. Shang, B. Zhao, W.-L. Xing, Y. Fu, Org. Lett., 19 (2017) 4291-4294.
[156] L. Candish, M. Teders, F. Glorius, J. Am. Chem. Soc., 139 (2017) 7440-7443.
[157] H.G. Yayla, H. Wang, K.T. Tarantino, H.S. Orbe, R.R. Knowles, J. Am. Chem. Soc., 138 (2016) 10794-10797.
[158] T. Xue, Z. Zhang, R. Zeng, Org. Lett., 24 (2022) 977-982.
[159] K. Wang, R. Zeng, Org. Chem. Front., 9 (2022) 3692-3696.
[160] Q. Wu, W. Liu, M. Wang, Y. Huang, P. Hu, Chem. Commun., 58 (2022) 9886-9889.
[161] W.-M. Zhang, K.-W. Feng, R.-G. Hu, Y.-J. Guo, Y. Li, Chem, 9 (2023) 430-442.
[162] Z. Zhang, G. Zhang, N. Xiong, T. Xue, J. Zhang, L. Bai, Q. Guo, R. Zeng, Org. Lett., 23 (2021) 2915-2920.
[163] A. Hu, J.-J. Guo, H. Pan, Z. Zuo, Science, 361 (2018) 668-672.
[164] A. Hu, J.-J. Guo, H. Pan, H. Tang, Z. Gao, Z. Zuo, J. Am. Chem. Soc., 140 (2018) 1612-1616.
[165] A. Hu, Y. Chen, J.-J. Guo, N. Yu, Q. An, Z. Zuo, J. Am. Chem. Soc., 140 (2018) 13580-13585.
[166] K. Zhang, L. Chang, Q. An, X. Wang, Z. Zuo, J. Am. Chem. Soc., 141 (2019) 10556-10564.
[167] S. Rohe, A.O. Morris, T. McCallum, L. Barriault, Angew. Chem. Int. Ed., 57 (2018) 15664-15669.
[168] W. Guo, Q. Wang, J. Zhu, Chem. Soc. Rev., 50 (2021) 7359-7377.
[169] S. Bonciolini, T. Noël, L. Capaldo, Eur. J. Org. Chem., 2022 (2022) e202200417.
[170] L. Capaldo, D. Ravelli, M. Fagnoni, Chem. Rev., 122 (2022) 1875-1924.
[171] D.P. Schwinger, M.T. Peschel, T. Rigotti, P. Kabaciński, T. Knoll, E. Thyrhaug, G. Cerullo, J. Hauer, R. de Vivie-Riedle, T. Bach, J. Am. Chem. Soc., 144 (2022) 18927-18937.
[172] Q. An, Y.-Y. Xing, R. Pu, M. Jia, Y. Chen, A. Hu, S.-Q. Zhang, N. Yu, J. Du, Y. Zhang, J. Chen, W. Liu, X. Hong, Z. Zuo, J. Am. Chem. Soc., 145 (2023) 359-376.
[173] S.M. Treacy, T. Rovis, J. Am. Chem. Soc., 143 (2021) 2729-2735.
[174] H. Na, M.B. Watson, F. Tang, N.P. Rath, L.M. Mirica, Chem. Commun., 57 (2021) 7264-7267.
[175] P. Lian, W. Long, J. Li, Y. Zheng, X. Wan, Angew. Chem. Int. Ed., 59 (2020) 23603-23608.
[176] R. Sang, W. Han, H. Zhang, C.M. Saunders, A. Noble, V.K. Aggarwal, J. Am. Chem. Soc., 145 (2023) 15207-15217.
[177] G. Wang, L. Gao, Y. Feng, L. Lin, Org. Lett., 25 (2023) 4340-4344.
[178] Q. An, Z. Wang, Y. Chen, X. Wang, K. Zhang, H. Pan, W. Liu, Z. Zuo, J. Am. Chem. Soc., 142 (2020) 6216-6226.
[179] P. Li, A.M. Deetz, J. Hu, G.J. Meyer, K. Hu, J. Am. Chem. Soc., 144 (2022) 17604-17610.
[180] C.-Y. Huang, J. Li, C.-J. Li, Nature Comm., 12 (2021) 4010.
[181] S. Rohe, A.O. Morris, T. McCallum, L. Barriault, Angew. Chem. Int. Ed., 57 (2018) 15664-15669.
[182] K. Ohkubo, A. Fujimoto, S. Fukuzumi, Chem. Commun., 47 (2011) 8515-8517.
[183] Y.C. Kang, S.M. Treacy, T. Rovis, Synlett, 32 (2021) 1767-1771.
[184] Y.C. Kang, S.M. Treacy, T. Rovis, ACS Catal., 11 (2021) 7442-7449.
[185] Y. Jin, Q. Zhang, L. Wang, X. Wang, C. Meng, C. Duan, Green Chem., 23 (2021) 6984-6989.
[186] Q. Zhang, S. Liu, J. Lei, Y. Zhang, C. Meng, C. Duan, Y. Jin, Org. Lett., 24 (2022) 1901-1906.
[187] Z. Jue, Y. Huang, J. Qian, P. Hu, ChemSusChem, 15 (2022) e202201241.

[188] X. Wu, H. Zhang, N. Tang, Z. Wu, D. Wang, M. Ji, Y. Xu, M. Wang, C. Zhu, Nature Comm., 9 (2018) 3343.
[189] X. Wu, M. Wang, L. Huan, D. Wang, J. Wang, C. Zhu, Angew. Chem. Int. Ed., 57 (2018) 1640-1644.
[190] G.-X. Li, X. Hu, G. He, G. Chen, Chem. Sci., 10 (2019) 688-693.
[191] N. Xiong, Y. Li, R. Zeng, Org. Lett., 23 (2021) 8968-8972.
[192] Z.-Y. Dai, S.-Q. Zhang, X. Hong, P.-S. Wang, L.-Z. Gong, Chem Catal., 2 (2022) 1211-1222.
[193] Y. Jin, L. Wang, Q. Zhang, Y. Zhang, Q. Liao, C. Duan, Green Chem., 23 (2021) 9406-9411.
[194] B. Niu, K. Sachidanandan, M.V. Cooke, T.E. Casey, S. Laulhé, Org. Lett., 24 (2022) 4524-4529.
[195] Z.-T. Pan, L.-M. Shen, F.W. Dagnaw, J.-J. Zhong, J.-X. Jian, Q.-X. Tong, Chem. Commun., 59 (2023) 1637-1640.
[196] J.-L. Tu, A.-M. Hu, L. Guo, W. Xia, J. Am. Chem. Soc., (2023).
[197] E.T. McBee, H.B. Hass, C.M. Neher, H. Strickland, Ind. End. Chem., 34 (1942) 296-300.
[198] G.A. Russell, J. Am. Chem. Soc., 80 (1958) 4987-4996.
[199] W. Liu, Q. Wu, M. Wang, Y. Huang, P. Hu, Org. Lett., 23 (2021) 8413-8418.
[200] G. Zhang, Z. Zhang, R. Zeng, Chin. J. Chem., 39 (2021) 3225-3230.
[201] A. Chinchole, M.A. Henriquez, D. Cortes-Arriagada, A.R. Cabrera, O. Reiser, ACS Catal., 12 (2022) 13549-13554.
[202] J.-J. Tang, X. Yu, Y. Wang, Y. Yamamoto, M. Bao, Angew. Chem. Int. Ed., 60 (2021) 16426-16435.
[203] Y.-K. Mei, X.-T. Min, S.-Y. Guo, C.-H. Liu, X.-X. Zhang, D.-W. Ji, B. Wan, Q.-A. Chen, Eur. J. Org. Chem., 2022 (2022) e202200043.
[204] X.-J. Wei, I. Abdiaj, C. Sambiagio, C. Li, E. Zysman-Colman, J. Alcázar, T. Noël, Angew. Chem. Int. Ed., 58 (2019) 13030-13034.
[205] S. Oh, E.E. Stache, J. Am. Chem. Soc., 144 (2022) 5745-5749.
[206] M. Wang, J. Wen, Y. Huang, P. Hu, ChemSusChem, 14 (2021) 5049-5056.
[207] Y.-C. Lu, J.G. West, Angew. Chem. Int. Ed., 62 (2023) e202213055.
[208] M. Zhang, J. Zhang, Q. Li, Y. Shi, Nature Comm., 13 (2022) 7880.
[209] K.-J. Bian, S.-C. Kao, D. Nemoto, X.-W. Chen, J.G. West, Nature Comm., 13 (2022) 7881.
[210] C.-L. Zhu, C. Wang, Q.-X. Qin, S. Yruegas, C.D. Martin, H. Xu, ACS Catal., 8 (2018) 5032-5037.
[211] C.S. Day, A. Fawcett, R. Chatterjee, J.F. Hartwig, J. Am. Chem. Soc., 143 (2021) 16184-16196.
[212] S.-J. Shen, C.-L. Zhu, D.-F. Lu, H. Xu, ACS Catal., 8 (2018) 4473-4482.
[213] S. Makai, E. Falk, B. Morandi, J. Am. Chem. Soc., 142 (2020) 21548-21555.
[214] L. Ge, M.-F. Chiou, Y. Li, H. Bao, Green Synthesis and Catalysis, 1 (2020) 86-120.
[215] A. Hossain, A. Vidyasagar, C. Eichinger, C. Lankes, J. Phan, J. Rehbein, O. Reiser, Angew. Chem. Int. Ed., 57 (2018) 8288-8292.
[216] G. Fumagalli, P.T.G. Rabet, S. Boyd, M.F. Greaney, Angew. Chem. Int. Ed., 54 (2015) 11481-11484.
[217] O.M. Kuzmina, A.K. Steib, A. Moyeux, G. Cahiez, P. Knochel, Synthesis, 47 (2015) 1696-1705.
[218] A. Guérinot, J. Cossy, Iron-Catalyzed C–C Cross-Couplings Using Organometallics, in: A. Correa (Ed.) Ni- and Fe-Based Cross-Coupling Reactions, Springer International Publishing, Cham, 2017, pp. 265-338.
[219] A. Piontek, E. Bisz, M. Szostak, Angew. Chem. Int. Ed., 57 (2018) 11116-11128.

[220] M. Neumeier, U. Chakraborty, D. Schaarschmidt, V. de la Pena O'Shea, R. Perez-Ruiz, A. Jacobi von Wangelin, Angew. Chem. Int. Ed., 59 (2020) 13473-13478.
[221] H. Rao, L.C. Schmidt, J. Bonin, M. Robert, Nature, 548 (2017) 74-77.
[222] X.-H. Ouyang, Y. Li, R.-J. Song, M. Hu, S. Luo, J.-H. Li, Sci. Adv., 5 (2019) eaav9839.
[223] N. Xiong, Y. Li, R. Zeng, ACS Catal., 13 (2023) 1678-1685.
[224] W. Zhao, R.P. Wurz, J.C. Peters, G.C. Fu, J. Am. Chem. Soc., 139 (2017) 12153-12156.
[225] J.-L. Tu, H. Gao, M. Luo, L. Zhao, C. Yang, L. Guo, W. Xia, Green Chem., 24 (2022) 5553-5558.
[226] S. Dadashi-Silab, K. Kim, F. Lorandi, D.J. Schild, M. Fantin, K. Matyjaszewski, Polymer Chemistry, 13 (2022) 1059-1066.
[227] S. Li, B. Zhu, R. Lee, B. Qiao, Z. Jiang, Org. Chem. Front., 5 (2018) 380-385.
[228] B. Huang, Y. Li, C. Yang, W. Xia, Green Chem., 22 (2020) 2804-2809.
[229] M.N. Sanabria, M.M. Hornink, V.G. Correia, L.H. Andrade, Org. Process Res. Dev., 24 (2020) 2288-2297.
[230] J. Prousek, Pure Appl. Chem., 79 (2007) 2325-2338.
[231] L. Clarizia, D. Russo, I. Di Somma, R. Marotta, R. Andreozzi, Applied Catalysis B: Environmental, 209 (2017) 358-371.
[232] J. Macías-Sánchez, L. Hinojosa-Reyes, J.L. Guzmán-Mar, J.M. Peralta-Hernández, A. Hernández-Ramírez, Photochem. Photobio. Sci., 10 (2011) 332-337.
[233] S. Hussain, E. Aneggi, D. Goi, Environmental Chemistry Letters, 19 (2021) 2405-2424.
[234] Z. Luo, Y. Meng, X. Gong, J. Wu, Y. Zhang, L.-W. Ye, C. Zhu, Chin. J. Chem., 38 (2020) 173-177.
[235] J.-H. Ye, M. Miao, H. Huang, S.-S. Yan, Z.-B. Yin, W.-J. Zhou, D.-G. Yu, Angew. Chem. Int. Ed., 56 (2017) 15416-15420.
[236] S. Dadashi-Silab, X. Pan, K. Matyjaszewski, Macromolecules, 50 (2017) 7967-7977.
[237] S. Dadashi-Silab, K. Matyjaszewski, ACS Macro Lett., 8 (2019) 1110-1114.
[238] J. Zhang, D. Campolo, F. Dumur, P. Xiao, J.P. Fouassier, D. Gigmes, J. Lalevée, ChemCatChem, 8 (2016) 2227-2233.
[239] J. Zhang, D. Campolo, F. Dumur, P. Xiao, J.P. Fouassier, D. Gigmes, J. Lalevée, J. Polym. Sci., Part A: Polym. Chem., 53 (2015) 42-49.
[240] L.L. Jamula, A.M. Brown, D. Guo, J.K. McCusker, Inorg. Chem., 53 (2014) 15-17.
[241] S.M. Fatur, S.G. Shepard, R.F. Higgins, M.P. Shores, N.H. Damrauer, J. Am. Chem. Soc., 139 (2017) 4493-4505.
[242] M.D. Woodhouse, J.K. McCusker, J. Am. Chem. Soc., 142 (2020) 16229-16233.
[243] M. Darari, A. Francés-Monerris, B. Marekha, A. Doudouh, E. Wenger, A. Monari, S. Haacke, P.C. Gros, Molecules, 25 (2020) 5991.
[244] A.K.C. Mengel, C. Förster, A. Breivogel, K. Mack, J.R. Ochsmann, F. Laquai, V. Ksenofontov, K. Heinze, Chem-Eur. J., 21 (2015) 704-714.
[245] C. Förster, M. Dorn, T. Reuter, S. Otto, G. Davarci, T. Reich, L. Carrella, E. Rentschler, K. Heinze, Inorganics, 6 (2018) 86.
[246] P. Dierks, A. Kruse, O.S. Bokareva, M.J. Al-Marri, J. Kalmbach, M. Baltrun, A. Neuba, R. Schoch, S. Hohloch, K. Heinze, M. Seitz, O. Kühn, S. Lochbrunner, M. Bauer, Chem. Commun., 57 (2021) 6640-6643.
[247] P. Dierks, A. Kruse, O.S. Bokareva, M.J. Al-Marri, J. Kalmbach, M. Baltrun, A. Neuba, R. Schoch, S. Hohloch, K. Heinze, M. Seitz, O. Kühn, S. Lochbrunner, M. Bauer, Chem. Commun., 59 (2023) 2990-2990.
[248] B.C. Paulus, S.L. Adelman, Lindsey L. Jamula, James K. McCusker, Nature, 582 (2020) 214-218.
[249] J. Steube, L. Burkhardt, A. Päpcke, J. Moll, P. Zimmer, R. Schoch, C. Wölper, K. Heinze, S. Lochbrunner, M. Bauer, Chem-Eur. J., 25 (2019) 11826-11830.

[250] W. Leis, M.A. Argüello Cordero, S. Lochbrunner, H. Schubert, A. Berkefeld, J. Am. Chem. Soc., 144 (2022) 1169-1173.
[251] T. Reuter, A. Kruse, R. Schoch, S. Lochbrunner, M. Bauer, K. Heinze, Chem. Commun., 57 (2021) 7541-7544.
[252] M. Darari, E. Domenichini, A. Francés-Monerris, C. Cebrián, K. Magra, M. Beley, M. Pastore, A. Monari, X. Assfeld, S. Haacke, P.C. Gros, Dalton Trans., 48 (2019) 10915-10926.
[253] L.A. Fredin, M. Pápai, E. Rozsályi, G. Vankó, K. Wärnmark, V. Sundström, P. Persson, J. Phys. Chem. Lett., 5 (2014) 2066-2071.
[254] P. Dierks, A. Päpcke, O.S. Bokareva, B. Altenburger, T. Reuter, K. Heinze, O. Kühn, S. Lochbrunner, M. Bauer, Inorg. Chem., 59 (2020) 14746-14761.
[255] L. Liu, T. Duchanois, T. Etienne, A. Monari, M. Beley, X. Assfeld, S. Haacke, P.C. Gros, Phys. Chem. Chem. Phys., 18 (2016) 12550-12556.
[256] A. Aydogan, R.E. Bangle, A. Cadranel, M.D. Turlington, D.T. Conroy, E. Cauët, M.L. Singleton, G.J. Meyer, R.N. Sampaio, B. Elias, L. Troian-Gautier, J. Am. Chem. Soc., 143 (2021) 15661-15673.
[257] D. Gygi, M.I. Gonzalez, S.J. Hwang, K.T. Xia, Y. Qin, E.J. Johnson, F. Gygi, Y.-S. Chen, D.G. Nocera, J. Am. Chem. Soc., 143 (2021) 6060-6064.
[258] M.I. Gonzalez, D. Gygi, Y. Qin, Q. Zhu, E.J. Johnson, Y.-S. Chen, D.G. Nocera, J. Am. Chem. Soc., 144 (2022) 1464-1472.
[259] C.B. Larsen, J.D. Braun, I.B. Lozada, K. Kunnus, E. Biasin, C. Kolodziej, C. Burda, A.A. Cordones, K.J. Gaffney, D.E. Herbert, J. Am. Chem. Soc., 143 (2021) 20645-20656.
[260] J. Chen, S. Stepanovic, A. Draksharapu, M. Gruden, W.R. Browne, Angew. Chem. Int. Ed., 57 (2018) 3207-3211.
[261] Y.-D. Du, C.-Y. Zhou, W.-P. To, H.-X. Wang, C.-M. Che, Chem. Sci., 11 (2020) 4680-4686.
[262] A. Gualandi, M. Marchini, L. Mengozzi, M. Natali, M. Lucarini, P. Ceroni, P.G. Cozzi, ACS Catal., 5 (2015) 5927-5931.
[263] M.A. Cismesia, T.P. Yoon, Chem. Sci., 6 (2015) 5426-5434.
[264] H.-K. Liu, Y.-F. Lei, P.-J. Tian, H. Wang, X. Zhao, Z.-T. Li, D.-W. Zhang, J. Mater. Chem. A, 9 (2021) 6361-6367.
[265] S. Parisien-Collette, A.C. Hernandez-Perez, S.K. Collins, Org. Lett., 18 (2016) 4994-4997.
[266] A.C. Hernandez-Perez, S.K. Collins, Angew. Chem. Int. Ed., 52 (2013) 12696-12700.
[267] J.E. Monat, J.K. McCusker, J. Am. Chem. Soc., 122 (2000) 4092-4097.
[268] D. Guo, T.E. Knight, J.K. McCusker, Science, 334 (2011) 1684-1687.
[269] R. Lindroth, A. Ondrejková, C.-J. Wallentin, Org. Lett., 24 (2022) 1662-1667.
[270] E.M.S. Maçôas, R. Kananavicius, P. Myllyperkiö, M. Pettersson, H. Kunttu, J. Phys. Chem. A, 111 (2007) 2054-2061.
[271] O. Prakash, L. Lindh, N. Kaul, N.W. Rosemann, I.B. Losada, C. Johnson, P. Chábera, A. Ilic, J. Schwarz, A.K. Gupta, J. Uhlig, T. Ericsson, L. Häggström, P. Huang, J. Bendix, D. Strand, A. Yartsev, R. Lomoth, P. Persson, K. Wärnmark, Inorg. Chem., 61 (2022) 17515-17526.
[272] N.W. Rosemann, P. Chábera, O. Prakash, S. Kaufhold, K. Wärnmark, A. Yartsev, P. Persson, Journal of the American Chemical Society, 142 (2020) 8565-8569.
[273] H. Kandori, K. Kemnitz, K. Yoshihara, J. Phys. Chem, 96 (1992) 8042-8048.
[274] E.W. Castner, D. Kennedy, R.J. Cave, J. Phys. Chem. A, 104 (2000) 2869-2885.
[275] N.V. Rees, O.V. Klymenko, R.G. Compton, M. Oyama, J. Electroanal. Chem., 531 (2002) 33-42.
[276] F. Cao, J. Kim, A.J. Bard, J. Am. Chem. Soc., 136 (2014) 18163-18169.

[277] A. Aydogan, R.E. Bangle, S. De Kreijger, J.C. Dickenson, M.L. Singleton, E. Cauët, A. Cadranel, G.J. Meyer, B. Elias, R.N. Sampaio, L. Troian-Gautier, Catal. Sci. Technol., 11 (2021) 8037-8051.
[278] R.N. Sampaio, D.C. Grills, D.E. Polyansky, D.J. Szalda, E. Fujita, J. Am. Chem. Soc., 142 (2020) 2413-2428.
[279] J. Schwarz, A. Ilic, C. Johnson, R. Lomoth, K. Wärnmark, Chem. Commun., 58 (2022) 5351-5354.
[280] P. Zimmer, P. Müller, L. Burkhardt, R. Schepper, A. Neuba, J. Steube, F. Dietrich, U. Flörke, S. Mangold, M. Gerhards, M. Bauer, Eur. J. Inorg. Chem., 2017 (2017) 1504-1509.
[281] P. Zimmer, L. Burkhardt, R. Schepper, K. Zheng, D. Gosztola, A. Neuba, U. Flörke, C. Wölper, R. Schoch, W. Gawelda, S.E. Canton, M. Bauer, Eur. J. Inorg. Chem., 2018 (2018) 5203-5214.
[282] M. Huber-Gedert, M. Nowakowski, A. Kertmen, L. Burkhardt, N. Lindner, R. Schoch, R. Herbst-Irmer, A. Neuba, L. Schmitz, T.-K. Choi, J. Kubicki, W. Gawelda, M. Bauer, Chem-Eur. J., 27 (2021) 9905-9918.
[283] A. Rodenberg, M. Orazietti, B. Probst, C. Bachmann, R. Alberto, K.K. Baldridge, P. Hamm, Inorg. Chem., 54 (2015) 646-657.
[284] N.W. Rosemann, L. Lindh, I. Bolaño Losada, S. Kaufhold, O. Prakash, A. Ilic, J. Schwarz, K. Wärnmark, P. Chábera, A. Yartsev, P. Persson, Chem. Sci., (2023).
[285] N. Kaul, R. Lomoth, J. Am. Chem. Soc., 143 (2021) 10816-10821.
[286] Y.J. Jang, H. An, S. Choi, J. Hong, S.H. Lee, K.-H. Ahn, Y. You, E.J. Kang, Org. Lett., 24 (2022) 4479-4484.
[287] E.P. Farney, S.J. Chapman, W.B. Swords, M.D. Torelli, R.J. Hamers, T.P. Yoon, J. Am. Chem. Soc., 141 (2019) 6385-6391.
[288] I.M. Dixon, F. Alary, M. Boggio-Pasqua, J.-L. Heully, Inorg. Chem., 52 (2013) 13369-13374.
[289] I.M. Dixon, S. Khan, F. Alary, M. Boggio-Pasqua, J.L. Heully, Dalton Trans., 43 (2014) 15898-15905.
[290] Y. Pellegrin, F. Odobel, C. R. Chim., 20 (2017) 283-295.
[291] A. Ilic, J. Schwarz, C. Johnson, L.H.M. de Groot, S. Kaufhold, R. Lomoth, K. Wärnmark, Chem. Sci., 13 (2022) 9165-9175.
[292] A. Ilic, J. Schwarz, C. Johnson, L.H.M. de Groot, S. Kaufhold, R. Lomoth, K. Wärnmark, Chem. Sci., 13 (2022) 9165-9175.
[293] S. S. Jayanthi, P. Ramamurthy, Phys. Chem. Chem. Phys., 1 (1999) 4751-4757.
[294] L. Troian-Gautier, M.D. Turlington, S.A.M. Wehlin, A.B. Maurer, M.D. Brady, W.B. Swords, G.J. Meyer, Chem. Rev., 119 (2019) 4628-4683.
[295] R.E. Bühler, M. Ebert, Nature, 214 (1967) 1220-1221.
[296] S.J. Hwang, B.L. Anderson, D.C. Powers, A.G. Maher, R.G. Hadt, D.G. Nocera, Organometallics, 34 (2015) 4766-4774.
[297] Q. Yang, Y.-H. Wang, Y. Qiao, M. Gau, P.J. Carroll, P.J. Walsh, E.J. Schelter, Science, 372 (2021) 847-852.
[298] Z. Pan, Q. Wang, X. Sheng, J.H. Horner, M. Newcomb, J. Am. Chem. Soc., 131 (2009) 2621-2628.
[299] J. Rosenthal, T.D. Luckett, J.M. Hodgkiss, D.G. Nocera, J. Am. Chem. Soc., 128 (2006) 6546-6547.
[300] I.M. Wasser, H.C. Fry, P.G. Hoertz, G.J. Meyer, K.D. Karlin, Inorg. Chem., 43 (2004) 8272-8281.
[301] H.C. Fry, P.G. Hoertz, I.M. Wasser, K.D. Karlin, G.J. Meyer, J. Am. Chem. Soc., 126 (2004) 16712-16713.
[302] M.W. Peterson, D.S. Rivers, R.M. Richman, J. Am. Chem. Soc., 107 (1985) 2907-2915.

[303] R.M. Richman, M.W. Peterson, J. Am. Chem. Soc., 104 (1982) 5795-5796.
[304] Y. Kato, T. Yoshino, S. Matsunaga, ACS Catal., (2023) 4552-4559.
[305] H. Qiao, S. Sun, F. Yang, Y. Zhu, J. Kang, Y. Wu, Y. Wu, Adv. Synth. Catal., 359 (2017) 1976-1980.
[306] R. Xu, C. Cai, Chem. Commun., 55 (2019) 4383-4386.
[307] L.C.M. Castro, J.-B. Sortais, C. Darcel, Chem. Commun., 48 (2012) 151-153.
[308] D. Bézier, F. Jiang, T. Roisnel, J.-B. Sortais, C. Darcel, Eur. J. Inorg. Chem., 2012 (2012) 1333-1337.
[309] L.C.M. Castro, D. Bézier, J.-B. Sortais, C. Darcel, Adv. Synth. Catal., 353 (2011) 1279-1284.
[310] D. Lehnherr, Y. Ji, A.J. Neel, R.D. Cohen, A.P.J. Brunskill, J. Yang, M. Reibarkh, J. Am. Chem. Soc., 140 (2018) 13843-13853.
[311] A. Raghuvanshi, A.K. Singh, S.M. Mobin, P. Mathur, ChemistrySelect, 2 (2017) 9245-9248.
[312] C. Zhu, H. Yue, L. Chu, M. Rueping, Chem. Sci., 11 (2020) 4051-4064.
[313] Y. Landais, G. Kurtay, F. Robert, J. Lusseau, Synlett, 0.
[314] H. Zhang, W. Zhong, Q. Gong, P. Sun, X. Fei, X. Wu, S. Xu, Q. Zhang, G. Fu, S. Xie, Y. Wang, Angew. Chem. Int. Ed., 62 (2023) e202303405.
[315] H. Gao, L. Guo, Y. Zhu, C. Yang, W. Xia, Chem. Commun., 59 (2023) 2771-2774.
[316] Q.-L. Zhang, W. Liu, Y. Zhou, F.-L. Zhang, Green Chem., 25 (2023) 5735-5740.
[317] A. Rogolino, J.B.G. Filho, L. Fritsch, J.D. Ardisson, M.A.R. da Silva, G.A. Atta Diab, I.F. Silva, C.A.F. Moraes, M.R. Forim, M. Bauer, T.D. Kühne, M. Antonietti, I.F. Teixeira, ACS Catal., 13 (2023) 8662-8669.
[318] H.-H. Wang, H. Shao, G. Huang, J. Fan, W.-P. To, L. Dang, Y. Liu, C.-M. Che, Angew. Chem. Int. Ed., 62 (2023) e202218577.
[319] W. Wei, S.L. Homölle, T. von Münchow, Y. Li, I. Maksso, L. Ackermann, Cell Reports Physical Science, 4 (2023) 101550.
[320] S.-C. Kao, K.-J. Bian, X.-W. Chen, Y. Chen, A.A. Martí, J.G. West, Chem Catal., 3 (2023) 100603.
[321] Z. Zhang, X. Li, D. Zhou, S. Ding, M. Wang, R. Zeng, J. Am. Chem. Soc., 145 (2023) 7612-7620.
[322] G.-D. Xia, Z.-K. Liu, Y.-L. Zhao, F.-C. Jia, X.-Q. Hu, Org. Lett., 25 (2023) 5279-5284.
[323] S. Ohmura, K. Katagiri, H. Kato, T. Horibe, S. Miyakawa, J.-y. Hasegawa, K. Ishihara, J. Am. Chem. Soc., 145 (2023) 15054-15060.
[324] A. Reddy-Marri, E. Marchini, V.D. Cabanes, R. Argazzi, M. Pastore, S. Caramori, P.C. Gros, Chem. Sci., 14 (2023) 4288-4301.
[325] K. Parkatzidis, N.P. Truong, K. Matyjaszewski, A. Anastasaki, J. Am. Chem. Soc., (2023).
[326] W.R. Kitzmann, K. Heinze, Angew. Chem. Int. Ed., 62 (2023) e202213207.
[327] C. Wegeberg, O.S. Wenger, JACS Au, 1 (2021) 1860-1876.
[328] F. Wilkinson, A. Farmilo, J. Chem. Soc., Faraday Trans. 2, 72 (1976) 604-618.
[329] C. Yin, M. Wang, Z. Cai, B. Yuan, P. Hu, Synthesis, 54 (2022) 4864-4882.